Ph.D. Thesis

Development of one-dimensional fluorescent nano-materials derived by chiral molecular hybridization

September, 2019

Double Degree Program between
Doctoral School of Chemical Sciences, University of Bordeaux
Graduate School of Science and Technology, Kumamoto University

Shaheen Hamidkhan PATHAN

To my parents

Acknowledgement

Doing science is a long journey; Ph.D. is the stepping stone to contribute in this journey and traveling through untrodden ways to solve the problems. This journey is not possible without the support, contribution, and motivation of several people who play a very important role in every phase of this beautiful journey of Ph.D. Here, I take an opportunity to thank and express my gratitude to all of them.

To start with, I would like to thank all the jury members, and specially Prof. Jérôme LACOUR, and Prof. Kazushi KINBARA who kindly agreed to be reviewers for the manuscript.

Besides, I received an opportunity to work in two groups of two universities: In ODA's group, the molecular assembly group chiral (CMA) in the Institute of Chemistry and Biology of Membranes and Nanoobjects (CBMN), University of Bordeaux, France and Prof. IHARA group, Department of Biochemistry, Kumamoto University, Japan.

I would like to express my sincere gratitude to my thesis supervisors Dr. Reiko ODA, Prof. Hirotaka IHARA, and Prof. Makoto TAKAFUJI, for giving me this opportunity. Right from the beginning of the first day of arrival at Bordeaux as well as in Kumamoto. They guided me, in all possible aspects, to learn, discuss science, work, how to become a thinker and a good researcher, and to be a good human being. The feeling and respect, especially for Dr. Reiko ODA, cannot be expressed in words. Words are not enough to praise her. She introduces me how to be a good scientific researcher, how to learn and look at the problem. In thesis writing, she helped me all the possible ways. About myself, ' I was like a rock found in the forest, to whom Dr. Reiko ODA chose, gave shape like a sculpturer, Prof. Hirotaka IHARA tried to utilized that shaped rock for some purpose, and Prof. Makoto TAKAFUJI tried to decorate that shaped rock to make it more beautiful.' Prof. IHARA is the man with an ocean of knowledge and expertise. I feel blessed for getting an opportunity to work in his team; he is one who trained me to be rough and tough, taught me to look for the positive side of every problem. Even though I made several mistakes until the end of the Ph.D., he patiently dealt with me. He was also there to motivate me during bad times. Prof. TAKAFUJI is the person who helped me to make life easier in Kumamoto, Japan. He was always there for me, tried to help out during

the discussions with Prof. IHARA, to solve my problems. I could not have imagined to have better advisors then them.

Apart from my supervisors, many people share their contribution providing expertise and assistance during this course of research. I would like to thank all of them. To begin with, in ODA's group, Dr. Emilie Pouget who was my first mentor in the beginning of the Ph.D course, she trained to do synthesis of gemini surfactant, to handle the instruments during the group meeting in discussion and doing administrative work, she was there whenever I needed her, she helped to feel comfortable in group and to socialize. Prof. Sylvain NLATE helped me giving a good piece of advice in scientific discussion, especially when it comes to organic chemistry. From IHARA's group, Prof. Yutaka KUWAHARA who helped to get the license for instruments to use, to deal with administrative work, in the absence of Prof. IHARA and Prof. TAKAFUJI, he is the person who use to take care and helped me to solve problems in work as well as other external matters. The collaborators, Prof. Takashi SAGAWA from Kyoto University, Japan for allowing me to work in his lab for a short duration of time, his help on the synthesis of quantum dots and advisory suggestion. Dr. Dario BASSANI from ISM, for providing spectroscopic characterization facilities and playing an essential role in the discussion as well as teaching spectroscopic studies.

Furthermore, I would like to thank to all engineers of IECB, CBMN and Kumamoto University, who help helped me to utilize the facility of equipments. Sisareuth TAN and Marion DECOUSSA-MENDOZA at CBMN for using FEI-120kV TEM. Yuka ONITSUKA and Tetsuya SATO from Kumamoto University for JEOL- 1400 plus TEM. Sonia BUFFIERE from PLACAMAT for HRTEM.

It is not possible to have a peaceful stay at the workplace and new place far away from the home country without the support of one's colleagues. I take this opportunity to thank all the people with whom I was working during the last 3.5 years: In ODA's group, Dr. Yutaka OKAZAKI, Dr. Mariam ATTOUI, Jie GAO, Antoine SCALABRE, Antoine AMESTOY, Peizhao LIU, Jian-Qiao JIANG, Wijak YOSPANYA and Dr. Marie-Christine DURRIEU group, especially Dr. Marie-Christine OERTHEL, Dr. Caroline ROYER, and Laurence PADIOLLEAU. When colleagues become friends, life becomes easier and colorful, my special thanks to Dr. Mariam ATTOUI, Jie GAO, and Antoine SCALABRE for giving moral support and staying there

for me, whenever I needed them. Antoine SCALABRE and I worked on the same project, so most of the time we worked together, he helped me several times in ISM as well as characterized samples in my absence. The best part is he always remain positive, cool and calm, never says no for anything whether we go out for dinner or do experiments. Jie and Mariam are two quiet girls who became very good friends, we shared uncountable moments from every part of life together with work and discussion. Dr. Y. OKAZAKI the postdoc in our group played an essential role for preparing myself going to JAPAN, as a senior he taught me every result of the experiment is a result nothing like good or bad is there. During the curial point, he taught me how to react with problems and find the solutions.

In IHARA's group, Dr. Hiroki NOGUCHI, Dr. Kyouhei YOSHIDA, Dr. Nanami HANO, Dr. Fataha Nur ROBEL, Dr. Nuruzzaman KHAN, Marziya Sultana, Nahid Sultana, Yoko RYU, Tianhang LIU, master's and bachelor's students. Special thanks to the postdoc Dr. H. NOGUCHI from whom I learned so many things during discussion, doing experiments most of the time in lab if any problem occurs he is the first person to whom we approach, management, team work, he played a very important role as senior and also in my project he helped me all possible ways. From each one of them, I learned uncountable things, it will help me to become a better human being and as a researcher.

I want to extend my sincere thanks to all my friends whom I met during the course of Ph.D. in two universities at Bordeaux and Kumamoto especially, Dr. Vikas SHARMA, Dr. Pooja SHARMA, Dr. Suraj KUMAR, Dr. Vibhor JAJOO, Dr. Anandi SRINIVASAN, Dr. Deewakar SHARMA, Dr. Swati KAUSHIK, Dr. Mrunali SONA, Dr. Tanima BISWAS, Meghna, Binu, Sirisha, and Arvind. Also, I would like to say thanks to my overseas friends who always supported and encouraged me, Disha PANDYA, Vidhi BHAVSAR, Jolly JOY, Binita THANKI, Gautam THANKI, Anup AGRAWAL, and Prashant CHOPRA.

Last but not least, I would like to express sincere thanks to parents, Mr. Hamidkhan PATHAN and Mrs. Parveenbanu PATHAN who always encourage and motivated me to follow up dreams and never give up, stood beside me as my strength. My younger siblings, sister Shabnam, and brother Shahrukh supported me spiritually throughout the journey and taken care of my strength in my absences. Moreover, the superpower of all, who gave me energy and good health.

Thank you very much for adding more colours and happy moments in my life.

Abstract

In this work, we focused on the creation of optically active chiral nanostructures by fabricating fluorescent silica nanohelices in order to obtain optically active nanoscale soft materials for applications as nano-photonics materials. For this purpose, silica chiral nanohelices were used for grafting and organizing achiral fluorescent inorganic nanocrystals such as quantum dots, dyes, molecules, and fluorescent polymers through different approaches. These inorganic helices were formed via sol-gel method using organic helical self–assemblies of surfactant molecules (achiral and cationic Gemini surfactant, with chiral counter-ion, tartrate) as templates. First, the surface of helical silica was functionalized by 3-aminopropyltriethoxysilane in order to graft inorganic quantum dots ZnS-$AgInS_2$ with different capping ligands. In the second part, fluorescent anthracene derivative polymer was organized via deposition and absorption on the surface of helical silica. To investigate the chiroptical properties, circular dichroism and circularly polarised luminescence characterization were performed.

In the first chapter, the bibliographic study on different chiral organic self-assembling systems and their chiroptical properties are shown. The studies on the formation of chiral self-assembled systems in different conditions, structural morphology, fabrication techniques and their applications are discussed followed by the use of fluorescent nanocrystals, i.e., quantum dots (QDs) and achiral fluorescent polymers on which chiroptical properties can be obtained and their applications in optical nano-devices, sensors, and nano-photonics.

In the first part of the second chapter, different characterization techniques such as transmission electron microscope (TEM), higher resolution transmission electron microscope (HRTEM), and confocal microscopy, UV-Vis spectroscopy and fluorescence spectroscopies, as well as circular dichroism (CD) and circularly polarised luminescence (CPL) spectroscopies are described. In the second part, the synthesis of Gemini 16-2-16 as well as their self-assemblies mechanism, and their transformation to silica replica via sol-gel chemistry are described. These silica nanohelices are functionalized by 3-aminopropyltriethoxysilane (APTES). Their analysis is performed by Thermogravimetric analysis (TGA) and elementary analysis (EA).

In the third Chapter, we focused on the synthesis of inorganic $(ZnS)_{x-1}(AgInS2)_x$ QDs with different compositions molar ratio (x=0.2, 0.4, 0.6, 0.8, and 1.0) and its characterizations by TEM, Fourier-transform infrared spectroscopy (FTIR), zeta potential measurements,

absorption, and emission spectroscopy. Four types of ligands were used to cap the QDs via phase ligand exchange as follows: ammonium sulphide (AS), 3-mercaptopropionic acid (MPA), l-cysteine (L-Cys) and the fourth one is oleylamine (OLA). These QDs are grafted on the surface of amine-modified silica helices through ionic interaction. Various techniques were used to show the grafting of QDs on the surface of silica helix, and their optical properties were studied using absorption and emission spectroscopy. After grafting, in each case of ligands, different results were observed as follows: The TEM characterization shows that QDs are grafted on the surface of silica helices. In the case of AS-capped QDs, the helical morphology of silica helices after grafting is destroyed; therefore the further analysis was not possible. While, in the cases of QDs with three other ligands MPA, OLA and L-cys, dense and homogeneous grafting of the QDs were observed by TEM and the helical morphology was preserved after their grafting. The HRTEM images were taken on the MPA-QDs@silica helices and energy-dispersive x-ray (EDX) analysis was performed in STEM mode, confirming the QDs elements present on the silica surfaces. For the OLA-QDs@silica helices, along with the TEM images, confocal microscopy was also used to observe fluorescent long fiber-like structures indicating that QDs are grafted on silica helices. In spectroscopic studies, no major changes were observed for the UV-Vis absorbance of MPA- and OLA capped QDs upon grafting, but it may be due to their broad absorbance with no particular peaks and no CD was observed for all three of them. On the other hand, in the case of L-cysteine ligand which is chiral, QDs alone show induced circular dichroism (CD) between the wavelength 250 nm - 300 nm (g-factor 10^{-5}). However, their grafting on the silica nanohelices does not seem to influence the ICD. For the fluorescence, blue shift was observed in the both cases of MPA and OLA. In sum, in spite of the homogeneous and dense grafting of the QDs and well preserved nanohelices (MPA, OLA, L-Cys), we could not observe induced CD or CPL. However, we are able to prepare fluorescent silica helix by grafting QDs which are stable in polar and non-polar solvents.

In the last chapter, the syntheses and the characterisation of polymer particles with size ranging from nm - µm from different monomer such as 2,6 -dihydroxynapthalene (DHN), 2,6-dihydroxy anthracene (DHA) and 9,9-bis(4-hydroxyphenyl)fluorene (BHF) with two different cross-linkers 1,3,5-trimethyl-1,3,5-triazinane (TMTA) and hexamethylenetetramine (HMT), are described. The size of the particles was investigated by transmission electron microscope (TEM) and scanning electron microscope (SEM). The other characterization such as FTIR, EA,

zeta potential were performed to study their physiochemical properties and optical properties were studied using absorption and emission spectroscopy. These polymers were then adsorbed or deposited on the surface of the silica twisted ribbons and nanohelices. For this study, two types of monomers, 1,5 -dihydroxynapthalene (1,5-DHN), 2,6-dihydroxy anthracene (DHA) were used with common cross-linker 1,3,5-trimethyl-1,3,5-triazinane (TMTA), respectively. The deposition of different types of polymers on the silica helix was confirmed with TEM. The further analysis of DHA polymer on silica helices was performed by using EA, absorption, and emission spectroscopy. The ensemble of these results showed that we are able to create the hybrid fluorescent one dimensional helical structure by organic polymer coating on silica nanohelices. The investigation on the chiroptical properties of these polymers@silica nanohelices did not show induced circular dichroism and circularly polarised luminescence in an excited state of the polymer after coating.

Keywords: Self-assembly, chirality, 16-2-16 Gemini surfactant, nano helical silica, $(ZnS)_{1-x}(AgInS_2)_x$ quantum dots, fluorescent polymer, anthracene-derivatives, optical properties, circular dichroism and circularly polarised luminescence.

Résumé

Dans ce travail, nous nous sommes concentrés sur la création de nanostructures chirales optiquement actives en fabriquant des nanohélices de silice fluorescente afin d'obtenir des matériaux souple, nanométriques, optiquement actifs pour des applications en tant que matériaux nanophotoniques. Pour cette fin, des nanohélices de silice chiraux ont été utilisés pour greffer et organiser des nanocristaux inorganiques fluorescents achiraux tels que des points quantiques, des chromophores, des molécules et des polymères fluorescents selon différentes approches. Ces hélices inorganiques ont été formées par procédé sol-gel en utilisant des auto-assemblages hélicoïdaux organiques de molécules amphiphiles (amphiphile gemini cationique, avec un contre-ion chiral le tartrate) en tant que modèles. Tout d'abord, la surface de la silice hélicoïdale a été fonctionnalisée par l'3-aminopropyltriéthoxysilane afin de greffer des points quantiques inorganiques ZnS-$AgInS_2$ avec différents ligands. Dans la deuxième partie, le polymère de dérivé anthracénique fluorescent a été organisé par dépôt et adsorption à la surface de silice hélicoïdale. Afin d'étudier les propriétés chiroptiques, différentes caractérisations ont été réalisées comme le dichroïsme circulaire (CD) et la caractérisation de la luminescence polarisée circulairement (CPL).

Le premier chapitre présente l'étude bibliographique sur différents systèmes d'auto-assemblage organiques chiraux et leurs propriétés chiroptiques. Les études sur la formation de systèmes auto-assemblés chiraux dans différentes conditions, la morphologie structurale, les techniques de fabrication et leurs applications sont discutées suivies de l'utilisation de nanocristaux fluorescents, à savoir, les points quantiques (QD) et les polymères fluorescents achiraux sur lesquels les propriétés chiroptiques peut être obtenus et leurs applications dans les nanodispositifs optiques, les capteurs et la nano-photonique.

Dans la première partie du deuxième chapitre, différentes techniques de caractérisation telles que le microscope électronique en transmission (TEM), le microscope électronique en transmission haute résolution (HRTEM), la microscopie, la spectroscopie UV-Vis et la spectroscopie de fluorescence, ainsi que le dichroïsme circulaire (CD) et la spectroscopie de luminescence polarisée circulairement (CPL) sont décrites. Dans la deuxième partie, la synthèse de Gemini 16-2-16 ainsi que leur mécanisme d'auto-assemblages, et leur transformation en réplique de silice par l'intermédiaire de la chimie sol-gel

sont décrits. Ces nanohélices de silice sont fonctionnalisés par le 3-aminopropyltriéthoxysilane (APTES). Leur analyse est effectuée par analyse thermogravimétrique (TGA) et analyse élémentaire (EA).

Dans le troisième chapitre, nous nous sommes concentrés sur la synthèse de QD inorganiques $(ZnS)_{x-1}(AgInS_2)_x$ avec différentes compositions (rapport molaire (x = 0.2, 0.4, 0.6, 0.8 et 1.0)) et leurs caractérisations par TEM, spectroscopie infrarouge à transformée de Fourier (FTIR), mesures de potentiel zêta, spectroscopie d'absorption et d'émission. Quatre types de ligands ont été utilisés pour recouvrir les QD par échange de ligand de phase comme suit: sulfure d'ammonium (AS), acide 3-mercaptopropionique (MPA), l-cystéine (L-Cys) et le quatrième est l'oléylamine (OLA). Ces QD sont greffés à la surface des hélices de silice modifiée par de l'amine suite à des interactions ioniques. Diverses techniques ont été utilisées pour confirmer le greffage de QD à la surface d'une hélice de silice, et leurs propriétés optiques ont été étudiées par spectroscopie d'absorption et d'émission. Après le greffage, différents résultats ont été observés selon le ligand utilisé: la caractérisation par la TEM montre que les QD sont greffés à la surface d'hélices de silice. Dans le cas de QD avec AS en tant que ligand, la morphologie hélicoïdale des hélices de silice est détruite après le greffage; par conséquent, l'analyse ultérieure n'était pas possible. Alors que, dans les cas des QD avec les trois autres ligands MPA, OLA et L-cys, un greffage dense et homogène des QD a été observée par TEM et la morphologie hélicoïdale a été conservée. Les images HRTEM ont été prises sur les hélices de silice @MPA-QDs et une analyse dispersive en énergie par rayons X (EDX) a été réalisée en mode STEM, confirmant la présence des éléments QD sur la surface de silice. Pour les hélices de silice@OLA-QDs, en plus des images TEM, une microscopie confocale a également été utilisée et a aidé à observer des structures fluorescentes ressemblant à des fibres longues indiquant que les QD sont greffés sur les hélices de silice. Concernant les études spectroscopiques, aucun changement majeur n'a été observé pour l'absorbance UV-Vis des QD recouvert par le ligand MPA et l'OLA lors du greffage, mais cela peut être dû à leur absorbance large sans pics particuliers, aucun CD n'a été observé pour les trois cas de greffage. D'autre part, dans le cas du ligand L-cystéine qui est chiral, les QD seuls montrent un dichroïsme circulaire (CD) induit entre la longueur d'onde 250 nm - 300 nm (facteur g 10^{-5}). Cependant, leur greffage sur les nanohelices de silice ne semble pas influencer le ICD. Pour la fluorescence, un décalage vers le bleu a été observé dans les deux cas de MPA

et de l'OLA. En résumé, malgré le greffage homogène et dense des QD et la conservation des structures des nanohélices (MPA, OLA, L-Cys), nous n'avons pas pu observer de CD ou de CPL induite. Cependant, nous sommes en mesure de préparer des hélices de silice fluorescentes en greffant des QD stables dans des solvants polaires et non polaires.

Dans le dernier chapitre, la synthèse et la caractérisation de particules de polymères d'une taille allant de nm à µm à partir de différents monomères, telles que le 2,6-dihydroxynapthalène (DHN), le 2,6-dihydroxy anthracène (DHA) et le 9,9-bis (4-hydroxyphényl) fluorène (BHF) avec deux agents de réticulation différents, le 1,3,5-triméthyl-1,3,5-triazinane (TMTA) et l'hexaméthylènetétramine (HMT), sont décrites. La taille des particules a été étudiée par le microscope électronique en transmission (TEM) et par le microscope électronique à balayage (SEM). Les autres caractérisations telles que FTIR, EA, potentiel zêta ont été réalisées pour étudier les propriétés physico-chimiques des polymères et les propriétés optiques ont été étudiées par spectroscopie d'absorption et d'émission. Ces polymères ont ensuite été adsorbés ou déposés à la surface des rubans torsadés de silice et des nanohélices de silice. Pour cette étude, deux types de monomères, le 1,5-dihydroxynapthalène (1,5-DHN) et le 2,6-dihydroxy anthracène (DHA) ont été utilisés avec l'agent de réticulation commun 1,3,5-triméthyl-1,3,5- triazinane (TMTA), respectivement. Le dépôt de différents types de polymères sur les hélices de silice a été confirmé par TEM. L'analyse ultérieure du polymère de DHA sur les hélices de silice a été réalisée en utilisant l'EA, la spectroscopie d'absorption et d'émission. L'ensemble de ces résultats a montré que nous sommes en mesure de créer la structure hélicoïdale hybride fluorescente monodimensionnelle par revêtement de polymère organique sur des nanohélices de silice. L'étude des propriétés chiroptiques de ces nanohélices de silice @polymères n'a pas montré de dichroïsme circulaire induit ni de CPL dans un état excité du polymère après revêtement.

Mots-clés: auto-assemblage, chiralité, amphiphile Gemini 16-2-16, nanohélices de silice, points quantiques $(ZnS)_{1-x}(AgInS_2)_x$, polymère fluorescent, dérivés d'anthracéne, propriétés optiques, dichroïsme circulaire et CPL.

List of Abbreviations

NMR – Nuclear magnetic resonance

TEM – Transmission electron microscopy

HRTEM - High Resolution Transmission electron microscopy

STEM – Scanning transmission electron microscopy

EDX – Energy Dispersive X-Ray spectroscopy

CD – Circular dichroism

ICD – Induced circular dichroism

CPL – Circularly polarised luminescence

ICPL – Induced circularly polarised luminescence

MeOH- Deuterated methanol

TMEDA – Tetramethylethylenediaine

TGA – thermogravimetric analysis

EA- Elementary analysis

TEOS - Tetraethoxysilane

APTES – (3-Aminopropyl)triethoxysilane

QDs – Quantum dots

XRD – X-ray diffraction analysis

OLA- Oleylamine

AS –Ammonium sulphide

MPA- 3- Mercaptopropionic acid

L-cys – L-Cysteine

DLS - Dynamic light scattering analysis

SEM- Scanning electron microscopy

FT-IR - Fourier transform infrared spectra

DHN - 2,6 -Dihydroxy naphthalene,

DHA - 2,6- Dihydroxy anthracene

BHF - 9,9-Bis(4-hydroxyphenyl) fluorene

TMTA- 1,3,5-Trimethyl-1,3,5-triazinane

HMT- Hexamethylenetetramine

QY- quantum yield

Ant10-T_8W_2 - 2,6-Dihydroxy anthracene polymer particles

DMSO- Diethyl sulfoxide

DMF- Dimethylformamide

THF- Tetrahydrofuran

EtOAc - Ethyl acetate

PMMA - Poly(methyl methacrylate)

Table of Contents

Chapter 1: Literature Review

Chapter 1: Literature review

Table of contents

1. Introduction

The chirality is a basic concept closely related to the origin of life on the earth as all living organism consist of chiral molecules in their enantiomer forms which are crucial for defining their structures and biological functions. Studies about chirality is one of the most exciting topic in the scientific community in various fields such as biology, chemistry, physics, and mathematics and chirality plays an essential role in modern science and technology. Applications are made in different area such as biomedical, pharmaceutical, catalysis, fundamental physics, and nanoscience.

In this chapter, the bibliography studies of different chiral systems are presented, especially in self-assemblies systems. We will then focus ourselves in the studies on chiral systems showing chiroptical properties, in particular Induction of chirality on achiral systems such as dyes, fluorescent nanocrystals or polymers.

1.1 What is Chirality?

The word 'chiral' is defined to describe the objects having non-superimposable mirror images. And the chirality is a property of asymmetry in shape which is commonly found in chiral objects.

French chemist Louis Pasteur discovered the molecular chirality in 1848, in tartaric acid. Later on, he discovered the enantio-selectivity of tartaric acid by microorganism. [3] Today, the studies on molecular chirality are well established in the field of biology, chemistry as well as in physics.

At the sub-atomic level, chirality is about parity conservation, such as in left-handed helical neutrinos, while at molecular level, molecule found in nature such as amino acids, sugars, and many more are naturally chiral. In general, one of the enantiomers is favored, either as L-amino acids (proteins and enzymes), or as D-sugar groups (DNA, and RNA). [1-3]

Many biological macromolecules or supramolecular system, micro-organism, the helix shaped virus, bacteria such as helicobacter pylori, tobacco mosaic virus are all chiral, snails are the example at macroscopic living systems. Furthermore, many plants express chiral sense during their growth. Our galaxy is also chiral at light year scale. [4]

The molecular chirality plays a crucial role in the design of drugs and functional molecules because of the enantioselective recognition between drugs and the biomolecules, and therefore asymmetric synthesis of chemical compound plays vital role in pharmaceutical industry. [3, 4] Supramolecular chirality can be described as the chirality expressed at supramolecular level based on non-covalent interaction such as hydrogen bonding, van der Waals interaction, $\pi-\pi$ stacking, hydrophobic and hydrophilic interactions. While it is closely related to the chirality of the constituent molecules, the spatial arrangements and self-assembling patterns structures in molecules are the determining factors for their construction. [5]

Hereafter, we will discuss in detail about supramolecular chirality in self-assembling systems.

1.2 Self-assembly systems:

Self-assembly is a process in which a disordered system of pre-existing monomers form an organized structures or patterns as a result of specific local interactions in between the monomers which results into larger- supramolecular structures. Self-assembly is the basic level of all living organisms such as membranes, proteins, or cytoskeleton. [6]

The amphiphilic molecules have ambivalent properties and form self-assembled aggregates in water. Lipids or surfactants constitute typical class of amphiphilic molecules, with polar, ionic or hydrogen- bond forming head groups, such as phosphate, sulfate, ammonium, amino acids, peptides, or sugar. Most often, the hydrophobic tail consist of hydrocarbon chains which can be linear or branched, saturated or unsaturated. [7]

The aggregation of these molecules can lead to 'micro-phase separation' in selected solvents due to the disruption of the cohesive energy. Typically, amphiphiles form micelle-like aggregates or small closed interfaces. [8, 9] Various factors affect the inter/intra molecular interaction inside these aggregates, which have strong impact on their morphologies. Some of these factors are, molecular concentration, temperature, pH and ionic strength. [9, 10, 11]

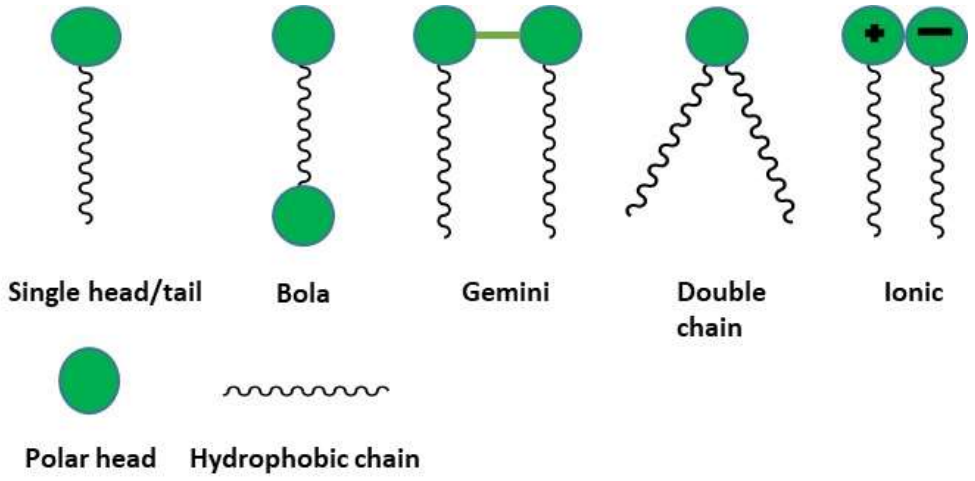

Figure 1.2.1: The classification of amphiphilic molecules.

In 1976, Israelachvili has proposed the critical packing factor *(Cpp)* which can be correlated to the shape and size of the molecules as follows, [11,12,13] *(Cpp)* = V_0/Al_c, where 'V_0' – volume occupied by hydrophobic chains in aggregates, '*A*'- surface area of hydrophilic headgroup in aggregate-solution. In 1976, Israelachvili has proposed the critical packing factor *(Cpp)* which can be correlated to the shape and size of the molecules as follows, [11,12,13] *(Cpp)* = V_0/Al_c, where 'V_0' – volume occupied by hydrophobic chains in aggregates, '*A*'- surface area of hydrophilic headgroup in aggregate-solution, and 'l_c' - chain length. [13]

Here, Cpp is determined by the balance between the hydrophobic effects of the amphiphiles' tails, and the tendency of hydrophilic headgroups to maximize their contact with water. The balance between these two main forces lead to optimal areas per amphiphilic headgroups and hydrophobic chains, for which the interaction energy is minimum. [13] Different structures such as spherical micelles, rod-like micelles, vesicles, bilayers can be formed as shown in figure 1.1.2. These self-assembled structures were first observed with lipid or lipid-like molecules, or natural amphiphilic macromolecules. In 1984, T. Kunitake co-workers reported bilayer-forming amphiphiles based on non-natural (synthetic) molecules. [14] Later on with year passed, it was discovered in lipids, nucleosides, sugar, and peptides based amphiphiles, bolaamphiphiles. [14-18]

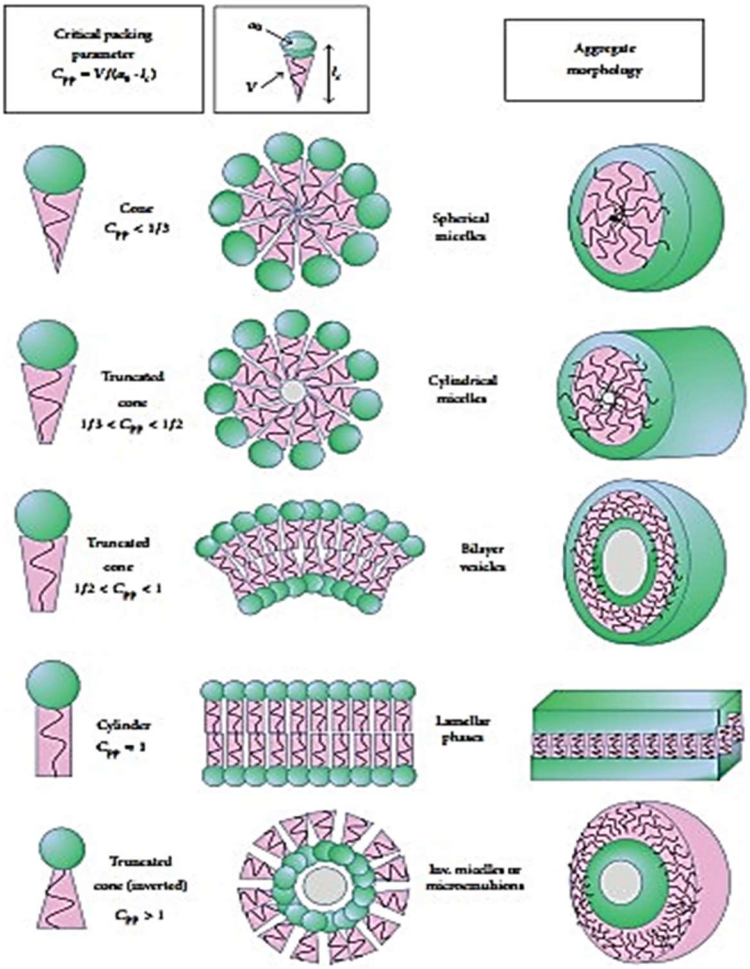

Figure 1.2.2: Amphiphile shape factors and summary of the aggregate structures that can be predicted from the critical packing parameter. [13]

1.3 A general review on chiral self-assembly systems:

In this section, our major focus is on chiral helical structures formed via self-assembly using variety of components including chiral and achiral molecules. A supramolecular organogels or hydrogels containing glutamide moiety and double long- alkyl chains have been reported to form chiral fibrillar structures. [19, 20, 21]. It can form strong intermolecular hydrogen bonds between amine and carbonyl groups from the neighboring molecules, leading to formation of bilayer and higher-order chiral structures. Aromatic functional groups or dyes with chiral center can also be introduced, for which π- π stacking can result to stable gel formation expressing mesoscopic chirality. [22] Figure 1.3.1 represents molecular structure of glutamide containing amphiphiles and corresponds to different fibrous structure

in different conditions with altering guest agents involved in the change of chirality expressions. [22- 25]

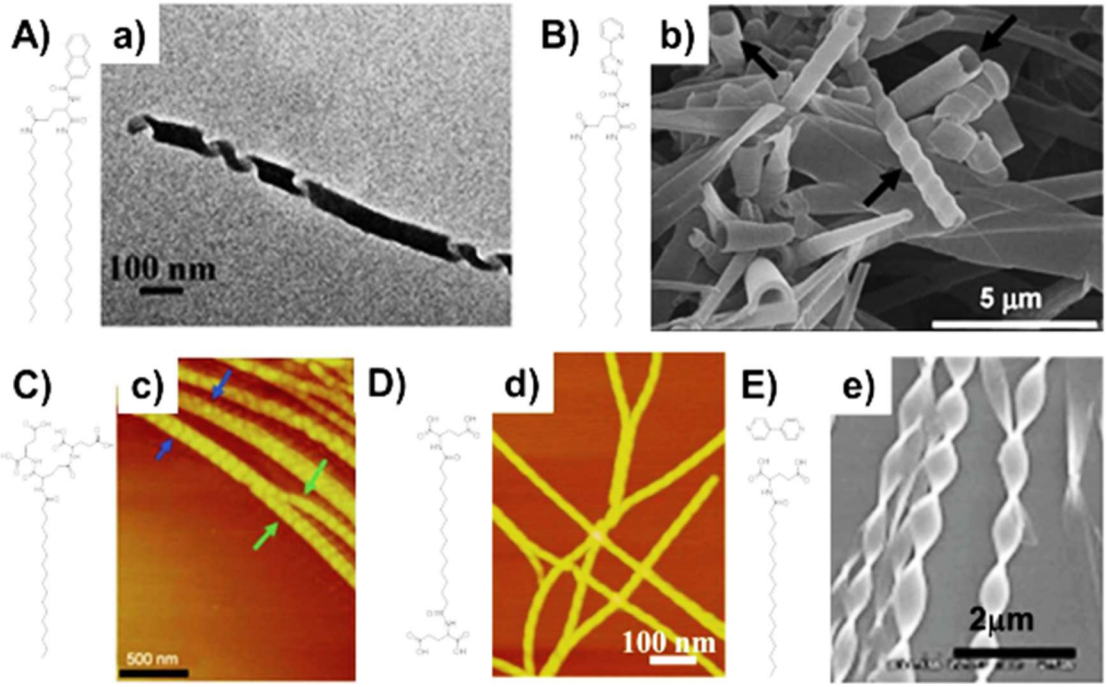

Figure 1.3.1. Molecular structure of glutamide-containing amphiphiles and corresponding chiral nanoarchitectures. A) Molecular structure of 2-naphthylglutamide amphiphile (2-NLG) and a) TEM image of it in acetonitrile. B) Molecular structure of glutamide amphiphile containing a pyridylpyrazole ring (PPLG) and b) SEM image of it in DMSO. C) Molecular structure of dendritic glutamic lipid (OGAC) and c) AFM image of its assembly.D) Molecular structure of bola-type glutamic amphiphile (HDGA) and d) AFM image of its assembly E) Molecular structure of glutamic lipid and 4,4-bipyridine and e) SEM image of the formed chiral twists.[20, 22-25]

There also are many chiral self-assembled systems based on peptides such as the system presented by Aggeli et al. (figure 1.3.2) where β-sheets forming peptides self-assemble to various structures such as helical tapes, twisted ribbons, fibrils or fibers as a function of concentration, which plays determining role for the competition between the free energy gain from attraction between ribbons and the penalty because of elastic distortion of the intrinsically twisted ribbons on incorporation into a growing fibril. [26]

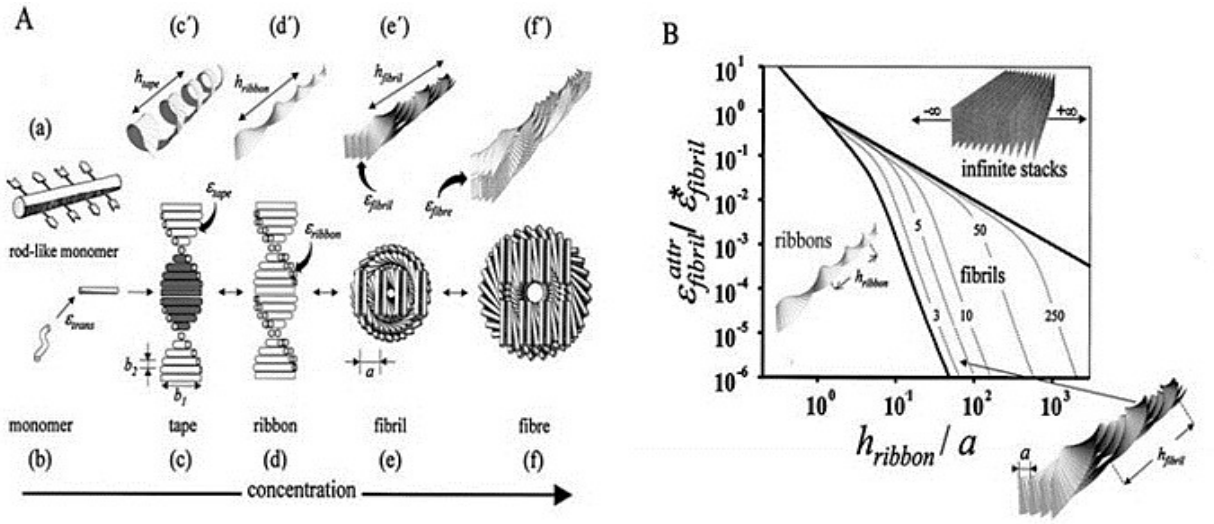

Figure 1.3.2: Model of hierarchical self-assembly of chiral rod-like units. (*A*) Local arrangements (*c*–*f*) and the corresponding global equilibrium conformations (c9–f9) for the hierarchical self-assembling structures formed in solutions of chiral molecules. (*B*) Phase diagram of a solution of twisted ribbons that form fibrils. The scaled variables are as follows: relative helix pitch of isolated ribbons *h*-ribbonya, and relative side-by-side attraction energy between ribbons. The areas divided by the thick lines reveal the conditions where ribbons, fibrils, and infinite stacks of completely untwisted ribbons are stable. The dotted lines are lines of stability for fibrils containing *p* ribbons (*p* are written on the lines). [26]

The polymer can also form chiral structures. For example, E. L. Thomas and co-workers reported the mechanisms of hierarchical chirality transfer at different scale via self-assembly of enantiomeric chiral block copolymers (BCPs). They demonstrated the evolution of homochirality from molecular level upto phase chirality (Figure 1.3.3). [27]

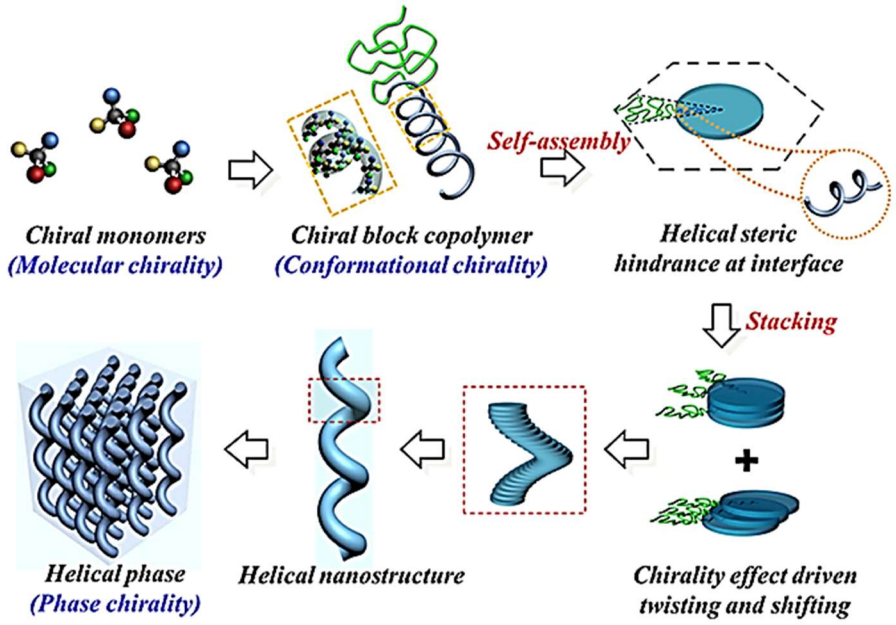

Figure 1.3.3: Schematic illustration of the hypothetical mechanism of transfer of chirality from molecular chirality into phase chirality in the self-assembly of BCPs. [27]

Oda's group has been investigating the self-assemblies of non-chiral gemini surfactant with chiral counterion tartrate (Figure 1.3.4), in which chirality can be varied and tuned from nm- µm scale. The n-2-n Gemini surfactant (n is the number of carbon in their hydrocarbon chain, and 2 represents the ethylene spacer between two ammonium head groups) forms self-assembled organic twisted or helical ribbons and tubes in the presence of chiral tartrate anions. The handedness of the chiral ribbons are determined by the enantiomers of the counter-ions L or D- tartrate ions (right-handed and left-handed respectively). The degree of twist and pitch of the ribbons can be tuned by the enantiomeric excess of the counterions. [28-31]

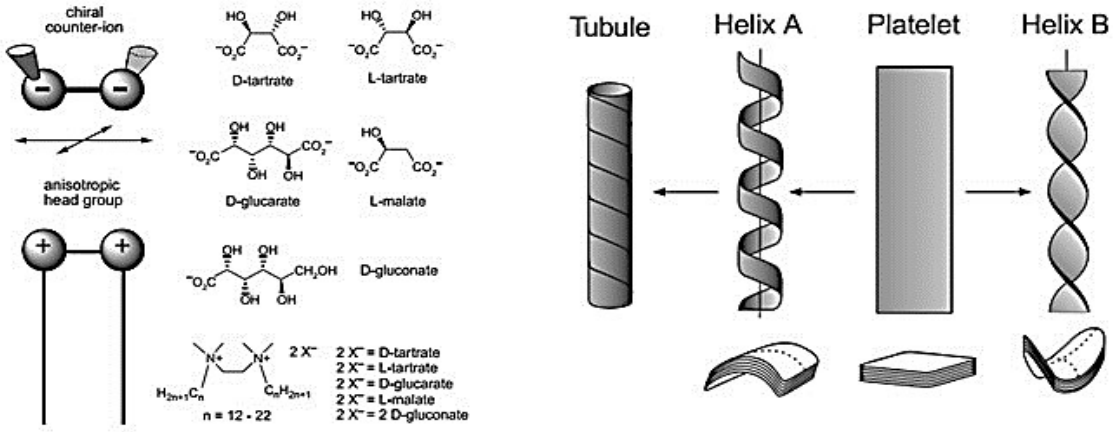

Figure 1.3.4: In Left, cationic gemini amphiphiles having chiral counterions. Shown are the structures of ethylene-1,2-bis(dimethylalkylammonium) surfactants with various chiral anions. In right, Schematic representation of helical and twisted ribbons. Top, platelet or flat ribbon. Helical ribbons (helix A), precursors of tubules, feature inner and outer faces. Twisted ribbons (helix B), formed by some *n*-2-*n* tartrate surfactants, have equally curved faces and a C2 symmetry axis. Bottom, the consequences of cylindrical and saddle-like curvatures in multilayered structures. In a stack of cylindrical sheets, the contact area from one layer to the next varies. This is not the case for saddle-like curvature, which is thus favored when the layers are coordinated. [28]

1.4 The chiroptical properties of chiral systems:

The fascinating chiroptical properties exhibited by the chiral macro/supra/molecular systems have attracted attention since several decades due to their promising use in applications. In this part of the section, we focus on different techniques used to characterize chirality in different systems, which are optically active. The details about characterization principles and the instrumentation part used for this thesis are discussed in Chapter 2.

In chiral systems, various characterization techniques are adapted depending on the environment and conditions in order to characterize the chirality in the systems. The characterization, such as nuclear magnetic resonance (NMR) and X-ray diffraction (XRD) structural analysis are to identify the conformation and configuration of chiral molecules. XRD studies apply to crystalline materials. In order to investigate the structural morphologies from micro –to nanometre scale, several techniques have been developed such as scanning electron microscopy (SEM), transmission electron microscopy (TEM), scanning tunnelling microscopy (STM), and atomic force microscopy (AFM). These techniques will help to understand the chiral morphologies and arrangements of atoms and molecules forming supramolecular structures such as chiral fibers which are typically helical or twisted in shape. [32]

Electronic circular dichroism (CD) and vibrational circular dichroism (VCD) allows to investigate the chiroptical properties directly in a solution, suspension, or solid state. These techniques can also identify the induction of chirality on an achiral molecule or a particle. The chiroptical properties in an excited states can be determined by using circularly polarised light (CPL) technique, this technique is useful in case of chiral fluorescent systems involving monomer, polymer, dyes, quantum dots which participate in formation of chiral structures.

1.5 Chiral induction on an achiral inorganic fluorescent and non-fluorescent nanoparticles:

(a) Inorganic fluorescent nanoparticles: Quantum dots

The development of the research on nanomaterials is closely related to nanotechnology, as nanomaterials have defined structure, shape, size and properties at nanoscale between 1.0 nm to 100 nm [33] in terms of dimensions. Often they have unique optical, electronic, or mechanical properties. Meanwhile, photoluminescence is the emission of light from any substance or a molecule that has absorbed light, and it arises from electronically excited states. The word luminescence origins from Latin root (*lumen: light*) introduced by the German physicist and science historian Eilhard Wiedeman as a *Luminescenz.*

The semiconductor crystals having fluorescent properties are termed as 'Quantum Dots' which are between 1.0 -10.0 nm in size and the color of the emitted light based on their quantum confinement principle depends on the energy difference between the conductance band and the valence band.[34] Quantum confinement effect is a phenomenon which occurs when electron and holes are restricted in one or more dimensions, which is close to or smaller than the exciton Bohr radius.[35] In last two decades, QDs are the most commonly reported nanomaterials, due to their outstanding features and promising applications employed in solar cells, light emitting diodes (LEDs), novel optoelectronic devices, the label for in-vivo imaging and many more. [36] QDs are stable and controllable alternatives compared to their "big brothers", the fluorescent organic dyes, which have limitations such as narrow excitation spectra, inherent susceptibility to proteolytic enzymes and poor stability, especially in applications like bio-imaging, lighting, and displaying. Apart from semiconductor quantum dots, there are other quantum dots perovskite QDs, carbon QDs, and graphene QDs synthesized from various sources, and different techniques were adopted. [37, 38] In this section, the literature on different types of quantum dots and their applications are discussed. In particular, detailed studies about the metal sulphide quantum dots, is shown which will be used in the context of the research conducted in this thesis.

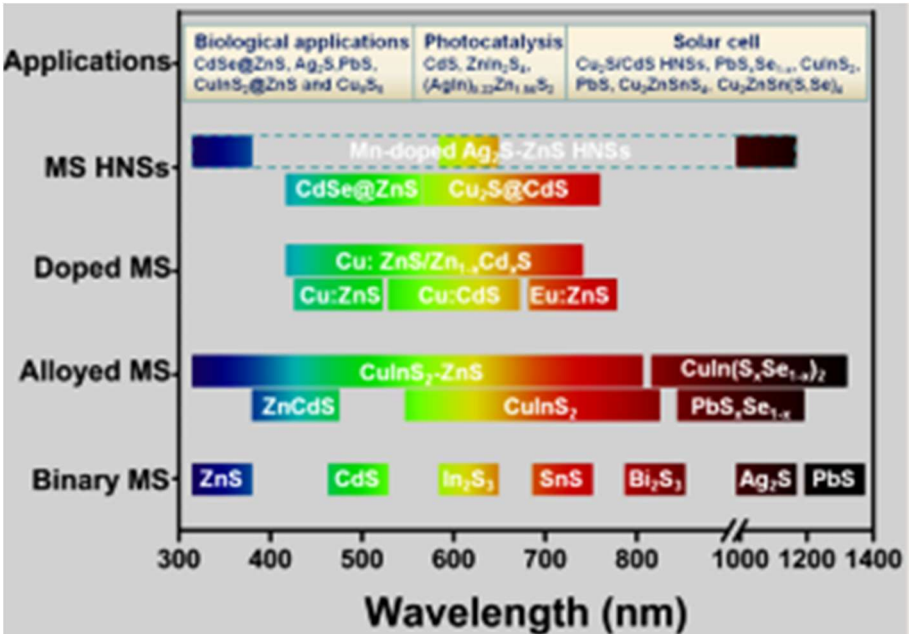

Figure 1.5.1. Schematic illustration of different type's semiconducting quantum dots with the application and emission wavelength. [39]

Metal sulphide (MS) nanocrystals (NCs) form an important class of semiconductor and attracted much attention over the past decade due to their unique optical properties, as well as multiple potential applications such as optoelectronic devices, solar cells, light emitting diodes, and lasers. [39, 40, 41] In particular, I-III-IV ternary alloyed semiconductors exhibit suitable band gaps, non-toxic and nonlinear optical properties which makes them a potential candidate for such applications. $CuInS_2$ and $AgInS_2$ quantum dots are most commonly used semiconductors; they are considered as environmentally friendly nanomaterials. The band gap energies of $CuInS_2$ (E_g = 1.5 eV) and $AgInS_2$ (E_g = 1.8 eV) quantum dots matches well with solar spectrum, high radiation stability, high absorption coefficient, and less toxicity properties are an asset for optoelectronic devices. [42-47] To synthesize them, many techniques were adopted. [48-55] For instance, from a single molecular source $CuInS_2$ QDs were synthesized with a quantum yield of 5% reported in Castro et al.; [56] The difficult problem was they were not able to tune the emission wavelength in a wide range regardless of having control over particle size with diameter of 2.0 – 4.0 nm, lesser than the Bohr radii approximately 4.1 nm for $CuInS_2$. [57] On the other hand, by increasing the Cu content, the absorption band can be adjusted in the case of Cu-In-S QDs from 560 nm to 870 nm, and it corresponds to tunable band gaps energies ranging from 2.30 to 1.48 eV. [58,59] Several techniques were adapted to fulfill the requirement.

(b) Chiroptical properties in inorganic nanoparticles including quantum dots:

There are different methods to induce chiroptical properties to inorganic nano structures, for example to induce chiroptical properties of nanoparticles from chiral capping ligands, chiral templates, or chiral organization of particles.

Chiral ligands: achiral CdSe QDs capped by a chiral ligand such as L-or D-cysteine demonstrated circular dichroism (CD) and circularly polarised luminescence (CPL) signals. [60, 61] While, chirality inversion was observed in CdSe and CdS quantum dots without changing the capping ligand reported by Choi et al. [62, 63] Such ligand-induced chirality was also observed with graphene quantum dots and silver nanocluster. [64, 65]

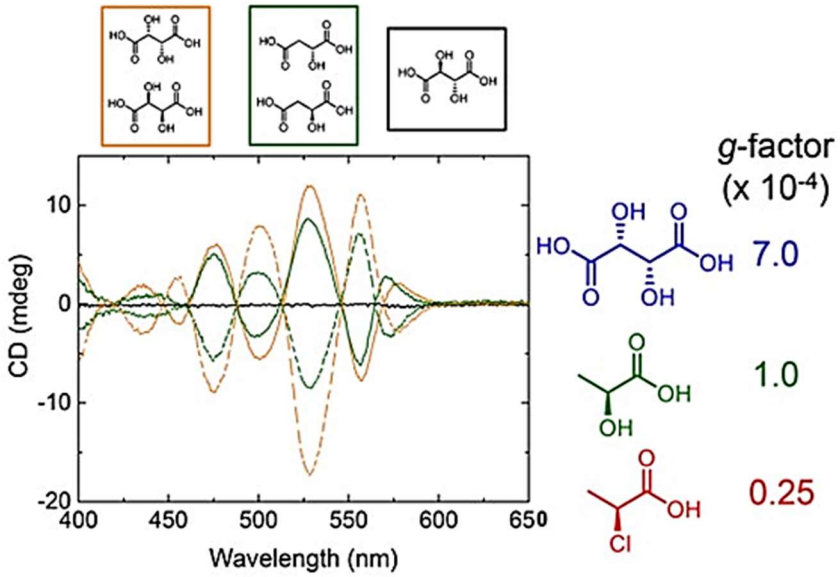

Figure 1.5.2: Overlaid CD spectra of CdSe nanoparticles (5 µM, DMF) bound by L-(+)-tartaric acid (dotted orange trace), D-(-)-tartaric acid (solid orange trace), D-(+)-malic acid (dotted green trace), L- (-)-malic acid (solid green trace), and meso-tartaric acid (black trace). The value of g-factor with respect to the capping ligand. [61]

T. Tatsuma and his co-worker reported plasmonic chiral nanostructure by using circularly polarised light. [66] Using twisted electric field distributions around the achiral gold nanocuboids under circularly polarized light, chiral plasmonic nanostructures were by means of site-selective deposition of PbO_2 based on plasmon-induced charge separation (PICS). When the light irradiated on TiO_2, the positive and negative charges are generated on nanocuboid and TiO_2, respectively. [67] Therefore, oxidation and reduction reactions occurs due to the generation of charge in the presence of a strong electric field. The Circular

dichroism (CD) spectra of the substrate gold nanocuboids were observed when circularly polarized light was irradiated on the suspension (figure 1.5.3-iid).

Figure 1.5.3: (i) Concept of chiral nanostructure preparation.Schematic illustration of chiral nanostructure fabrication by PICS using circularly polarized light as the sole chiral source. (ii) Optical properties of the chiral nanostructures. (a) Experimental and simulated extinction spectra of the TiO2 substrate with gold nanocuboids irradiated from the back side. (b) CD spectra of the TiO2 substrate with gold nanocuboids before (black line) and after PbO2 deposition by RCP (blue line) or LCP (red line) light irradiation. (c) Simulation model of a left-handed gold nanocuboid with one or two PbO2 moieties. (d) Simulated CD spectra of the models shown in panel c. [67]

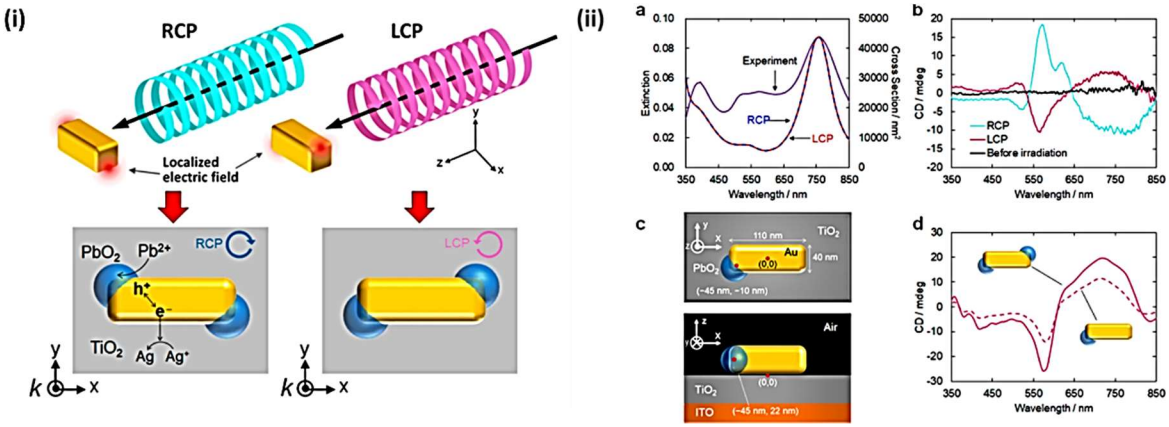

The molecular recognition plays a vital role to understand a natural mechanism in the process like metabolism or immune response, due to the chiral recognition between receptors on biomolecules and the target molecules. M. V. et al., [68] reported the enantioselective recognition of l-cysteine molecules on the chiral surfaces of the CdSe and CdS nanocrystals.

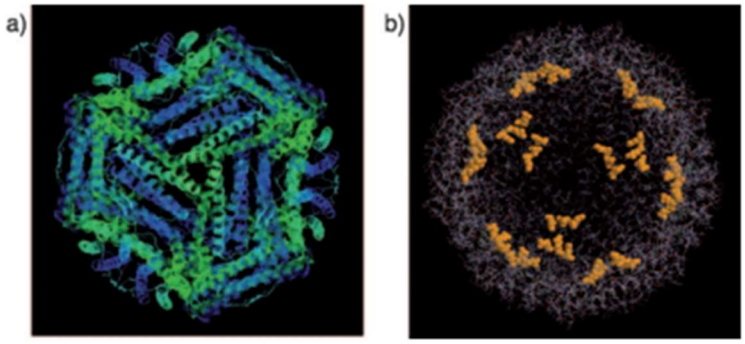

Figure 1.5.4: a) Illustration of apoferritin from a threefold channel (ribbon model) and b) a cross-sectional view (slab 65%). The 72 glutamate residues on the interior surface are depicted as a yellow space-filling model. [68]

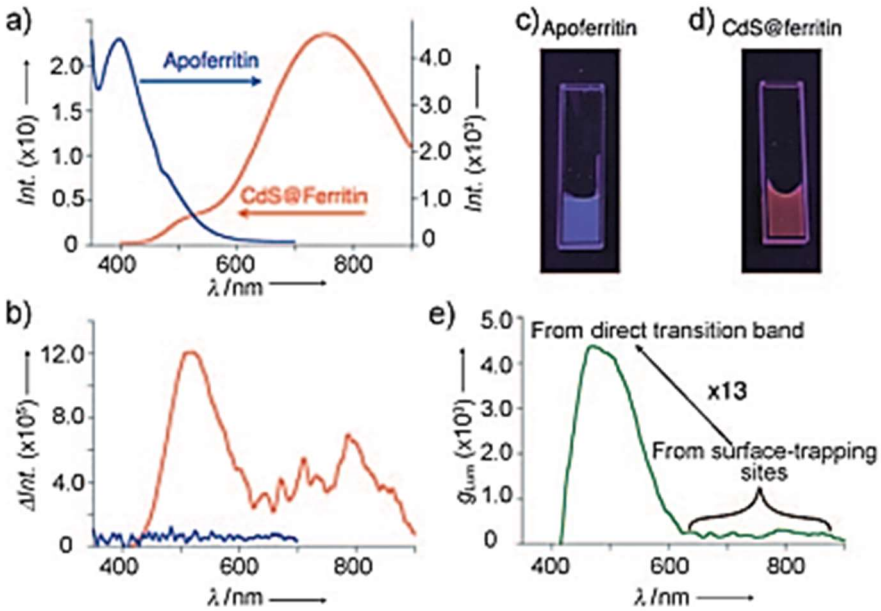

Figure 1.5.5: a) PL and b) CPL spectra of apoferritin (blue) and CdS@ferritin (red). All spectra were obtained using excitation at 325 nm. Photographs of c) apoferritin and d) CdS@ferritin. The samples were irradiated by a UV lamp with an emission wavelength of 310 nm. e) Kuhn's anisotropy factor (gLum) as a function of wavelength. [68]

Also, by using a hollow chiral template, the quantum dots were prepared (figure 1.5.4). M. Naito and his co-workers have reported that chiral quantum dots can be synthesized using rhombic dodecahedral protein, which is a horse spleen ferritin, as a hollow chiral template. CdS water-soluble quantum dots were synthesized accomplishing ferritin, 72 glutamate residues on the interior surface of the apoferritin shell are the initiators, to form quantum dots. These quantum dots emit left handed CPL emission. The emergence of CPL emission is due to the surface trapping sites of quantum dots and the direct transitions (figure 1.5.5), respectively. [69] The modulation for normal emission and chiral emission is done by laser photoetching.

Induction of chirality in plasmonic nanoparticles presents unique properties as compared to other inorganic nanoparticles and quantum dots. Nanoparticles of gold, silver, and other noble metals show surface plasmon. Chiral induction through the capping ligand can then be observed for the surface plasmon signals. [70, 71] While, synthesizing Ag nanoparticles in helical DNA results into chiral induction, which is observed in circular dichroism (CD). [72] DNA acts as a template to control the size of the particles and at the same time, particles are arranged inside the DNA (figure 1.5.6). Due to helical arrangement of Ag nanoparticles along the DNA, their plasmonic signal shows induced CD. [72]

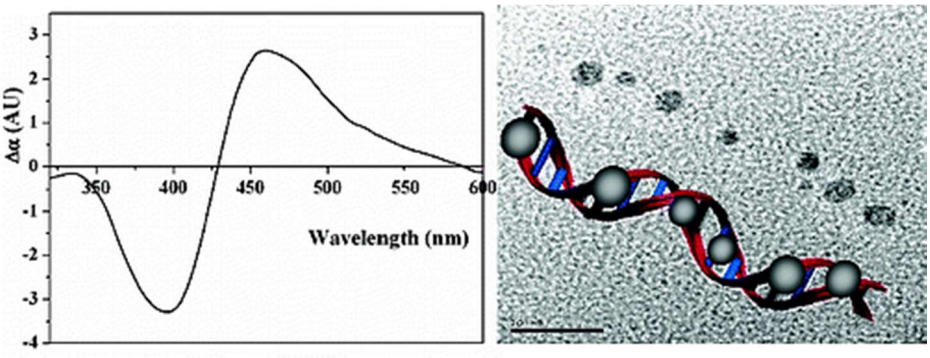

Figure 1.5.6: CD spectra measured on Ag nanoparticles grown directly on the DNA and TEM image of Ag nanoparticle with the scheme. [72]

Fisher and coworkers created nanocolloids with anisotropic three-dimensional shapes, with a size of 20 nm (figure 1.5.7a) such as plasmonic Au nanohelices and other shapes such as nano hooks containing Cu, Ti, Al_2O_3, and Au. The chiral morphology-originated circular dichroism and tunable optical chiroptical properties were observed (figure 1.5.7). [73]

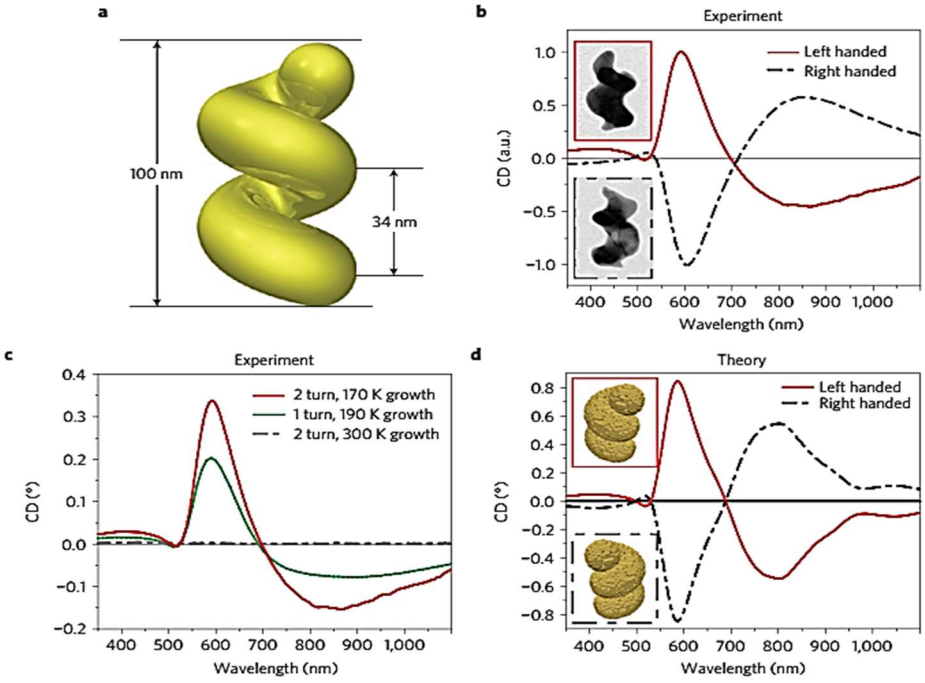

Figure 1.5.7: The chiroptical response of solutions of Au nanohelices. a, Model two-turn gold nanohelix showing critical dimensions. b, Normalized circular dichroism (CD) spectra of left-handed and right-handed helices. Inset: TEM images of grown structures with left (top) and right (bottom) chirality (image dimensions: 85 nm×120 nm). c, Circular dichroism spectra of two- and one-turn helices grown under cooling conditions, and of nominal two-turn helices grown at room temperature. The spectra are plotted against an absolute *y* axis calibrated according to the optical density of the λmax peaks (at around 600 nm) in the corresponding ultraviolet–visible spectra. d,

Simulated CD spectra for a based on model dimensions taken from TEM images. The insets show the discrete dipole models used in the calculations. [73]

In Oda's group, plasmonic nanoparticles were organized on chiral template. Strong circular dichroism (CD) has been observed for their surface plasmon resonance (SPR). The anisotropy factor is of the order of 10^{-4} -10^{-3}. The chiroptical properties depend on the size and organization of the gold nanoparticles (figure 1.5.8). This is an example of secondary chirality induction on the optical properties of gold due to the template [32, 74, 75]

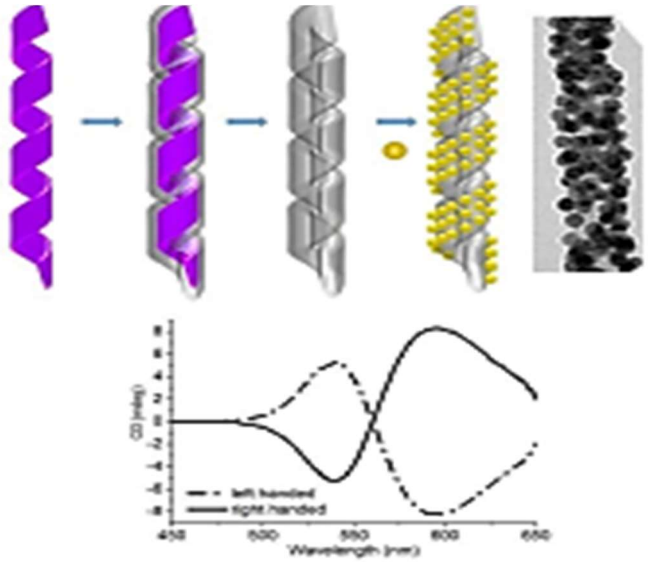

Figure 1.5.8: Silica nanohelices synthesized from sol-gel condensation of TEOS on self-assembled organic nanostructures are used as a matrix to prepare helical GNPs superstructures (Goldhelix) with tunable and well-defined handedness. Goldhelix made using GNPs with various sizes. Top: representative TEM images of 5-10 nm GNPs@ SiO2 helix. Bottom: corresponding electronic ECD spectra of the Goldhelices. Dashed lines represent right-handed Goldhelix, and solid lines represent left-handed Goldhelix. [32]

Huo and coworkers have used, as template, the organic lipid gelator N,N'-bis(octadecyl)-l-glutamic diamide (LGAm) and its enantiomer DGAm, which have been reported to form organogels with tubular nanostructures. [76] The achiral phototunable core-shell QDs including CdSe/ZnS, CdS/ZnS, and ZnSe/ZnS were used, these QDs were adsorbed on the surface of nanotube by ionic interaction between the free amine group at the chiral center of the tube and the carboxylic group of ligand capped on QDs (figure 1.5.9A). Induced chirality was observed in absorbance and emission of achiral QDs and the circular dichroism (CD) and circularly polarised luminesce (CPL) signals with different handedness can be generated in the co-gels were observed (figure 1.5.9B).

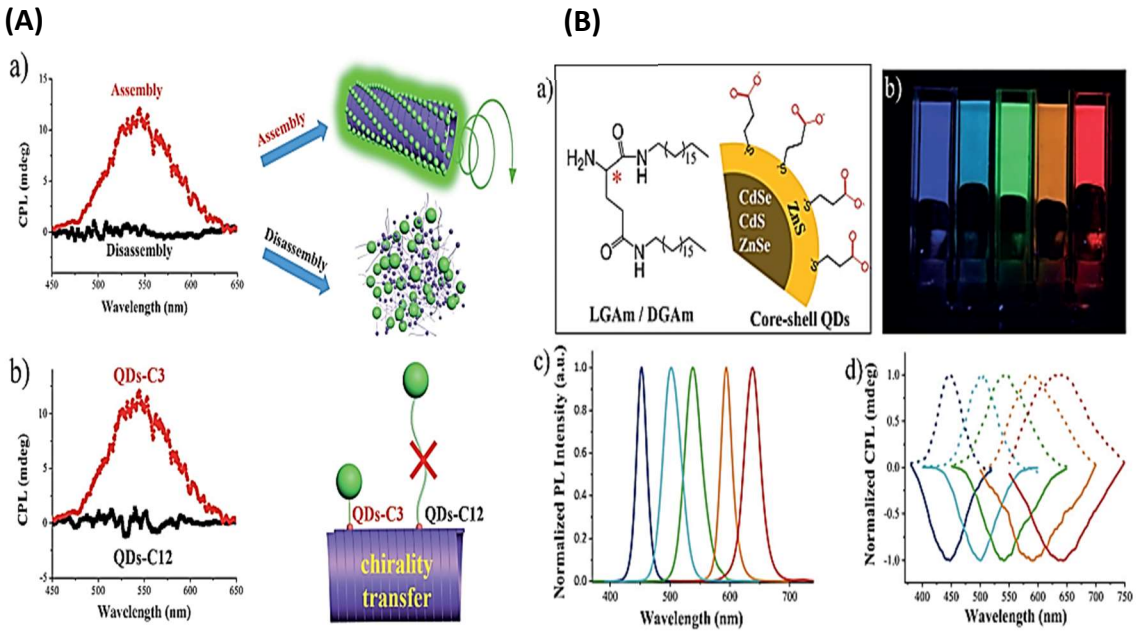

Figure 1.5.9: A: a) CPL spectra of green-emissive QD doped co-gels in the state of assembly and disassembly. The disassembly spectrum was obtained from a DGAm gel in THF/H2O (10:1 v/v); [DGAm]= 10 mg mL@1, [QD]=0.2 mg mL@1. b) The spacer length of the capping reagent determines the feasibility of chirality transfer from the chiral nanotube to the QDs. The spectrum of the QDs-C12 doped co-gel was obtained from a DGAm gel in EtOH/H2O (10:1 v/v); [DGAm]=20 mg mL@1, [QDs-C12]=[QDs-C3]=0.2 mg mL@1, B: (a) Molecular structure of the gelators and the QDs used in this work. Three core–shell QDs with the same ZnS shell capped with 3-mercaptopropionic acid and different cores (CdSe, CdS, and ZnSe) were investigated. b) Photograph of various CdSe/ZnS QD doped cogels in EtOH/H2O (10:1 v/v) under UV light. EtOH/H2[LGAm]= 20 mg mL@1, [QD]=0.2 mg. c) Fluorescence spectra of the corresponding co-gels; lex=360 nm. d) Mirror-image CPL spectra of the corresponding co-gels; lex=360 nm. [76]

1.6 Chiral induction in chiral and achiral polymer:

Helical polymer is synthesized through controlled polymerization of an enantiomerically pure isocyanide which creates both *static* diastereomeric right- and left-handed helical polyisocyanides whose helical sense can be controlled by the polymerization solvent and temperature (figure 1.6.1a). The AFM images (figure 1.6.1c) show the helical morphology of the polymer and the ICD spectra on the aromatic group of both the enantiomer which is determined by the helical sense, indicating that the polymer is optically active at the ground state due to the induced chirality. [77]

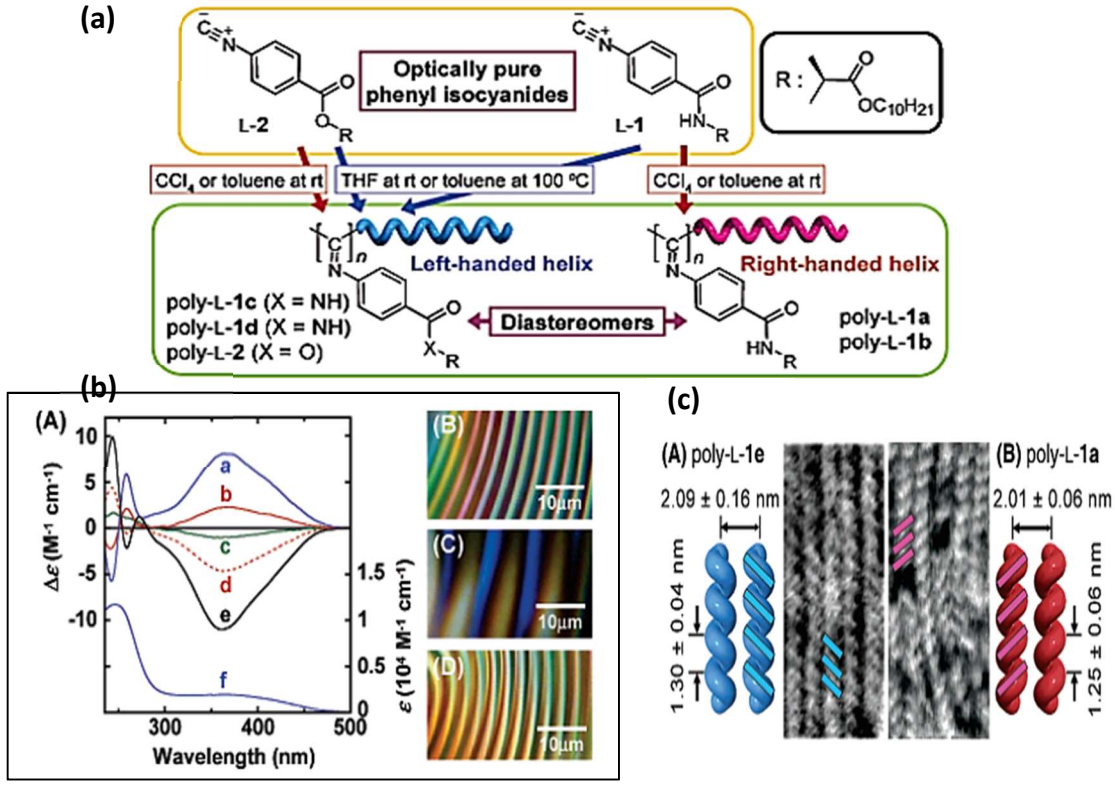

Figure 1.6.1: (a) Structures of L-1 and L-2 and schematic illustration of diastereomeric helical polyisocyanides produced by the helix-sense controlled polymerization of L-1. The helix-sense can be controlled by the solvent polarity and temperature during the polymerization, resulting in the formation of static diastereomeric helical polyisocyanides, while L-2 yields only the left-handed helical poly-L-2 independent of the polymerization conditions, (b) : (A) CD spectra of poly-L-1a (a, blue line), poly-L-1b (b, red solid line), and poly-L-1c (c, green line) polymerized in CCl_4, toluene, and THF, respectively, at ambient temperature; poly-L-1d (d, red dotted line) polymerized in toluene at 100 °C; and poly-L-1e (e, black line) after polyL-1d annealed in toluene at 100 °C for 6 days. The absorption spectrum of poly-L-1a (f) is also shown. The CD and absorption spectra were measured in CHCl3 at 25 °C (0.2 mg/mL). (B-D) Polarized optical micrographs of cholesteric LC phases of poly-L-1a (B), a 1:1 mixture of poly-L-1a and poly-L-1e (C), and poly-L-1e (D) in $CHCl_3$ (15 wt %), and (c) : AFM phase images of self-assembled poly-L-1e (A) and polyL-1a (B) on HOPG. Schematic representations of the left-handed helical poly-L-1e (left) and right-handed helical poly-L-1a (right).

2D helix-bundles with periodic oblique pendant arrangements (blue and pink lines, respectively). [77]

An example of ICD on achiral azobenzene liquid crystalline polymer was observed. Here, it was reported that under circularly polarized light, induction of chirality in an initially achiral Sm-A liquid crystalline azobenzene polymer and formation of TGB-like phase was observed. [78] This was the first example of an optical switch based on the change of the chirality in a pro-chiral polymer film B as a source of asymmetric induction (figure 1.6.2c).

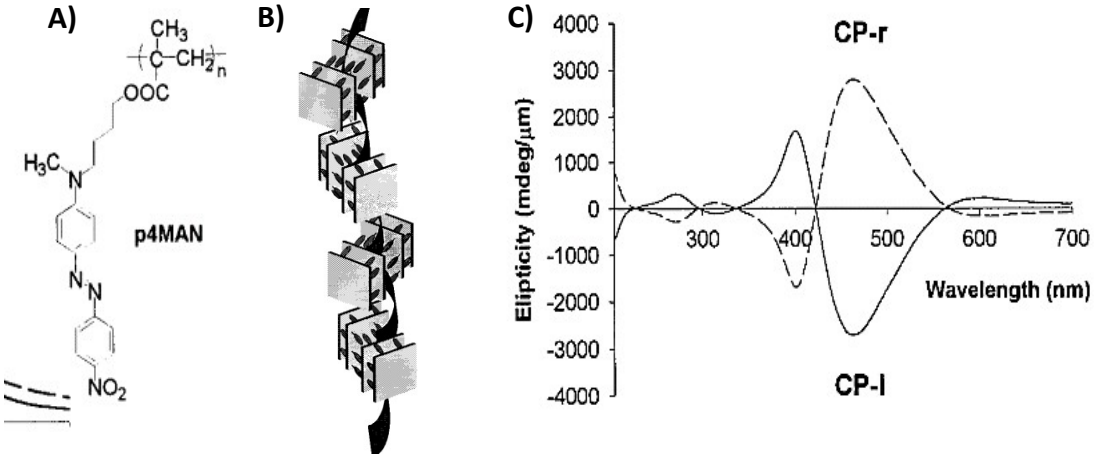

Figure 1.6.2 (A) the molecular structure of p4MAN, (b) the scheme of helical organization of the molecules, and (c) CD spectra of thin films (140 nm) of p4MAN recorded after irradiation with circularly polarized light (514 nm, 75 mW/cm2): induced with CP-l (s) and with CP-r (---), respectively. [78]

In H. Ihara's group, since 1980s, self-assembly of glutamine molecule which form chiral nanotubes has been investigated. These molecules are used as template to induce chirality to dyes, polymer, metal ions etc. [79, 80, 81] Using glutamide nanotubes as a template, polymerization of styrene was performed, and ICD was observed on the polymerized styrene. [81, 82, 83] Chiral stacking of benzothiophene on the glutamide nanotubes show phosphorescent with a lifetime of milliseconds and also results into ICD when incorporated in a thin polymer film. [84] Other achiral fluorophores such as pyrene, anthracene, phenylanthracene and diphenylanthracene in interaction with glutamide nanotubes also showed induction of chiral emission and absorbance. [85-87]

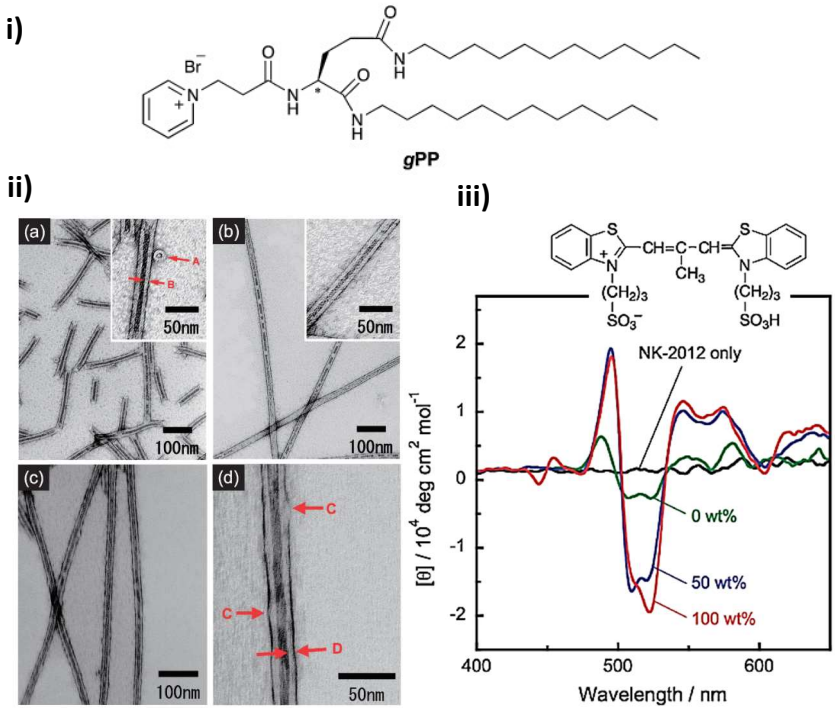

Figure 1.6.3: (i) Scheme of glutamide molecule, (ii) TEM images of gPP aggregates: (a) without a monomer; (b) with styrene (100 wt % for gPP); (c), (d) with styrenedivinylbenzene (65 wt % and 35 wt % for gPP, repsectively) after photo-irradiated for 4 h. These samples were stained by 1.0 wt % uranyl acetate, and (iii) CD spectra of aqueous mixed systems composed of gPP and NK-2012 at 10 °C. [gPP] = 0.5 mM, [NK-2012] = 0.025 mM, [styrene] = 0100 wt % for gPP. [83]

Various examples shown above demonstrated how chiral system in interaction with achiral component can induce chirality to the latter and affect their optical properties. A concept which can be used for creation of optically active nanomaterials.

References

1. Brandt, J. R.; Salerno, F.; Fuchter, M. J. The Added Value of Small-Molecule Chirality in Technological Applications. *Nature Reviews Chemistry* **2017**, *1*, 0045.
2. https://joeleriksson.com/amphidromus-wikiwand.html
3. Gal, J. The Discovery of Biological Enantioselectivity: Louis Pasteur and the Fermentation of Tartaric Acid, 1857—A Review and Analysis 150 Yr Later. *Chirality* **2008**, *20* (1), 5–19. https://doi.org/10.1002/chir.20494.
4. Wang, Y.; Xu, J.; Wang, Y.; Chen, H. Emerging Chirality in Nanoscience. *Chem. Soc. Rev.* **2013**, *42* (7), 2930–2962. https://doi.org/10.1039/C2CS35332F.
5. Yang, Y.; Zhang, Y.; Wei, Z. Supramolecular Helices: Chirality Transfer from Conjugated Molecules to Structures. *Advanced Materials* **2013**, *25* (42), 6039–6049. https://doi.org/10.1002/adma.201302448.
6. Safinya, C. R.; Raviv, U.; Needleman, D. J.; Zidovska, A.; Choi, M. C.; Ojeda-Lopez, M. A.; Ewert, K. K.; Li, Y.; Miller, H. P.; Quispe, J.; et al. Nanoscale Assembly in Biological Systems: From Neuronal Cytoskeletal Proteins to Curvature Stabilizing Lipids. Advanced Materials 2011, 23 (20), 2260–2270. https://doi.org/10.1002/adma.201004647.
7. Sorrenti, A.; Illa, O.; Ortuño, R. M. Amphiphiles in Aqueous Solution: Well beyond a Soap Bubble. Chemical Society Reviews 2013, 42 (21), 8200.
8. M. J. Rosen, Surfactants and Interfacial Phenomena, Wiley, New York, NY, USA, 2nd edition, 1989.
9. K. Holmberg, B. Jonsson, B. Kronberg, and B. Lindman, Surfactants and Polymers in Aqueous Solution, John Wiley & Sons, Chichester, UK, 2nd edition, 2002
10. Chandler, D. Interfaces and the Driving Force of Hydrophobic Assembly. *Nature* **2005**, *437* (7059), 640–647. https://doi.org/10.1038/nature04162
11. a) Tanford C., The Hydrophobic Effect: Formation of Micelles and Biological Membranes. 1973, New York: John Wiley & Sons Inc; b) Tanford, C. Theory of Micelle Formation in Aqueous Solutions. *The Journal of Physical Chemistry* **1974**, *78* (24), 2469–2479. https://doi.org/10.1021/j100617a012.
12. Israelachvili, J. N. Intermolecular and Surface Forces Revised Third Edition. Elsevier Science & Technology Books 2011.
13. Lombardo, D.; Kiselev, M. A.; Magazù, S.; Calandra, P. Amphiphiles Self-Assembly: Basic Concepts and Future Perspectives of Supramolecular Approaches. *Advances in Condensed Matter Physics* **2015**, *2015*, 1–22. https://doi.org/10.1155/2015/151683.
14. Nakashima, N., Asakuma, S., & Kunitake, T. (1985). Optical Microscopic Study of Helical Superstructures of Chiral Bilayer Membranes. *Journal of the American Chemical Society*, *107*(2), 509-510. https://doi.org/10.1021/ja00288a043
15. Fyfe, M. C. T.; Stoddart, J. F. Synthetic Supramolecular Chemistry. *Accounts of Chemical Research* **1997**, *30* (10), 393–401. https://doi.org/10.1021/ar950199y.
16. Alfonsi, K.; Colberg, J.; Dunn, P. J.; Fevig, T.; Jennings, S.; Johnson, T. A.; Kleine, H. P.; Knight, C.; Nagy, M. A.; Perry, D. A.; et al. Green Chemistry Tools to Influence a Medicinal Chemistry and Research Chemistry Based Organisation. *Green Chem.* **2008**, *10* (1), 31–36. https://doi.org/10.1039/B711717E.
17. Tachibana, T.; Kambara, H. Enantiomorphism in the Helical Aggregate of Lithium 12-Hydroxystearate. *Journal of the American Chemical Society* **1965**, *87* (13), 3015–3016.

https://doi.org/10.1021/ja01091a046.
18. Cornelissen, J. J. Helical Superstructures from Charged Poly(Styrene)-Poly(Isocyanodipeptide) Block Copolymers. *Science* **1998**, *280* (5368), 1427–1430. https://doi.org/10.1126/science.280.5368.1427.
19. Ihara, H.; Hachisako, H.; Hirayama, C.; Yamada, K. Specific Bindings of Methyl Orange to Chiral Bilayer Membranes with β-Alanyl-L-Glutamoyl Head Groups [1]. *Liquid Crystals* **1987**, *2* (2), 215–221. https://doi.org/10.1080/02678298708086292.
20. Zhang, L.; Wang, T.; Shen, Z.; Liu, M. Chiral Nanoarchitectonics: Towards the Design, Self-Assembly, and Function of Nanoscale Chiral Twists and Helices. *Advanced Materials* **2016**, *28* (6), 1044–1059. https://doi.org/10.1002/adma.201502590.
21. Miao, W.; Yang, D.; Liu, M. Multiple-Stimulus-Responsive Supramolecular Gels and Regulation of Chiral Twists: The Effect of Spacer Length. *Chemistry - A European Journal* **2015**, *21* (20), 7562–7570. https://doi.org/10.1002/chem.201500097.
22. Wang, X.; Duan, P.; Liu, M. Self-Assembly of π-Conjugated Gelators into Emissive Chiral Nanotubes: Emission Enhancement and Chiral Detection. *Chemistry - An Asian Journal* **2014**, *9* (3), 770–778. https://doi.org/10.1002/asia.201301518.
23. Shen, Z.; Wang, T.; Liu, M. H-Bond and π–π Stacking Directed Self-Assembly of Two-Component Supramolecular Nanotubes: Tuning Length, Diameter and Wall Thickness. *Chemical Communications* **2014**, *50* (17), 2096. https://doi.org/10.1039/c3cc48350a.
24. Jin, Q.; Zhang, L.; Liu, M. Solvent-Polarity-Tuned Morphology and Inversion of Supramolecular Chirality in a Self-Assembled Pyridylpyrazole-Linked Glutamide Derivative: Nanofibers, Nanotwists, Nanotubes, and Microtubes. *Chemistry - A European Journal* **2013**, *19* (28), 9234–9241. https://doi.org/10.1002/chem.201300612.
25. Zhu, X.; Duan, P.; Zhang, L.; Liu, M. Regulation of the Chiral Twist and Supramolecular Chirality in Co-Assemblies of Amphiphilic L-Glutamic Acid with Bipyridines. *Chemistry-A European Journal* **2011**, *17* (12), 3429–3437. https://doi.org/10.1002/chem.201002595.
26. Aggeli, A.; Nyrkova, I. A.; Bell, M.; Harding, R.; Carrick, L.; McLeish, T. C. B.; Semenov, A. N.; Boden, N. Hierarchical Self-Assembly of Chiral Rod-like Molecules as a Model for Peptide -Sheet Tapes, Ribbons, Fibrils, and Fibers. *Proceedings of the National Academy of Sciences* **2001**, *98* (21), 11857–11862. https://doi.org/10.1073/pnas.191250198.
27. Ho, R.-M.; Li, M.-C.; Lin, S.-C.; Wang, H.-F.; Lee, Y.-D.; Hasegawa, H.; Thomas, E. L. Transfer of Chirality from Molecule to Phase in Self-Assembled Chiral Block Copolymers. *Journal of the American Chemical Society* **2012**, *134* (26), 10974–10986. https://doi.org/10.1021/ja303513f.
28. Oda, R.; Huc, I.; Schmutz, M.; Candau, S. J.; MacKintosh, F. C. Tuning Bilayer Twist Using Chiral Counterions. *Nature* **1999**, *399* (6736), 566–569. https://doi.org/10.1038/21154.
29. Oda, R.; Huc, I.; Homo, J.-C.; Heinrich, B.; Schmutz, M.; Candau, S. Elongated Aggregates Formed by Cationic Gemini Surfactants. *Langmuir* **1999**, *15* (7), 2384–2390. https://doi.org/10.1021/la9814889
30. Oda, R.; Artzner, F.; Laguerre, M.; Huc, I. Molecular Structure of Self-Assembled Chiral Nanoribbons and Nanotubules Revealed in the Hydrated State. *Journal of the American Chemical Society* **2008**, *130* (44), 14705–14712.

https://doi.org/10.1021/ja8048964.
31. Oda, R.; Pouget, E.; Buffeteau, T.; Nlate, S.; Ihara, H.; Okazaki, Y.; Ryu, N. A Tale of Chirality Transfer, Multistep Chirality Transfer from Molecules to Molecular Assemblies, Organic to Inorganic Materials, Then to Functional Materials. In *Molecular Technology*; Yamamoto, H., Kato, T., Eds.; Wiley-VCH Verlag GmbH & Co. KGaA: Weinheim, Germany, 2019; pp 107–136. https://doi.org/10.1002/9783527823987.vol3_c6
32. Oda, R.; Pouget, E.; Buffeteau, T.; Nlate, S.; Ihara, H.; Okazaki, Y.; Ryu, N. A Tale of Chirality Transfer, Multistep Chirality Transfer from Molecules to Molecular Assemblies, Organic to Inorganic Materials, Then to Functional Materials. In *Molecular Technology*; Yamamoto, H., Kato, T., Eds.; Wiley-VCH Verlag GmbH & Co. KGaA: Weinheim, Germany, 2019; pp 107–136. https://doi.org/10.1002/9783527823987.vol3_c6
33. Moon, R. J.; Martini, A.; Nairn, J.; Simonsen, J.; Youngblood, J. Cellulose Nanomaterials Review: Structure, Properties and Nanocomposites. *Chemical Society Reviews* **2011**, *40* (7), 3941. https://doi.org/10.1039/c0cs00108b.
34. Park, J. P.; Lee, J.-J.; Kim, S.-W. Highly Luminescent InP/GaP/ZnS QDs Emitting in the Entire Color Range via a Heating up Process. *Scientific Reports* **2016**, *6* (1). https://doi.org/10.1038/srep30094.
35. Bawendi, M. G.; Steigerwald, M. L.; Brus, L. E. The Quantum Mechanics of Larger Semiconductor Clusters ("Quantum Dots"). *Annual Review of Physical Chemistry* **1990**, *41* (1), 477–496. https://doi.org/10.1146/annurev.pc.41.100190.002401.
36. Chaudhary, S.; Ozkan, M.; Chan, W. C. W. Trilayer Hybrid Polymer-Quantum Dot Light-Emitting Diodes. *Applied Physics Letters* **2004**, *84* (15), 2925–2927. https://doi.org/10.1063/1.1699476V
37. Li, X.; Rui, M.; Song, J.; Shen, Z.; Zeng, H. Carbon and Graphene Quantum Dots for Optoelectronic and Energy Devices: A Review. *Advanced Functional Materials* **2015**, *25* (31), 4929–4947. https://doi.org/10.1002/adfm.201501250.
38. Huang, H.; Susha, A. S.; Kershaw, S. V.; Hung, T. F.; Rogach, A. L. Control of Emission Color of High Quantum Yield $CH_3NH_3PbBr_3$ Perovskite Quantum Dots by Precipitation Temperature. *Advanced Science* **2015**, *2* (9), 1500194. https://doi.org/10.1002/advs.20150019.
39. Shen, S.; Wang, Q. Rational Tuning the Optical Properties of Metal Sulfide Nanocrystals and Their Applications. *Chemistry of Materials* **2013**, *25* (8), 1166–1178. https://doi.org/10.1021/cm302482d.
40. Xie, R.; Rutherford, M.; Peng, X. Formation of High-Quality I−III−VI Semiconductor Nanocrystals by Tuning Relative Reactivity of Cationic Precursors. *Journal of the American Chemical Society* **2009**, *131* (15), 5691–5697. https://doi.org/10.1021/ja9005767.
41. Uematsu, T.; Doko, A.; Torimoto, T.; Oohora, K.; Hayashi, T.; Kuwabata, S. Photoinduced Electron Transfer of ZnS–AgInS 2 Solid-Solution Semiconductor Nanoparticles: Emission Quenching and Photocatalytic Reactions Controlled by Electrostatic Forces. The Journal of Physical Chemistry C 2013, 117 (30), 15667–15676. https://doi.org/10.1021/jp403898z.
42. Chen, F.; Lin, Q.; Wang, H.; Wang, L.; Zhang, F.; Du, Z.; Shen, H.; Li, L. S. Enhanced Performance of Quantum Dot-Based Light-Emitting Diodes with Gold Nanoparticle-

Doped Hole Injection Layer. Nanoscale Research Letters 2016, 11 (1). https://doi.org/10.1186/s11671-016-1573-8.
43. Koo, B.; Patel, R. N.; Korgel, B. A. Wurtzite−Chalcopyrite Polytypism in CuInS 2 Nanodisks. Chemistry of Materials 2009, 21 (9), 1962–1966.
44. Kruszynska, M.; Borchert, H.; Parisi, J.; Kolny-Olesiak, J. Synthesis and Shape Control of CuInS 2 Nanoparticles. Journal of the American Chemical Society 2010, 132 (45), 15976–15986. https://doi.org/10.1021/ja103828f.
45. Mao, B.; Chuang, C.-H.; Wang, J.; Burda, C. Synthesis and Photophysical Properties of Ternary I–III-VI AgInS 2 Nanocrystals: Intrinsic versus Surface States. The Journal of Physical Chemistry C 2011, 115 (18), 8945–8954. https://doi.org/10.1021/jp2011183.
46. Santangelo, S. A.; Hinds, E. A.; Vlaskin, V. A.; Archer, P. I.; Gamelin, D. R. Bimodal Bond-Length Distributions in Cobalt-Doped CdSe, ZnSe, and Cd 1 - x Zn x Se Quantum Dots. Journal of the American Chemical Society 2007, 129 (13), 3973–3978. https://doi.org/10.1021/ja068260p.
47. Hu, L.; Peng, Q.; Li, Y. Selective Synthesis of Co $_3$ O $_4$ Nanocrystal with Different Shape and Crystal Plane Effect on Catalytic Property for Methane Combustion. *Journal of the American Chemical Society* **2008**, *130* (48), 16136–16137. https://doi.org/10.1021/ja806400e.
48. Peng, Y.; Brynda, M.; Ellis, B. D.; Fettinger, J. C.; Rivard, E.; Power, P. P. Addition of H2 to Distannynes under Ambient Conditions. *Chemical Communications* **2008**, No. 45, 6042. https://doi.org/10.1039/b813442a.
49. Subramaniam, P.; Lee, S. J.; Shah, S.; Patel, S.; Starovoytov, V.; Lee, K.-B. Generation of a Library of Non-Toxic Quantum Dots for Cellular Imaging and SiRNA Delivery. *Advanced Materials* **2012**, *24* (29), 4014–4019. https://doi.org/10.1002/adma.201201019.
50. Kameyama, T.; Ishigami, Y.; Yukawa, H.; Shimada, T.; Baba, Y.; Ishikawa, T.; Kuwabata, S.; Torimoto, T. Crystal Phase-Controlled Synthesis of Rod-Shaped AgInTe $_2$ Nanocrystals for in Vivo Imaging in the near-Infrared Wavelength Region. *Nanoscale* **2016**, *8* (10), 5435–5440. https://doi.org/10.1039/C5NR07532G.
51. Kurokawa, M.; Tanaka, K.; Moriya, K.; Uchiki, H. Fabrication of Three-Dimensional-Structure Solar Cell with Cu$ {2}$ZnSnS$_{4}$. *Japanese Journal of Applied Physics* **2012**, *51*, 10NC33. https://doi.org/10.1143/JJAP.51.10NC33.
52. Loudon, J. C.; Mathur, N. D.; Midgley, P. A. Charge-Ordered Ferromagnetic Phase in La0.5Ca0.5MnO3. *Nature* **2002**, *420* (6917), 797–800. https://doi.org/10.1038/nature01299.
53. Chen, D.; Chen, X. Luminescent Perovskite Quantum Dots: Synthesis, Microstructures, Optical Properties and Applications. *Journal of Materials Chemistry C* **2019**, *7* (6), 1413–1446. https://doi.org/10.1039/C8TC05545A.
54. Li, L.; Coates, N.; Moses, D. Solution-Processed Inorganic Solar Cell Based on in Situ Synthesis and Film Deposition of CuInS $_2$ Nanocrystals. *Journal of the American Chemical Society* **2010**, *132* (1), 22–23. https://doi.org/10.1021/ja908371f.
55. Dabbousi, B. O.; Rodriguez-Viejo, J.; Mikulec, F. V.; Heine, J. R.; Mattoussi, H.; Ober, R.; Jensen, K. F.; Bawendi, M. G. (CdSe)ZnS Core−Shell Quantum Dots: Synthesis and Characterization of a Size Series of Highly Luminescent Nanocrystallites. The Journal of Physical Chemistry B 1997, 101 (46), 9463–9475. https://doi.org/10.1021/jp971091y.

56. Castro, S. L.; Bailey, S. G.; Raffaelle, R. P.; Banger, K. K.; Hepp, A. F. Synthesis and Characterization of Colloidal CuInS $_2$ Nanoparticles from a Molecular Single-Source Precursor. *The Journal of Physical Chemistry B* **2004**, *108* (33), 12429–12435. https://doi.org/10.1021/jp049107p.
57. Zhong, H.; Zhou, Y.; Ye, M.; He, Y.; Ye, J.; He, C.; Yang, C.; Li, Y. Controlled Synthesis and Optical Properties of Colloidal Ternary Chalcogenide CuInS2 Nanocrystals. Chemistry of Materials 2008, 20 (20), 6434–6443. https://doi.org/10.1021/cm8006827.
58. Chen, Y.; Li, S.; Huang, L.; Pan, D. Green and Facile Synthesis of Water-Soluble Cu–In–S/ZnS Core/Shell Quantum Dots. Inorganic Chemistry 2013, 52 (14), 7819–7821. https://doi.org/10.1021/ic400083w.
59. Rao, M. J.; Shibata, T.; Chattopadhyay, S.; Nag, A. Origin of Photoluminescence and XAFS Study of (ZnS)1– x (AgInS 2) x Nanocrystals. The Journal of Physical Chemistry Letters 2014, 5 (1), 167–173. https://doi.org/10.1021/jz402443y.
60. Tohgha, U.; Deol, K. K.; Porter, A. G.; Bartko, S. G.; Choi, J. K.; Leonard, B. M.; Varga, K.; Kubelka, J.; Muller, G.; Balaz, M. Ligand Induced Circular Dichroism and Circularly Polarized Luminescence in CdSe Quantum Dots. *ACS Nano* **2013**, *7* (12), 11094–11102. https://doi.org/10.1021/nn404832f
61. Puri, M.; Ferry, V. E. Circular Dichroism of CdSe Nanocrystals Bound by Chiral Carboxylic Acids. *ACS Nano* **2017**, *11* (12), 12240–12246. https://doi.org/10.1021/acsnano.7b05690.
62. Choi, J. K.; Haynie, B. E.; Tohgha, U.; Pap, L.; Elliott, K. W.; Leonard, B. M.; Dzyuba, S. V.; Varga, K.; Kubelka, J.; Balaz, M. Chirality Inversion of CdSe and CdS Quantum Dots without Changing the Stereochemistry of the Capping Ligand. *ACS Nano* **2016**, *10* (3), 3809–3815. https://doi.org/10.1021/acsnano.6b00567.
63. Varga, K.; Tannir, S.; Haynie, B. E.; Leonard, B. M.; Dzyuba, S. V.; Kubelka, J.; Balaz, M. CdSe Quantum Dots Functionalized with Chiral, Thiol-Free Carboxylic Acids: Unraveling Structural Requirements for Ligand-Induced Chirality. *ACS Nano* **2017**, *11* (10), 9846–9853. https://doi.org/10.1021/acsnano.7b03555.
64. Suzuki, N.; Wang, Y.; Elvati, P.; Qu, Z.-B.; Kim, K.; Jiang, S.; Baumeister, E.; Lee, J.; Yeom, B.; Bahng, J. H.; et al. Chiral Graphene Quantum Dots. *ACS Nano* **2016**, *10* (2), 1744–1755. https://doi.org/10.1021/acsnano.5b06369.
65. Nishida, N.; Yao, H.; Kimura, K. Chiral Functionalization of Optically Inactive Monolayer-Protected Silver Nanoclusters by Chiral Ligand-Exchange Reactions. *Langmuir* **2008**, *24* (6), 2759–2766. https://doi.org/10.1021/la703351p.
66. Saito, K.; Tatsuma, T. Chiral Plasmonic Nanostructures Fabricated by Circularly Polarized Light. *Nano Letters* **2018**, *18* (5), 3209–3212. https://doi.org/10.1021/acs.nanolett.8b00929.
67. Kazuma, E.; Tatsuma, T. In Situ Nanoimaging of Photoinduced Charge Separation at the Plasmonic Au Nanoparticle-TiO $_2$ Interface. *Advanced Materials Interfaces* **2014**, *1* (3), 1400066. https://doi.org/10.1002/admi.201400066.
68. Mukhina, M. V.; Korsakov, I. V.; Maslov, V. G.; Purcell-Milton, F.; Govan, J.; Baranov, A. V.; Fedorov, A. V.; Gun'ko, Y. K. Molecular Recognition of Biomolecules by Chiral CdSe Quantum Dots. *Scientific Reports* **2016**, *6* (1). https://doi.org/10.1038/srep24177.
69. Naito, M.; Iwahori, K.; Miura, A.; Yamane, M.; Yamashita, I. Circularly Polarized

Luminescent CdS Quantum Dots Prepared in a Protein Nanocage. *Angewandte Chemie International Edition* **2010**, *49* (39), 7006–7009.https://doi.org/10.1002/anie.201002552.
70. Lieberman, I.; Shemer, G.; Fried, T.; Kosower, E. M.; Markovich, G. Plasmon-Resonance-Enhanced Absorption and Circular Dichroism. *Angewandte Chemie International Edition* **2008**, *47* (26), 4855–4857. https://doi.org/10.1002/anie.200800231.
71. Maoz, B. M.; van der Weegen, R.; Fan, Z.; Govorov, A. O.; Ellestad, G.; Berova, N.; Meijer, E. W.; Markovich, G. Plasmonic Chiroptical Response of Silver Nanoparticles Interacting with Chiral Supramolecular Assemblies. *Journal of the American Chemical Society* **2012**, *134* (42), 17807–17813. https://doi.org/10.1021/ja309016k.
72. Shemer, G.; Krichevski, O.; Markovich, G.; Molotsky, T.; Lubitz, I.; Kotlyar, A. B. Chirality of Silver Nanoparticles Synthesized on DNA. *Journal of the American Chemical Society* **2006**, *128* (34), 11006–11007. https://doi.org/10.1021/ja063702i.
73. Mark, A. G.; Gibbs, J. G.; Lee, T.-C.; Fischer, P. Hybrid Nanocolloids with Programmed Three-Dimensional Shape and Material Composition. *Nature Materials* **2013**, *12*, 802.
74. Cheng, J.; Le Saux, G.; Gao, J.; Buffeteau, T.; Battie, Y.; Barois, P.; Ponsinet, V.; Delville, M.-H.; Ersen, O.; Pouget, E.; et al. GoldHelix: Gold Nanoparticles Forming 3D Helical Superstructures with Controlled Morphology and Strong Chiroptical Property. *ACS Nano* **2017**, *11* (4), 3806–3818. https://doi.org/10.1021/acsnano.6b08723.
75. Tamoto, R.; Lecomte, S.; Si, S.; Moldovan, S.; Ersen, O.; Delville, M.-H.; Oda, R. Gold Nanoparticle Deposition on Silica Nanohelices: A New Controllable 3D Substrate in Aqueous Suspension for Optical Sensing. *The Journal of Physical Chemistry C* **2012**, *116* (43), 23143–23152. https://doi.org/10.1021/jp307784m.
76. Huo, S.; Duan, P.; Jiao, T.; Peng, Q.; Liu, M. Self-Assembled Luminescent Quantum Dots To Generate Full-Color and White Circularly Polarized Light. *Angewandte Chemie International Edition* **2017**, *56* (40), 12174–12178. https://doi.org/10.1002/anie.201706308.
77. Kajitani, T.; Okoshi, K.; Sakurai, S.; Kumaki, J.; Yashima, E. Helix-Sense Controlled Polymerization of a Single Phenyl Isocyanide Enantiomer Leading to Diastereomeric Helical Polyisocyanides with Opposite Helix-Sense and Cholesteric Liquid Crystals with Opposite Twist-Sense. *Journal of the American Chemical Society* **2006**, *128* (3), 708–709. https://doi.org/10.1021/ja0576536.
78. Iftime, G.; Labarthet, F. L.; Natansohn, A.; Rochon, P. Control of Chirality of an Azobenzene Liquid Crystalline Polymer with Circularly Polarized Light. *Journal of the American Chemical Society* **2000**, *122* (51), 12646–12650. https://doi.org/10.1021/ja001244m.
79. Nikolova, L.; Nedelchev, L.; Todorov, T.; Petrova, Tz.; Tomova, N.; Dragostinova, V.; Ramanujam, P. S.; Hvilsted, S. Self-Induced Light Polarization Rotation in Azobenzene-Containing Polymers. *Applied Physics Letters* **2000**, *77* (5), 657–659. https://doi.org/10.1063/1.127076.
80. Jintoku, H.; Okazaki, Y.; Ono, S.; Takafuji, M.; Ihara, H. Incorporation and Template Polymerization of Styrene in Single-Walled Bilayer Membrane Nanotubes. *Chemistry Letters* **2011**, *40* (6), 561–563. https://doi.org/10.1246/cl.2011.561.
81. Jintoku, H.; Sagawa, T.; Miyamoto, K.; Takafuji, M.; Ihara, H. Highly Efficient and Switchable Electron-Transfer System Realised by Peptide-Assisted J-Type Assembly of

Porphyrin. *Chemical Communications* **2010**, *46* (38), 7208. https://doi.org/10.1039/c0cc01190h.
82. Takafuji, M.; Kira, Y.; Tsuji, H.; Sawada, S.; Hachisako, H.; Ihara, H. Optically Active Polymer Film Tuned by a Chirally Self-Assembled Molecular Organogel. *Tetrahedron* **2007**, *63* (31), 7489–7494. https://doi.org/10.1016/j.tet.2007.02.036.
83. Jintoku, H.; Okazaki, Y.; Ono, S.; Takafuji, M.; Ihara, H. Incorporation and Template Polymerization of Styrene in Single-Walled Bilayer Membrane Nanotubes. *Chemistry Letters* **2011**, *40* (6), 561–563. https://doi.org/10.1246/cl.2011.561.
84. Yoshida, K.; Kuwahara, Y.; Miyamoto, K.; Nakashima, S.; Jintoku, H.; Takafuji, M.; Ihara, H. A Room-Temperature Phosphorescent Polymer Film Containing a Molecular Web Based on One-Dimensional Chiral Stacking of a Simple Luminophore. *Chemical Communications* **2017**, *53* (36), 5044–5047. https://doi.org/10.1039/C7CC00395A.
85. Okazaki, Y.; Goto, T.; Sakaguchi, R.; Kuwahara, Y.; Takafuji, M.; Oda, R.; Ihara, H. Facile and Versatile Approach for Generating Circularly Polarized Luminescence by Non-Chiral, Low-Molecular Dye-on-Nanotemplate Composite System. *Chemistry Letters* **2016**, *45* (4), 448–450. https://doi.org/10.1246/cl.160047.
86. (2) Jintoku, H.; Dateki, M.; Takafuji, M.; Ihara, H. Supramolecular Gel-Functionalized Polymer Films with Tunable Optical Activity. *Journal of Materials Chemistry C* **2015**, *3* (7), 1480–1483. https://doi.org/10.1039/C4TC02948H.
87. Jintoku, H.; Dateki, M.; Takafuji, M.; Ihara, H. Supramolecular Gel-Functionalized Polymer Films with Tunable Optical Activity. *Journal of Materials Chemistry C* **2015**, *3* (7), 1480–1483. https://doi.org/10.1039/C4TC02948H.

Chapter 2: Characterization techniques and synthesis of chiral template

Chapter 2: Characterization techniques and synthesis of chiral *template*

Table of contents

2. Introduction

In the Chapter 1, we reviewed the construction of various chiral supramolecular system. Here, we will discuss different characterization techniques in order to study their structures, chemical components and chiroptical properties at different stages of synthesis and fabrication of nanomaterials. In the second part, the synthesis of the amphiphilic molecule, gemini tartrate (16-2-16), is presented, the self-assembly of which is used as a template to create chiral optically active nanostructures. We will then discuss the synthesis of the inorganic fluorophore, quantum dots ($(ZnS)_{1-x}(AgInS_2)_x$) which will be grafted on the surface of silica helix, as well as and the organic naphthalene and anthracene derivatives forming cross-link polymer on the surface of silica helix.

The proton (1H) NMR is used to characterize the gemini tartrate amphiphiles in each stage of syntheses. These gemini tartrate molecules self-assemble to form organic twisted nanoribbons, nanohelices, and nanotubes depending on various parameters, respectively; And, finally transcripted to silica twisted ribbons, helices, and nanotubes. To characterize the morphology of organic and inorganic helical nanostructures, Transmission Electron Microscopy (TEM, HR-TEM, STEM) is performed. TEM was also used to observe QDs or polymer grafting on the silica nanohelices. To quantify the amount of QDs grafted on the silica nanohelices X-ray spectroscopy with energy dispersion (EDX) was used. Also, thermogravimetric analysis (TGA) and elementary analysis were performed to quantify ligand on the surface of QDs as well as a polymer on silica helix. Confocal microscopy is used to observe fluorescent fiber-like structure in both the case of fluorophores on silica nanohelices to show the after organizing fluorophores helical silica is fluorescent. UV-Vis absorption and emission spectroscopies, electronic circular dichroism (CD) and circularly polarized luminescence (CPL) were used to characterize the optical and chiroptical properties of the nanostructures.

2.1 Microscopic techniques:

In order to determine the structural morphology of organic and inorganic silica helices TEM performed. Later to quantify and prove the grafting of quantum dots on silica helices

HRTEM, STEM and EDX spectroscopy are used, therefore to understand more in detail, the microscopic techniques are explained below.

2.1.1 Transmission Electron Microscope (TEM):

With an electron microscope (EM), the beam of electrons is used to produce images of the samples from micrometer to nanometer range. The information about the specimen or sample can be gathered as follows: Topography, Morphology, Composition, and Crystallographic information. [1, 2]

Transmission Electron Microscopy (TEM) is a technique where an electron beam interacts and passes through a specimen. The source of electrons is a V-shaped filament which is made of lanthanum hexaboride (LaB_6) or tungsten (W). The filament is covered with wehnelt electrode (wehnelt cap). The beam of electrons is focused, magnified by a system of magnetic lenses. The two condenser lenses control the brightness of the beam; it passes through the condenser aperture and hits the surface of the TEM grid containing the sample.

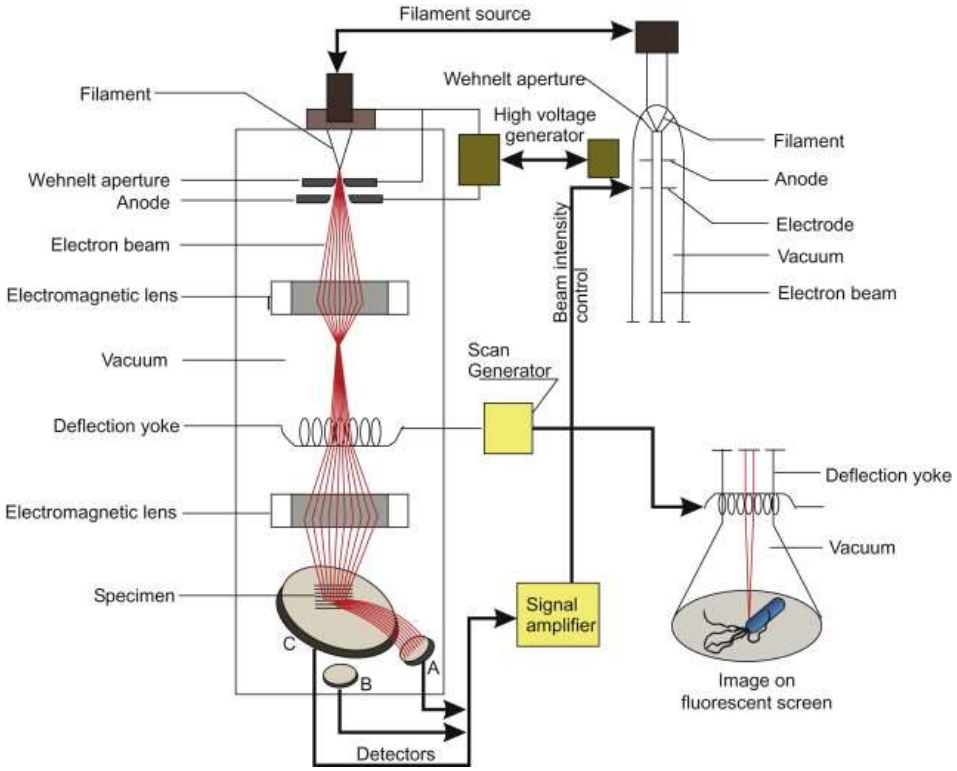

Figure 2.1.1.1: Transmission electron microscope with all of its components. [2]

The transmitted beams of electrons are elastically scattered, travel through an objective lens. The image display constructed by an objective lens. The objective aperture selects the area for elastically scattered electrons to construct the final image. The beam travels through three

lenses which magnify and controlled the magnification of the image as well as projector lens. The final image is shown on the fluorescent screen as well as on the monitor of the computer and collected on the printed version or soft copy. [1]

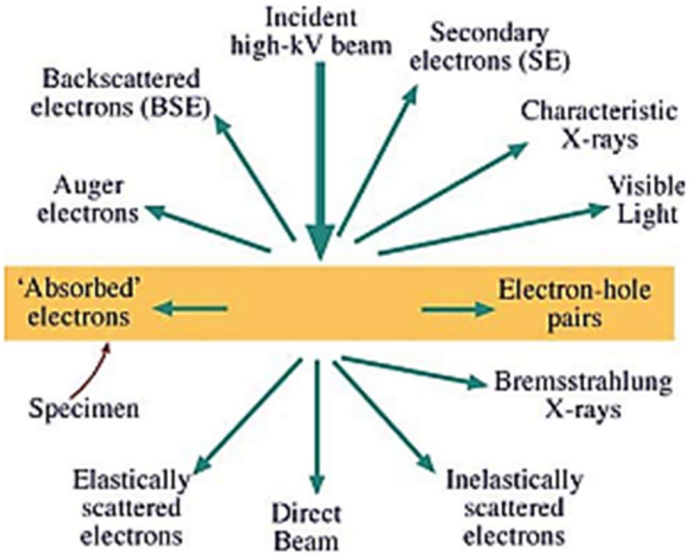

Figure 2.1.2: Signals generated when a high-energy beam of electrons interacts with a thin specimen. Most of these signals can be detected in different types of TEM. The directions shown for each signal do not always represent the physical direction of the signal, but indicate, in a relative manner, where the signal is strongest or where it is detected. [3]

Various types of images can be taken from TEM. In general, when the incident high electron beam interacts with the specimen generates a different type of electron combination. Electrons are one type of ionizing radiation. These radiations have the potential to remove the tightly bound, inner-shell electrons from atoms and molecules on the surface of the active specimen. The advantage of ionizing radiation is its ability to generate secondary signals from the specimen, as shown in figure 2.1.1.2. [2, 3] The inelastic and elastic scattered electrons will create bright field images and dark field images, respectively due to diffraction patterns. In addition, Energy Dispersive X-ray (EDX), Electron Energy Loss Spectrum (EELS), Energy Filtered Transmission Electron Microscopy (EFTEM), etc., can be performed under TEM.

2.1.2 High-resolution transmission electron microscopy (HRTEM):

High-resolution TEM provides accurate information about measurements and chemical components present in the samples of the different types at the atomic scale. In

HRTEM, due to high resolving power, it permits to perform imaging of the crystallographic structures of the given sample. The highest resolution obtained in HRTEM is 0.05 nm. [4]

HRTEM offers surface studies and computerized data acquisition for quantitative image analysis. HRTEM operated in two modes (A) Image mode and (B) Diffraction mode.

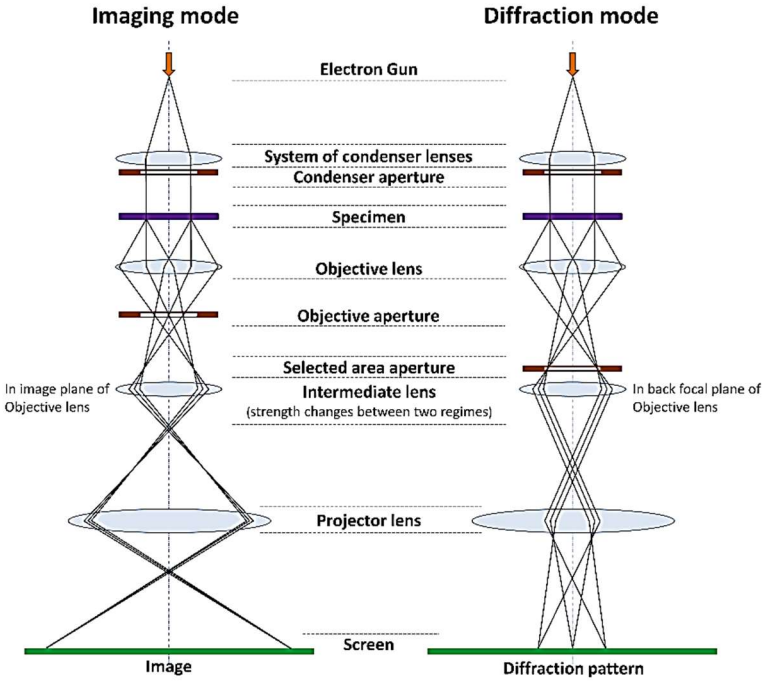

Figure 2.1.1.2: Two basic operations modes (a) Image mode, and (b) Diffraction mode. [5]

The diffraction mode has an advantage to detect even the weakest diffracted spot, which is not possible to detect in powder XRD due to much higher atomic scattering factor of electrons. Due to this, the HRTEM in diffraction mode has become a powerful tool to investigate the crystal symmetry and space groups. [4]

2.1.3 Scanning transmission electron microscopy (STEM):

Scanning transmission electron microscopy (STEM) is a versatile tool to characterize metals and alloys. By changing the imaging conditions such as camera length, probe size, and foil tilt, the image contrast can be readily adjusted based on several guiding principles.

In addition, STEM can be used to image nanoclusters (NCs) and precipitates, while simultaneously analysing micro-chemical changes under the same imaging conditions. In STEM mode, as in the case of a transmission electron microscope (TEM), images are formed by electrons passing through a sample sufficiently fine. Unlike TEM, in STEM mode, the beam

of electrons is focused into a thin spot which is then scanned onto the surface of the sample in using a system of magnetic lenses (scan coils) and generates the image point by point (Figure 2.1.3.1).

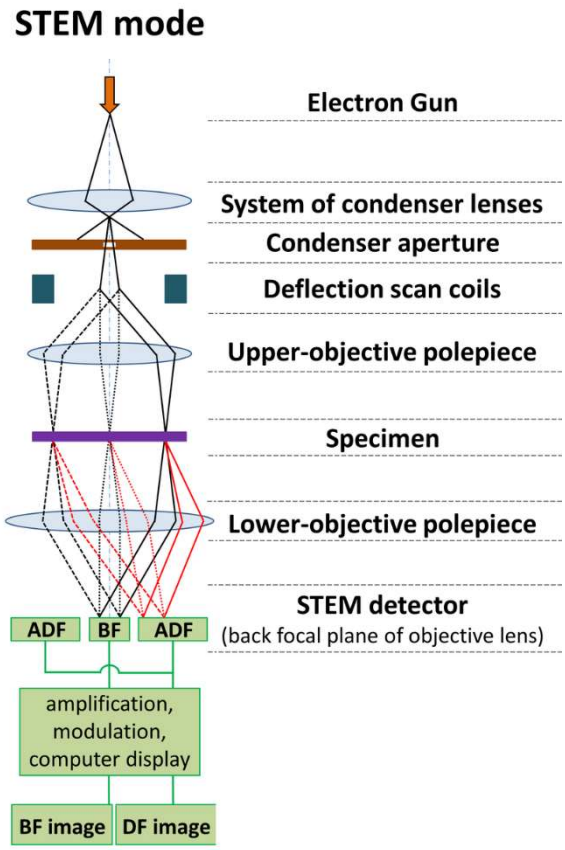

Figure 2.1.3.1: Scheme of STEM mode. [5]

The resolution in image and analysis is directly related to the diameter of the electronic probe. Observations can be made in bright field or in dark field. In the annular dark field, the images are formed by previously scattered electrons that fall on a detector located outside the path of the transmitted beam. Using an ADF detector (Annular Dark-field imaging) at wide angle, it is possible to form atomic resolution images where the contrast of a column atomic is directly related to the atomic number (Z contrast image). [6]

2.1.4 Energy dispersive X-ray spectrometry (EDX):

Energy dispersive X-ray spectrometry (EDX) consists in studying the X-rays emitted by a sample when it is bombarded by an electron beam. [7] The electron beam passing through the sample causes ionization of the atoms, which then emit X-rays during their de-excitation. The energy of Emitted radiation can be used to determine the elemental chemical

composition of the sample. EDX analysis is a multi-element chemical analysis technique. The detector most commonly used in EDX spectrometers is a photodiode of Si doped with lithium, which converts the energy of incident photons into electric voltage. This process is mainly done in three steps: the X-rays are converted into electric charges by ionization of the atoms of the crystal of the semiconductor. Then these Loads are converted into voltage and amplified through a FET (Field Effect Transistor). Finally, this voltage is isolated from the others inside specific channels that allow the counting and obtaining a dispersive spectrum in energy. It is this spectrum that allows to qualitative and quantitative analysis by comparing with the recorded standards.

An EDX spectrum usually consists of a family of peaks (lines) superimposed on a continuous background of relatively low intensity. The characteristic rays, accompanying electronic transitions between the atomic layers (K, LI, LII, LIII, etc.), appear in series. In each series, the lines are distinguished by an index (Kα, Kβ ...) indicating the level origin of the transition (Figure 2.1.4.1).

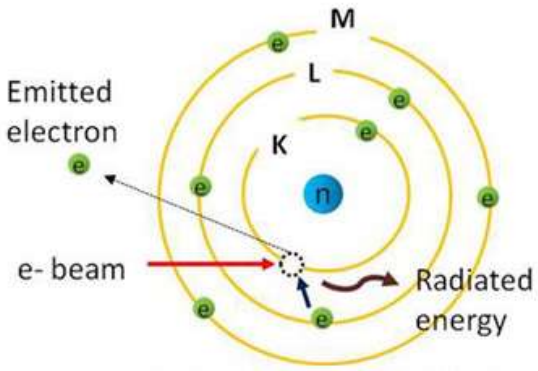

Figure 2.1.4.1: Scheme of EDS Principle. [9]

In EDX, it is possible to detect all elements from beryllium (Z = 4). However, the analysis of light elements is often complicated, because the intensity of the lines characteristics depends on the atomic number Z. Basic X-ray mapping is done by scanning an electronic probe on a selected region and at each breakpoint (several seconds), the entire X spectrum is checked in. Signals recorded in this way are represented in shot distribution cards collected for each position of the electronic probe. The signal strength is indicated by color levels for each element.

2.2 Chiroptical Measurement techniques:

To study the chiroptical properties of fluorescent silica helices, fabricated by grafting quantum dots and polymer coating on surface of silica helices, respectively circular dichroism (CD) and circularly polarized luminescence (CPL) were utilized, we estimate the induction of chirality at ground and excited states of fluorescent silica nanohelices in both the cases. Therefore, the brief descriptions with detailed terminology explanation is mentioned below, to understand these techniques

2.2.1 Circular Dichroism (CD):

Dichroism means the property possessed by some molecule or material to absorb light at different extents depending on the polarization of incident light. The absorption of left-handed circularly polarised light (L-CPlight) is different from the absorption of right-handed circularly polarised light (R-CP light) in the UV-visible region. Then, the difference of absorption of (L-CPlight) and (R-CPlight) is called as circular dichroism.

It is only observable for the chiral molecules which have chromophore moeties. [9] Basically, this spectroscopy obeys the same set of rules as UV-visible absorption spectroscopy with an extensive study of chiral molecules of all types and size. [10]

$$CD = \Delta A(\lambda) = A(\lambda)_{LCPL} - A(\lambda)_{RCPL}, \qquad ..(2.2.1.1)$$

Where A- absorption, and λ is the wavelength.

Circular dichroism is extensively used to analyse the secondary structures or conformation of macromolecules and biological molecules such as proteins and peptides, DNA/RNA or sugars.

In addition, by using circular dichroism, the structural, kinetic, and thermodynamic information about macromolecules can be obtained. Since the chiral molecules exist as enantiomers with the pair of non-super-imposable mirror-image isomer. Therefore, the enantiomers has the differential absorption of opposite sign at the same wavelength. And the bands observed in CD spectrum are commonly called as Cotton effect.

(i)

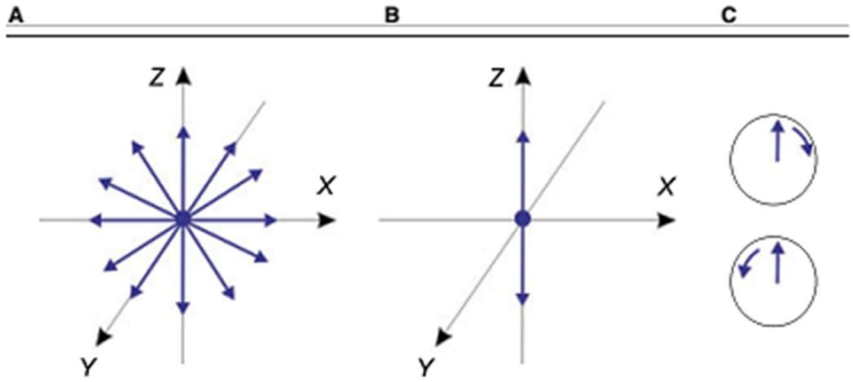

(ii)

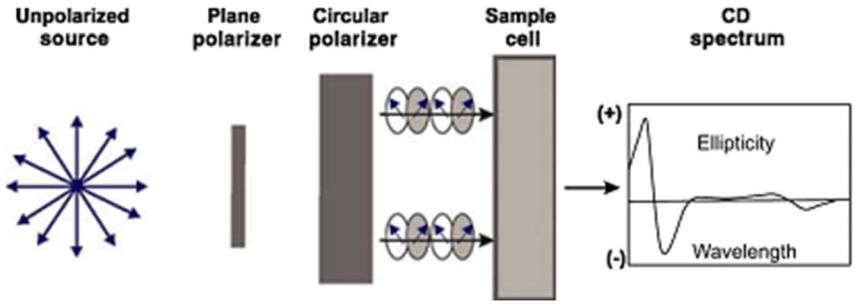

Figure 3.1.1: (i) Schemes of the electric field components of unpolarized (A), linearly or plane polarized light (B). The light is moving along the y-axis. For unpolarized light, all directions occur, whereas for linearly or plane polarized light only the z-direction is found. For circularly polarized light (C), the direction of rotation can be clockwise or counterclockwise, and (ii) Scheme of CD in which a difference in absorption is measured. [11]

According to the Beer-Lambert law,

$$\Delta\varepsilon = \Delta A / (C \times l) \qquad ..(2.2.1.2)$$

$$\Delta\varepsilon = \varepsilon_{LCPL} - \varepsilon_{RCPL} \qquad ..(2.2.1.3)$$

Where ε_{LCPL} and ε_{RCPL} are the molar extinction coefficients for LCP and RCP light, respectively.

C - molar concentration ($mol.L^{-1}$), and l - pathlength in centimeters (cm). The molar extinction coefficient unit is $L.mol^{-1}cm^{-1}$.

CD can be expressed in terms of degrees of ellipticity (θ), which is a legacy of polarimetry. Linearly polarised light has zero degrees of ellipticity (**θ**), while fully LCP or RCP will have ' + or – 45' degrees, respectively. The tangent of the ratio between the minor to the major elliptical axis is known as the degree of ellipticity (θ).

The relation between θ and ΔA can be written as:

$$\Delta A = \theta/32.982 \qquad ..(2.2.1.4)$$

Where θ is in millidegrees (m˚) or 1/1000 of a degree. The unit of molar ellipticity in terms of ΔA in degrees cm^2 $dmol^{-1}$, or degrees M^{-1} m^{-1}.

Therefore, molar ellipticity can be expressed as,

$$[\theta] = 100x\theta/(Cxl) \qquad ..(2.2.1.5)$$

C - the concentration in a molar, l - the cell pathlength in cm.

The factor of 100 is to converts the pathlength in meters. While the molar circular dichroism and molar ellipticity converted as:

$$\Delta\varepsilon = [\theta]/3298.2 \qquad ..(2.2.1.6)$$

Whereas,

$$\Delta\varepsilon = \varepsilon_{LCPL} - \varepsilon_{RCPL} \qquad ..(2.2.1.3)$$

$$g_{abs}(\lambda) = \Delta\varepsilon(\lambda)/\varepsilon(\lambda) \qquad .. (2.2.1.7)$$

Where ε_{LCPL} and ε_{RCPL} are the molar extinction coefficients for LCP and RCP light, respectively. In practice, circular dichroism can be measured in two different ways. (1) To generate circularly polarized waves and then to measure the absorption difference of the middle ΔA between the two states of polarization (right and left), and (2) to measure the ellipticity induced on a polarized wave rectilinearly. The first method is most commonly used on spectrophotometers. The rectilinear polarization of the incident light beam is transformed and modulated between a left circular polarization and a circular polarization right using a photoelastic modulator. [10,12]

2.2.2 Circularly Polarized Luminescence (CPL):

Circularly polarized luminescence (CPL) spectroscopy is based on the differential *spontaneous* emission of left and right circularly polarized radiations by luminescent chiral systems in excited states. The differential emission of left and right circularly polarized radiation can be observed for both atomic and molecular chiral luminescent systems in variety of conditions, and it can originate from a variety of radiative relaxation processes. [13]

CPL is associated with electronic transitions in molecular systems, considering that the molecular vibrational motions only will affect the radiative transition probabilities of electronic transitions via vibrionic coupling interactions. Electronic CPL spectroscopy is the emission analogue of electronic circular dichroism (CD) spectroscopy. [12,13]

The emission circular intensity differential (ECID),

$$\Delta I(\lambda) = I_{LCPL}(\lambda) - I_{RCPL}(\lambda) \qquad ..(2.2.2.1)$$

Where, λ – excited state wavelength of luminophore, and the emission dissymmetry factor

$$g_{em}(\lambda) = 2\Delta I(\lambda) / I(\lambda) \qquad ..(2.2.2.2)$$

$I_{LCPL}(\lambda)$ and $I_{RCPL}(\lambda)$ are the intensities of the left circularly polarized light (LCPL) and right circularly polarized light (RCPL) of the emitted radiation.

The characteristics of CPL are as follow: [13]

(1) CPL provides an information of chirality of molecular excited states related to geometry of the chiral systems whereas CD gives information at ground state of chiral system.

(2) CPL is uniquely featured for the study of emissive transitions, which do not terminate in a thermally accessible ground state. These states cannot he studied by ordinary CD/absorption experiments.

(3) In large molecular systems, it is quite common to have a number of electronically similar, but structurally distinct, chromophores. In these systems, it is generally found that emission occurs from only one of the chromophores. This selectivity is important in interpretation of spectra.

2.3 Synthesis of the chiral template: Nano helical silica

2.3.1 Synthesis of 16-2-16 Tartrate:

In this section, we present the synthesis of gemini 16-2-16 tartrate. [14] The name gemini, coined in 1991 by Fred Menger, [15] comes from the di-cationic structure of the amphiphiles and the nomination n-s-n is based on the hydrocarbon chain length, n, and the spacer length.

(1) Synthesis of 16-2-16 Br

1 molar equivalent of tetramethylethylenediamine (TMEDA) was used for 3 molar equivalents of alkyl bromide in 50mL of acetonitrile in a 250mL round-bottom flask. The reaction was carried out for 48 hours under reflux at 80-85°C with continuous stirring (400rpm). After that, the major part of acetonitrile will be evaporated with a rotary

evaporator until there is only a little amount of liquid. Then, acetone will be added, and the mixing will be stirred for 30min. The acetone is used to wash the product because the alkyl bromide and the monoalkylated by-products are soluble in this solvent. For the washing, to avoid any problem of filtration, the samples will be centrifuged, the supernatant will be removed, some acetone will be added, etc. for 3 times and dried under the vaccum 1H NMR was performed to observe the true product formation.

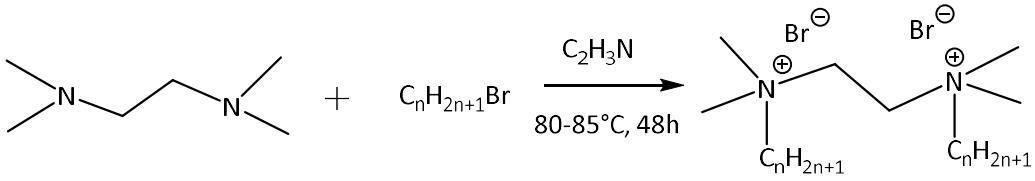

TMEDA **16-2-16Br**

NMR analysis (16-2-16Br) at 25°C, 300 MHz, in MeOD with 0.01% TMS was performed δ ppm: 4.04 (4H, s, 3.45 (4H, m), 3.3 (12H, s), 1.90 (4H, s) 1.29 (52H,m) 1.0 (6H,t, ^3J = 6.71Hz).

(2) Counter-Ion exchange from Bromide to acetate (16-2-16Ac)

Gemini bromide (2g, 1eq.) was dissolved in 50mL of methanol. The flask in covered with aluminum foil and put in a 50°C, oil bath. Then the silver acetate (1,34g 3 eq.) was added, and the reaction mixture was stirred at that temperature for 24 hours. The suspension was filtrated on Celite to remove the formed precipitate of silver bromide. The filtrated solution was put in a flask, and then the methanol was evaporated on a rotary evaporator. The product was dissolved in as small as possible amount of methanol (few drops) and after that acetone was added. For the washing, the samples will be centrifuged, the supernatant will be removed, and some acetone will be added, etc. for 3 times. Finally, the product will be dried under vacuum all night.

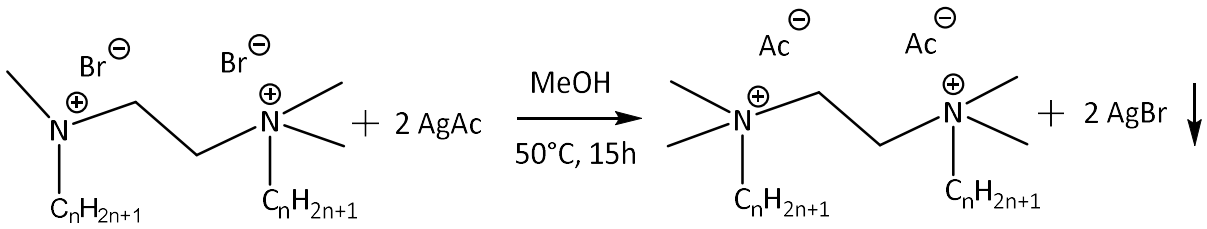

16-2-16Br **16-2-16Ac**

NMR analysis (16-2-16Ac) at 25°C, 300 MHz, in MeOD with 0.01% TMS was performed δ ppm: 4.04 (4H, s, 3.45 (4H, m), 3.3 (12H, s), 1.90(6H, s), 1.85 (4H,m) 1.29 (52H,m) 0.89 (6H,t, ^3J = 6.63Hz).

(3) Counter-Ion exchange from acetate to tartrate

1 molar equivalent of gemini acetate was used for 2 molar equivalents of tartaric acid. Both of them are dissolved separately in a mixture of MeOH/Acetone (1:9) (10ml for 100mg of gemini acetate) .The gemini acetate was added then drop wise into the tartaric acid with a drop tunnel. Then the product is transferred in a 50mL Falcon tube. For the washing, the product will be centrifuged, the supernatant will be removed, some mixture of MeOH/Acetone will be added, then centrifuged again, and supernatant will be removed. After that, some cold water (previously putted at 4°C) will be added to fill up the tube. The tube will be sonicated for 5min and then centrifuged. There will be finally 5 times washing with cold water and 2 times with acetone after that and product was dry under the vaccum. NMR was performed both 16-2-16 tartrate. The NMR result indicates that the product is ready for use for organic self-assembly.

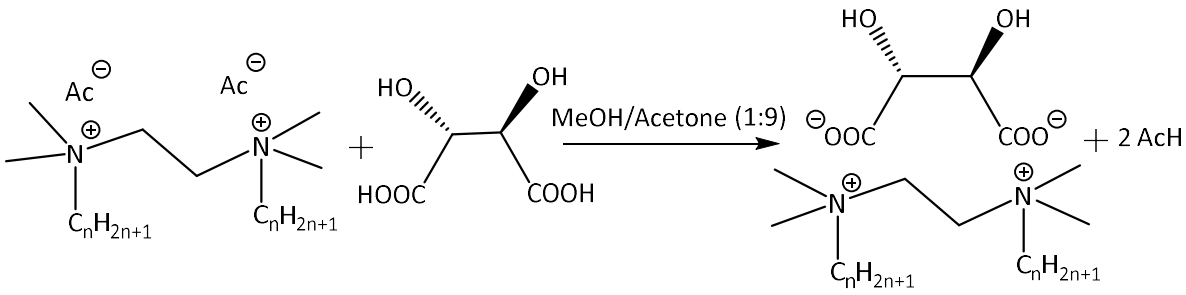

16-2-16 Ac **16-2-16 L**

NMR analysis (16-2-16L) at 25°C, 300 MHz, in MeOD with 0.01% TMS was performed δ ppm: 4.27(2H,s), 4.10 (4H, s) , 3.40 (4H, m), 3.25 (12H, s), 1.86 (6H, s), 1.85 (4H,m) 1.29 (52H,m) 0.90 (6H,t, ^3J = 6.5Hz).

2.3.2 Formation of organic gel and silica transcriptions:

In the gemini surfactant 16-2-16 tartrate, due to the presence of chiral counter-ion, the chirality can be expressed at the supramolecular level. Gemini surfactant forms a bilayer structure and results in the formation of an organic gel at 20°C, forming organic twisted ribbons, twisted helical ribbons, and nanotubes depending on the aging time of organic gel and other parameters such as concentration, enantiomer excess, pH, etc.

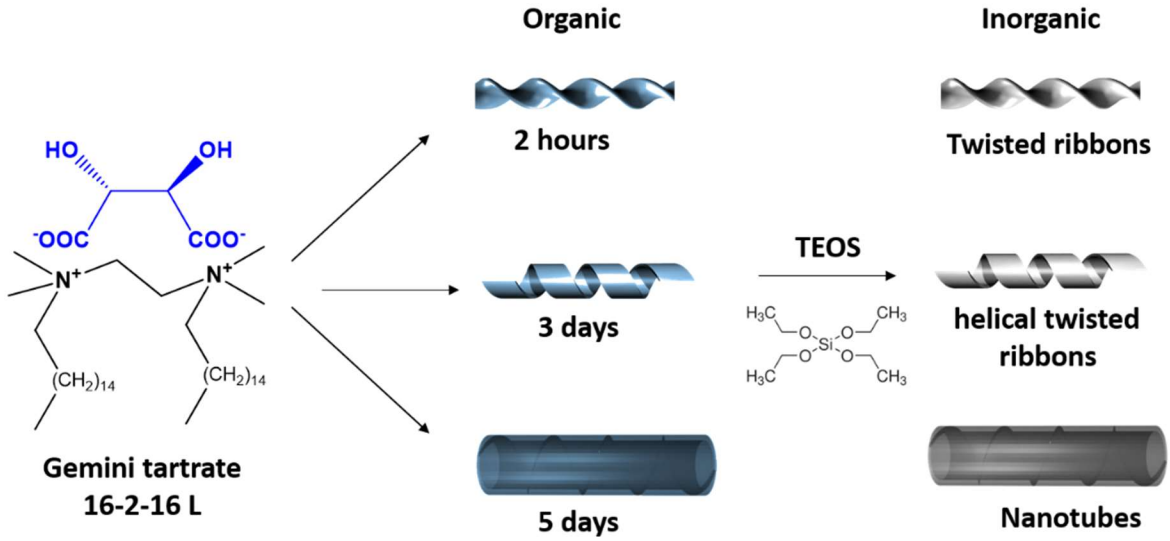

Figure 2.3.2.1: Scheme of self-assembling forming twisted ribbons, helical twisted ribbons and nanotubes for the gemini tartrate.

The formation of helical structure can be controlled by playing with parameters. Depending on the stereochemistry of counter-ion of gemini surfactant, the handedness of organic nanostructure can be countered, as left handed (L-tartrate) and right handed (D-tartrate) helical structures. For the present work, the gemini tartrate was solubilized in Milli-Q water to obtain a concentration of 1mM tartrate in the tube. Then, the solutions of gemini tartrate were heated up above the Krafft temperature (at 60°C in water bath) for few minutes, sonicated for 5min, heated up at 60°C again, naturally cooled down and putted without mixing at 20°C for different ageing time. The ageing time will have an influence on the structure. Typically, to obtain ribbons the gel was aged for 1-2 hour, 3days for helices and more than 5 days for tubes.

The organic self-assembly is dynamic, can be disrupted easily by small changes in the parameters. These self-assembles are formed due to weak interaction of inter-intramolecular hydrogen bond, van der Waals forces, and hydrophobic effect. Therefore, we need a robust

system to increase the stability of organic nano helical structures. The organic nanostructures transcribed into silica nanostructure via sol-gel chemistry. [16,17] Due to polycondensation reaction during the sol-gel process of SiO_2 from prehydrolysed TEOS, polymerized on the surface of organic nanostructures, leads to the formation of inorganic silica nanostructure, the reaction occurs in the ambient conditions.

Inorganic transcription:

Once the adequate aging time was reached, the organic gels were used as templates to prepare silica nanostructures through sol-gel transcription.

Generally, 0.5mL of tetraethoxysilane (TEOS) was added to 10mL of L or D tartaric acid aqueous solution with a concentration of 10^{-4}M. The pre-hydrolyzation was then realized by putting the solution at 20°C under stirring on a roller-mixer for 7 hours. At the end of the 7 hours (that must coincide with the end of the ageing time of the gel), equal volume of pre-hydrolyzed TEOS was added to the organic gels and mixed. Then the mixtures were stirred over night at 20°C on the roller-mixer. The washing was realized as the usual way: centrifuge, removing the supernatant, adding the corresponding solvent, sonicating to have homogeneous solution, centrifuge again, etc. The usual washing would be 2 times with ethanol to remove the excess of TEOS, 1 time (or more) with isopropanol to remove the organic template (the gemini), 2 times again with the ethanol.

We used the silica twisted nanoribbon and helical nanoribbons (nanohelices) as a template for organizing quantum dots and polymer on the surface of nano helical structures. (Figure 2.3.2.2)

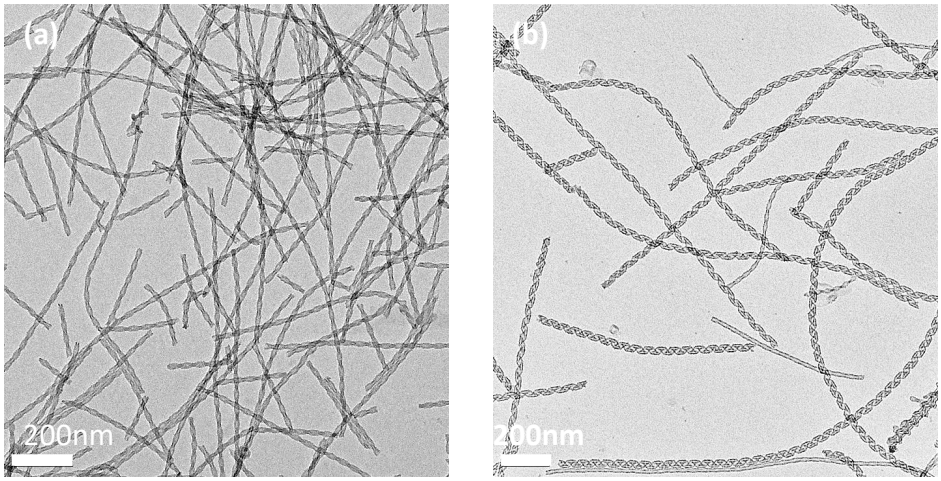

Figure 2.3.2.2: TEM image of chiral template: (a) silica twisted nanoribbon, and (b) helical nanohelices.

The nano helical silica is much longer several micrometers is in length. Therefore, by using tip sonication method, the length of silica nanohelices can be controlled in nm r and dispersity checked in various solvents.[17] Only, in the case of grafting quantum dots, the silica nanohelices length were controlled, ethanol and isopropanol were used in 1:1 ratio of volume. TEM images before and after sonication are as shown in the figure 2.3.2.3. After tip sonication, the surface of silica helices can be modified and functionalized with any molecule.

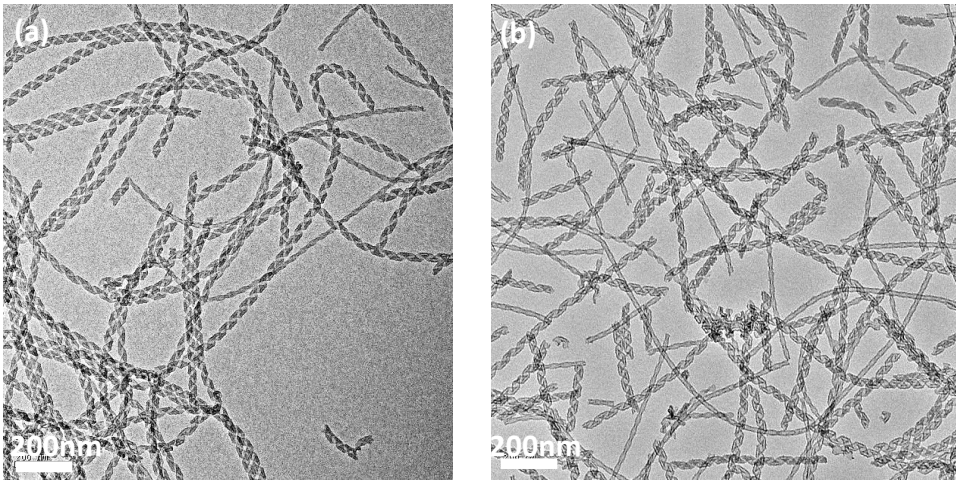

Figure 2.3.2.3: TEM image of silica nanohelices (a) before, and (b) after submitted to tip-sonication in ethanol and isopropanol solvent mixture.

2.3.3 Surface modification of silica nanohelices

The surface of silica nanohelices functionalized by 3-Aminopropyl triethoxysilane (APTES), in order to obtain the amine groups on the surface of silica. [15]

Amine functionalization will be performed with APTES and thiol functionalization with MPTES. Solutions of APTES and will be realized in ethanol with a concentration of 100mM. Generally, 50µL of APTES will be added per mL of silica helices/ribbons solutions (1mg/mL). The reaction mixture will be sonicated for 5min and then kept overnight at 80°C in oil bath. The solutions will be washed 3 times with isopropanol. The modification procedure can be repeated one time to be sure to coat all the surface with amine/thiol groups.

The amine-modified silica helices were used to graft quantum dots $(ZnS)_{1-x}(AgInS_2)_x$, which is capped by different ligands(discussed in chapter 3). The zeta potential measurement was performed to estimate the amount of amine immobilized on the surface of silica, as shown in figure 2.3.3.1. The zeta potential of amine-modified silica was positively charged between pH 5.0 – pH 8.0.

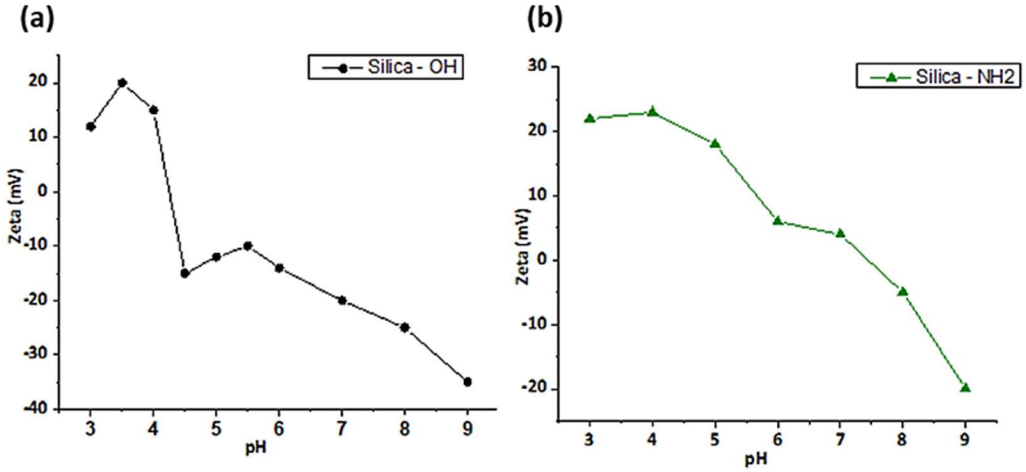

Figure 2.3.3.1: Zeta potential of (a) bare silica and (amine modified silica).

Thermogravimetric analysis (TGA) and elementary analysis (EA) were performed in order to quantify the amount of APTES grafted on the silica nanohelices. TGA was performed under N_2 condition, the weight loss in the figure indicates the amount APTES was there on the surface of silica, it was 23.79% by weight and EA confirms the % of each element present in

organic part, 2.9% H, 9.86% C and 3.52 N%, which indicates that APTES is on the surface of silica.

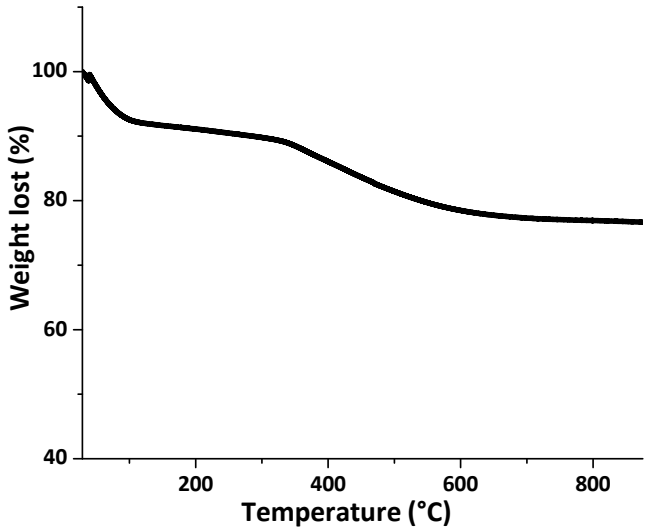

Figure 2.3.3.2: Thermogravimetric analysis of amine-modified silica nanohelices.

Conclusion:

In this chapter, we described the techniques to characterize silica nanohelices such as different modes of TEM and chiroptical techniques such as CD and CPL. In the second half of the chapter, the synthesis of gemini surfactant and the fabrication of silica nanohelices was described, which will be used in the Chapter 3 and 4 as chiral template to organized quantum dots and polymer.

Experimental Section:

Nuclear Magnetic Resonance spectroscopy (NMR): To follow up the synthesis of gemini tartrate ^{1}H NMR, 300 MHz was utilized. To analyse the spectra topspin 2.0 software was used.

Zeta potential: The surface charge of bare silica helix and polymer coated silica helix was done by using Zeta potential. The QDs was prepared in Milli-Q water with concentration 0.1 mg/ml. In 10mm cuvette of zeta potential sample were passed on with scanning of 10 scans with 3 times. The measurement was by Malvern Zeta sizer.

Absorption and emission spectroscopy: The study of quantum dots grafting and polymer coating was done by using absorption spectroscopy, this is carried out by using UV- machine UV 3600 plus. The data recorded with by setting the parameter as follows: scan speed 200nm/min with data interval of 0.5 nm at 25°C. The cuvette path length was 5mm. The emission spectra was studied by using Spectrofluorometer FP-6500. The parameters of fluorescence remains the same absorption spectroscopy, the additionally with excitation slit width and emission slit width is 3 nm for both respectively. The cuvette path length was 5mm.
Transmission electron microscopy: TEM was performed at room temperature by three different TEM machine (a) JEM -1400 plus Images taken at the voltage range between 80kV-100 kV in the form of TIFF format from camera and, (b) Philips EM 120, (c) HRTEM. The TEM grid prepared by dropping the product 6- 8 µl on copper TEM grid, let it to become dry and solvent get evaporated.

The Confocal Microscopy: The dilute solution of product was prepared with concentration 0.1mg/ml in ethanol and water. The excitation of laser done at 405 nm. The images were taken in TIFF format.

Thermogravimetric analysis (TGA): Quantum dots were dried under the vacuum. The parameters. Temperature rise 10° C/ min, inert atmosphere, instrument TG/DTA6200.

Reference:

1. Transmission Electron Microscopy; Carter, C. B., Williams, D. B., Eds.; Springer International Publishing: Cham, 2016. https://doi.org/10.1007/978-3-319-26651-0.
2. Drew R.; Van O. Environmental Forensics, *Asbestos;* Elsevier, 1964; pp 19-33. https://doi.org/10.1016/B978-012507751-4/50024-0.
3. Williams, D. B.; Carter, C. B. Transmission Electron Microscopy: A Textbook for Materials Science, 2nd ed.; Springer: New York, 2008.
4. Spence, J. C. H.; Spence, J. C. H. High-Resolution Electron Microscopy, Fourth edition.; Oxford University Press: Oxford, United Kingdom ; New York, NY, 2017
5. https://en.wikipedia.org/wiki/Scanning_transmission_electron_microscopy
6. Nellist, P. D. Scanning Transmission Electron Microscopy. In Science of Microscopy; Hawkes, P. W., Spence, J. C. H., Eds.; Springer New York: New York, NY, 2007; pp 65–132. https://doi.org/10.1007/978-0-387-49762-4_2.
7. Shindo, D.; Oikawa, T. Energy Dispersive X-Ray Spectroscopy. In Analytical Electron Microscopy for Materials Science; Shindo, D., Oikawa, T., Eds.; Springer Japan: Tokyo, 2002; pp 81–102. https://doi.org/10.1007/978-4-431-66988-3_4.
8. http://www.faantech.com/EDAX.html
9. Comprehensive Chiroptical Spectroscopy; Berova, N., Ed.; Wiley: Hoboken, NJ, 2012.
10. https://chem.libretexts.org/Bookshelves/Physical_and_Theoretical_Chemistry_Textbook_Maps/Supplemental_Modules_(Physical_and_Theoretical_Chemistry)/Spectroscopy/Electronic_Spectroscopy/Circular_Dichroism.
11. Ranjbar, B.; Gill, P. Circular Dichroism Techniques: Biomolecular and Nanostructural Analyses- A Review. Chemical Biology & Drug Design **2009**, 74 (2), 101–120. https://doi.org/10.1111/j.1747-0285.2009.00847.x.
12. Berova, N.;Polavarapu, L P.; Nakanishi, K.; Woody, W. R.; Comprehensive Chiroptical Spectroscopy: Instrumentation, Methodologies, and Theoretical Simulations, Volume 1, Wiley-VCH Verlag GmbH & Co. KGaA: Weinheim, Germany, 2011; https://doi.org/10.1002/9781118120187.
13. Riehl, P. J.;Richardson, S, F, *Chem. Rev.,* 1986, 8611-16. https://doi.org/10.1021/cr00071a001
14. Oda, R.; I. Huc, I.; Schmutz, M., Candau, J. S.; MacKintosh, C. F.; Nature **1999**, 399, 566-569.
15. Menger, M. F.; Keiper, S. J., Review, Angewandte Chemie International Edition, 2000, 39, 11, 1906-1920. https://doi.org/10.1002/1521-3773(20000602)39:11<1906::AID-ANIE1906>3.0.CO;2-Q.
16. Delclos, T.; Aimé, C.; Pouget, E.; Brizard, A.; Huc, I.; Delville, H. M; Oda, R.; Nano. Letter, 8, 1929-1935.
17. Okazaki, Y.; Cheng, J.; Dedovets, D.; Kemper, G.; Delville, H. M.; M.-C. Durrieu, C. M; Ihara, H.; Takafuji, M.; Pouget, E.; Oda, R.; ACS Nano **2014**, 8, 6863–6872.

Chapter 3: Synthesis of quantum dots, quantum dots grafted on the surface of helical silica, characterization and chiroptical properties

Chapter 3: Synthesis of quantum dots, quantum dots grafted on the surface of helical silica, characterization and chiroptical properties

Table of Contents

3. Introduction

In chapter 1, a brief description about various quantum dots has been given along with their optical properties and applications. When combined with chiral matrices, induced chiroptical properties can be observed.

In order to understand and implement the chiral induction on optical properties of quantum dots in this chapter, the fabrication of quantum dots grafted on chiral nano-helical silica has been demonstrated. The chiral nano-helical silica is used as a template to create hybrid structure. The quantum dots $(ZnS)_{1-x}(AgInS_2)_x$ has photo-tunable properties with average size 5.0 nm. Various ligands such as ammonium sulphide, 3-mercaptopropionic acid oleylamine and l-cysteine were used as capping ligand on the surface of quantum dots. As the surface of the silica nanohelices are functionalized by APTES, the nature of the interaction between nano-helical silica and quantum dots is electrostatic.

Here, we show the detailed study about $(ZnS)_{1-x}(AgInS_2)_x$ quantum dots grafting on the surface of amine modified silica helix and discuss how quantum dots grafted on the nanohelices show chiral optical properties.

3.1 Synthesis and Characterization of Quantum dots $(ZnS)_{1-x}(AgInS_2)_x$

3.1.1 Preparation of Quantum dots (QDs) with different ligands:

Oda's group has previously shown that nanoparticles can be organized on the surface of nanohelical silica and chiral properties of the nanohelices were transferred to the optical properties of these nanoparticles. [2,3] It was observed that for the effective chirality induction to nanoparticles, the size of the nanoparticle needs to be less than 10 nm. The $AgInS_2$-ZnS QDs as presented in Chapter 1 have perfect size with respect to the diameter of these silica helices. Torimoto and his co-workers have reported a synthesis of $AgInS_2$-ZnS quantum dots (QDs) with high quantum yield. [1] By changing the composition ratio of metal ions the emission wavelength can be tuned between 500 nm-750 nm. The particle size is between 1.0 nm – 5.0 nm in size. We choose these $AgInS_2$-ZnS quantum dots due to their strong luminescent features regardless of their size.

In order to have chiral organization of nanocrystals, we used $(AgInS_2)_x(ZnS)_{1-x}$ group of QDs, varying 'x' molar composition ratio as shown in figure 3.1.1.1. We used four different

types of capping ligands for quantum dots namely ammonium sulphide (AS), 3-mercaptoprionic acid (MPA), oleylamine (OLA), and L – cysteine. The ligand exchange was done by phase transition method from nonpolar media to polar media for ligands like ammonium sulphide, 3-mercaptoprionic acid and L – cysteine. [4-9].

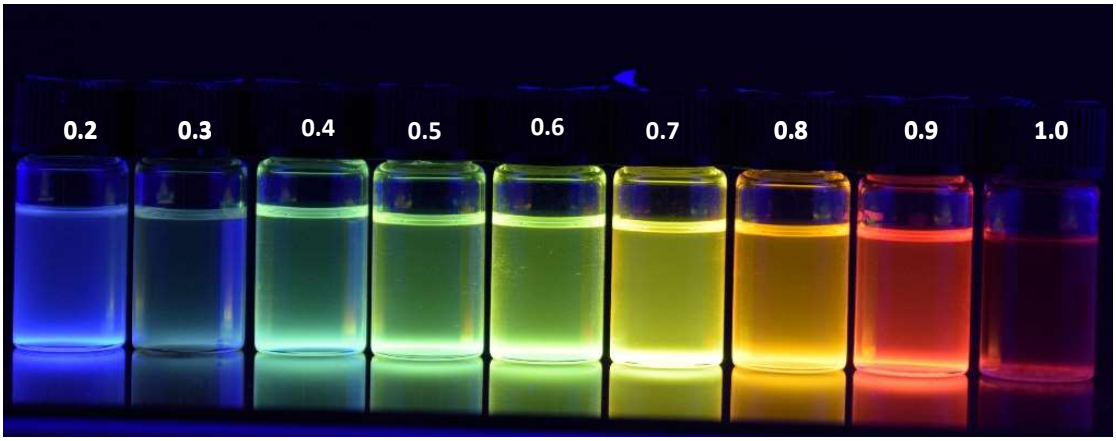

Figure 3.1.1.1: A group of $(AgInS_2)_x(ZnS)_{1-x}$ quantum dots suspension in toluene where x = 0.2, 0.3, 0.4, 0.5, 0.6, 0.7, 0.8, 0.9, and 1.0 excited at 365 nm wavelength.

In general, the capping ligands (often with long hydrocarbon chains) forming ionic or covalent bond with metal ions at the surface of the crystal, act as organic shell around the semiconductor core of QDs, avoiding their aggregations and control the growth of crystals during synthesis, and allow QDs to be soluble in organic solvents. [5] The initial capping ligand of $AgInS_2$- ZnS during its synthesis is oleylamine (OLA). [1] In order to disperse them in polar solvent, the surface capping ligand can be altered by new ligands having different functional group and also chain length of ligand can be tailored. We used the phase transfer method which has an advantage to preserve the quantum yield of QDs, surface encapsulation and allows to play with pH and ionic strengths, in order to change capping ligand. [5] In particular, we used the strategy implemented by A. Nag and his co-worker for all ligands mentioned above for changing the capping ligand reported Nag et al. [10] Three different capping ligands were used namely ammonium sulphide (AS), [5] 3-mercaptoprionic acid (MPA) [6] and L – cysteine (L-cys). [7] The schematics of ligand exchange presented in figure 3.1.1.2.

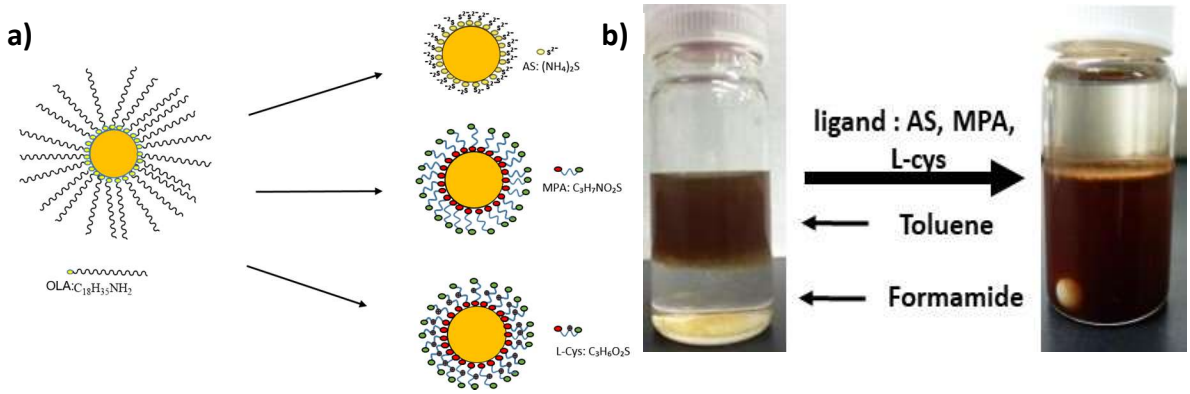

Figure 3.1.1.2: a) Scheme for ligand exchange with various ligand, and (b) An illustration of $(AgInS_2)_x(ZnS)_{1-x}$ quantum dots suspension undergone into ligand exchange by phase transfer method from toluene to formamide by replacing the original oleylamine(OLA) to new ligand. Here, the new ligand is 3-mercaptopropionic acid and composition ratio x=1.

3.1.2 Characterizations of nanocrystals:

The quantum dots were first characterized alone using transmission electron microscopy (TEM), XRD, emission and absorption spectroscopy, zeta-potential, FT-IR, elementary analysis in order to know the particle size, the optical properties and the surface chemistry

The transmission electron microscopy (TEM) images showing in figure 3.1.2.2(A-D) show QDs $(AgInS_2)_x(ZnS)_{1-x}$ capped by oleylamine with different composition x. They have different drying behaviours and contrasts due to the variation of ZnS doping. The sizes of particles analysed using image J software ranges between 2.0 nm – 5.0 nm according to statistics of measurement done on TEM images as shown in figure 3.1.2.2(a-d). This is slightly smaller than the reported values in the literature. [1]

X-ray powder diffraction (XRD) performed for two compositions of the same QDs $(AgInS_2)_x(ZnS)_{1-x}$ as x = 0.6 and 0.8 respectively as shown in the figure 3.1.2.1 and their crystal structure were confirmed . Three broad peaks resemble the bulk cubic structure of ZnS and trigonal structure of $AgInS_2$. Slight shift in the peaks is due to the variation of the ZnS ratio. [1, 11-13].

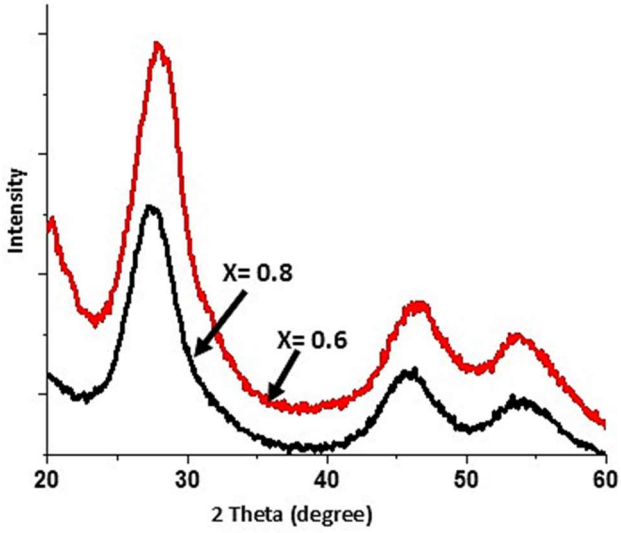

Figure 3.1.2.1: XRD plot for $(AgInS_2)_x(ZnS)_{1-x}$ quantum dots with different molar compositions x = 0.6 and x = 0.8.

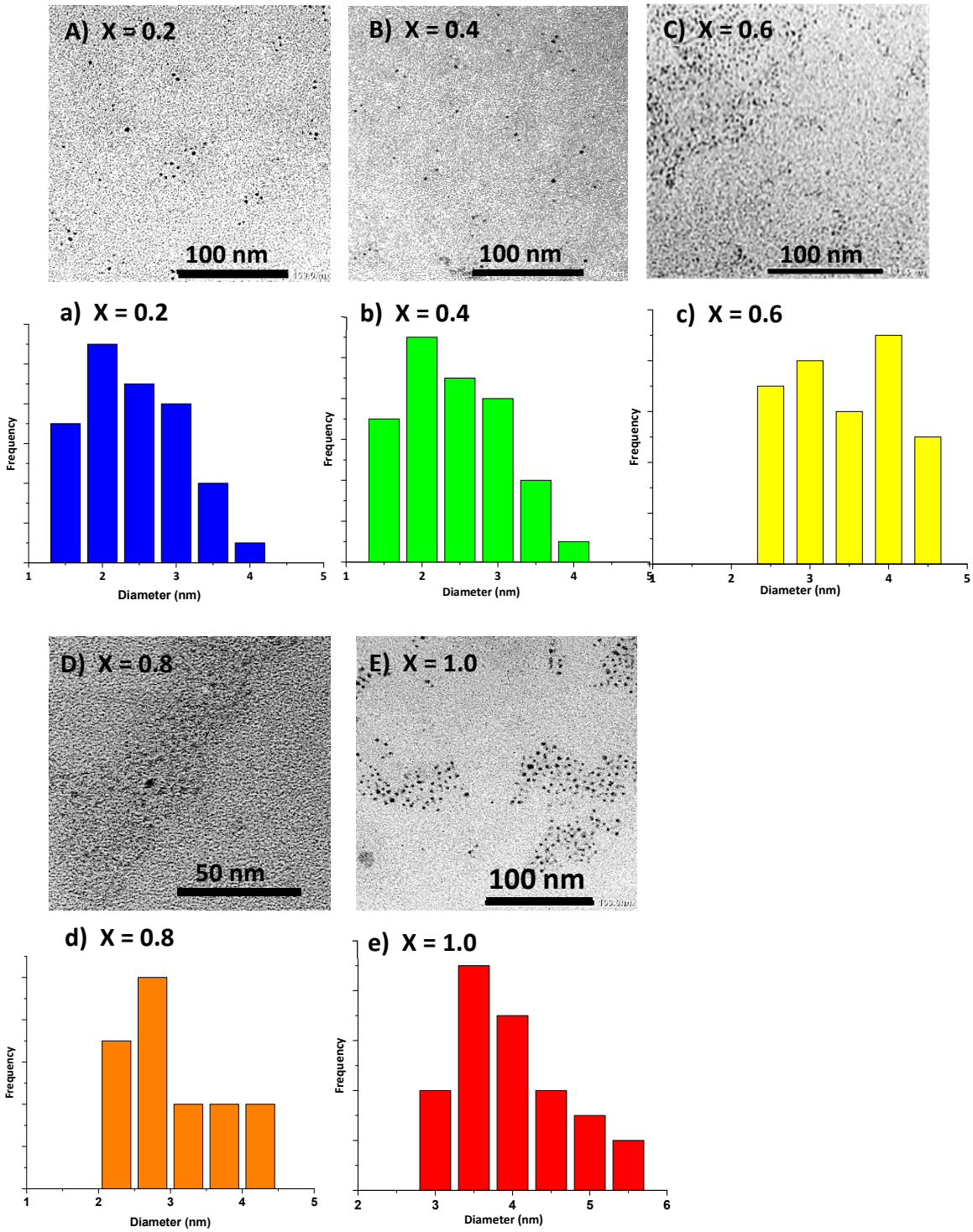

Figure 3.1.2.2: TEM image$(AgInS_2)_x(ZnS)_{1-x}$ quantum dots without staining with different molar composition ratio (A) x= 0.2, (B) x= 0.4, (C) x= 0.6, (D) x= 0.8, and (E) x= 1.0, and the plot of particle size measurement of quantum dots corresponding to each molar composition ratio (a) x= 0.2, (b) x= 0.4, (c) x= 0.6, (d) x= 0.8, and (e) x= 1.0.

The FT-IR measurement performed for dry sample of QDs capped by oleylamine (OLA), KBr pallet prepared by mixing 1% of QDs with known amount of KBr power. The FT-IR spectra (figure 3.1.2.3) show the presence of oleylamine on the surface on QDs. The characteristics of oleyl group were observed at the region between 2800 cm^{-1} – 3075 cm^{-1}. The peaks at 2873 cm^{-1} and 2927 cm^{-1} are due to the symmetric and asymmetric CH_2 stretching mode, respectively. Other peaks at 1563 cm^{-1} and 3327 cm^{-1} resembles to NH_2 scissoring and N-H stretching mode similar to peaks of OLA reported in N. Shukla et al. [1, 14].

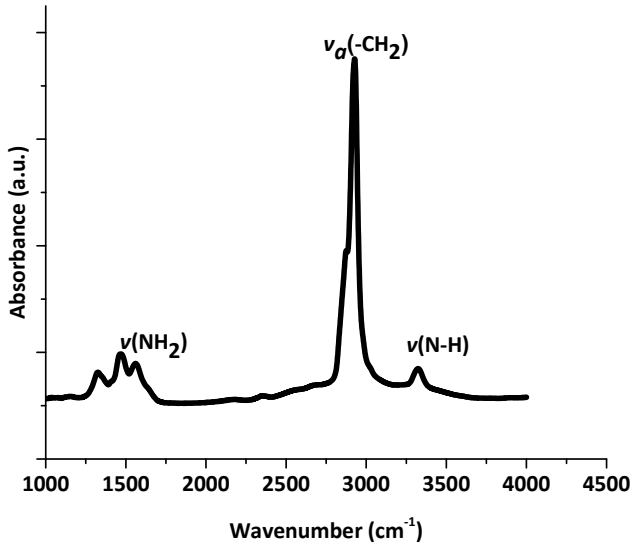

Figure 3.1.2.3: FTIR spectra of $(AgInS_2)_x(ZnS)_{1-x}$ quantum dots capped by oleylamine for dry sample.

We have then performed ligand exchange of these QDs in order to replace the oleyamine with new ligand on their surfaces in order to make dispersible in polar solvent. The ligands we chose were ammonium sulphide (AS) and 3-mercaptopropionic acid (MPA).

To determine the surface charge of quantum dots capped by ammonium sulphide (AS) and 3-mercaptopropionic acid (MPA) after the ligand exchange, zeta potential measurement was performed. The zeta potential measurement curve, performed at 0.1 mg/ml (figure 3.1.2.4) indicates that the quantum dots are overall highly negatively charged in both ligands beyond pH 4. [4, 6] The zeta potential of QDs capped by initial ligand oleylamine was not performed due to alkyl chain of ligand does not have and charge effect in non-polar solvent.

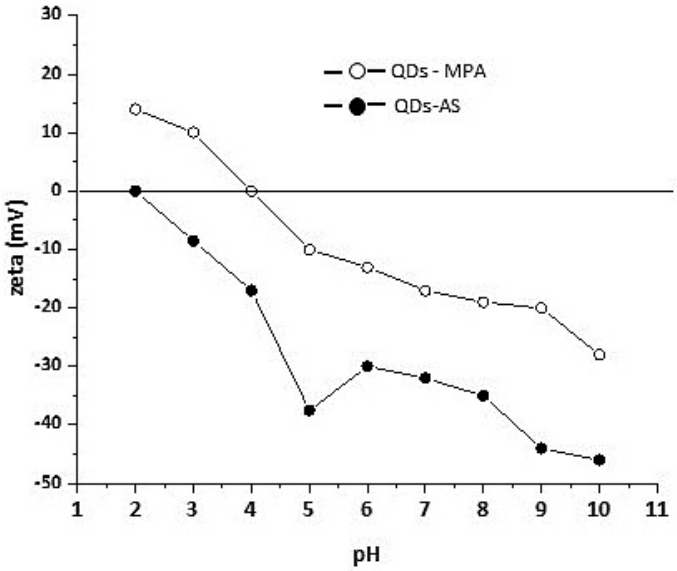

Figure 3.1.2.4: ξ potential curve of quantum dots capped by different ligand in (a) ammonium sulphide (AS), and (b) 3-mercaptopropionic acid (MPA). Concentration of QDs 0.1 mgml^{-1}.

Optical properties of Quantum dots:

The optical properties of quantum dots capped by oleylamine, dispersed in toluene is shown in figure 3.1.2.5; Figure 3.1.2.5 (a and b) represents the absorption and emission spectra of quantum dots capped by oleylamine excited at 365nm wavelength with different composition ratio of x = 0.2, 0.4, 0.6, 0.8 and 1.0 respectively. As reported previously, with increase molar composition ratio x, red shift is observed due to the decrease in ZnS component in the composite mixture of QDs. [1]

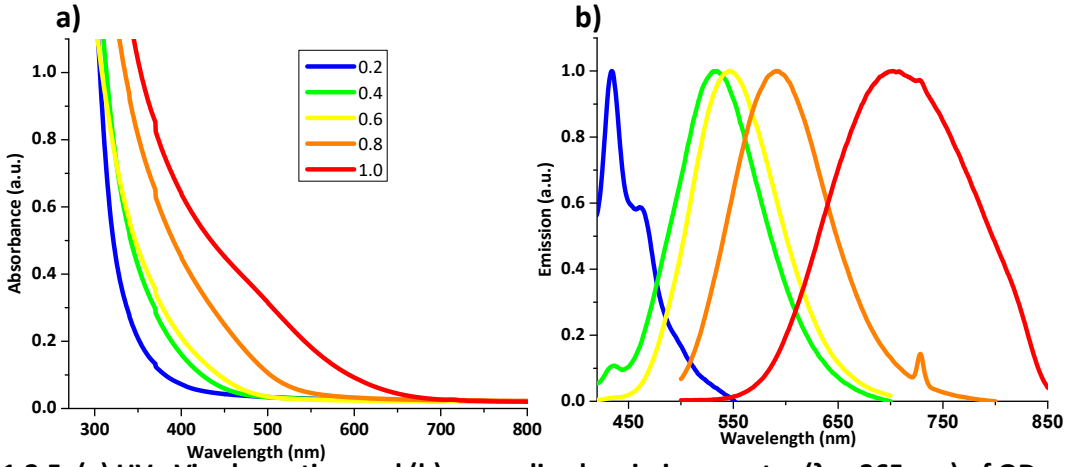

Figure 3.1.2.5: (a) UV –Vis absorption and (b) normalised emission spectra (λ_{ex}=365 nm) of QDs with even times composition ratio in toluene after synthesis.

The optical properties of quantum dots capped by oleylamine, dispersed in toluene is shown in figure 3.1.2.5; Figure 3.1.2.5 (a and b) represents the absorption and emission spectra of quantum dots capped by oleylamine excited at 365nm wavelength with different

composition ratio of x = 0.2, 0.4, 0.6, 0.8 and 1.0 respectively. As reported previously, with increase molar composition ratio x, red shift is observed due to the decrease in ZnS component in the composite mixture of QDs. [1]

The absorbance and emission spectra of the both AS capped, and MPA capped QDs in water (figure 3.1.2.6) showed similar properties as oleylamine capped QDs (figure 3.1.2.5). They all show red shift due to change of ligand and solvent (figure 3.1.2.6b) in case of all compositions. However, we will not discuss in detail about the AS capped quantum dots , as the silica helix were destroyed after grafting of these QDs as discussed in the next section 3.1.1. In case of QDs capped MPA, the comparison between figure 3.1.2.5b and figure 3.1.2.6b was done with respect to maxima wavelength of each emission spectra of QDs such as composition x=0.2 initial wavelength was 434 nm shifted to 541 nm large red shift was observed in x=0.2, and second larger shift was observed in case of x=1.0 QDs, while other composition x= 0.4, 0.6 and 0.8 have difference 18 – 33 nm in red shift as compare to composition x=0.2 and 1.0. The values of λ_{max} are mentioned in table 3.1.

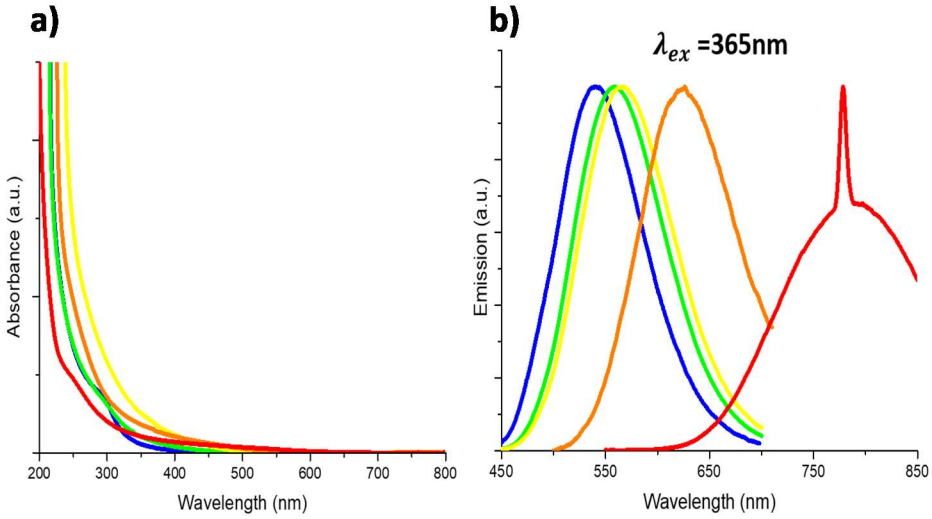

Figure 3.1.2.6: (a) UV –Vis absorption and (b) normalised emission spectra (λ_{ex}=365 nm) of QDs with even times composition ratio in milli-q water after ligand exchange. QDs capped by MPA in milli-Q water.

Table 3.1: Comparison of emission (λ_{max}) of QDs capped by OLA and MPA.

QDs x	QDs capped by OLA (λ_{max}) nm	QDs capped by MPA (λ_{max}) nm	Red shift nm
0.2	434	540	106
0.4	534	559	25
0.6	546	564	18
0.8	591	624	33
1.0	702	743	41

To understand more in deal the optical properties of QDs capped by MPA after the ligand exchange, QDs were excited at different wavelength to observe better excitation wavelength then 365 nm, and effect of acid and base respectively, on quantum dots. These experiments were performed in order to grafted the on silica helices, where few conditions will be required for grafting in section 3.2.2 we have discussed about grafting of QDs –MPA on silica helices, here the discussion is about QDs alone.

(a) Excitation in different wavelength for MPA capped QDs:

According to literature of ZnS-$AgInS_2$ nanocrystals dispersed in water, the strongest excitation was observed at the wavelength, 365 nm. [1] In order to see how this wavelength moves when the QDs are grafted on silica walls, excitation at different wavelength was performed for the QDs capped by MPA (Figure 3.1.2.7). The result indicates that there is no shift. These experiment was done on composition x=0.6 in milli-q water with concentration 1.0 mg ml^{-1} of QDs. Therefore, for all the sets of experiments the excitation wavelength was kept to be 365nm.

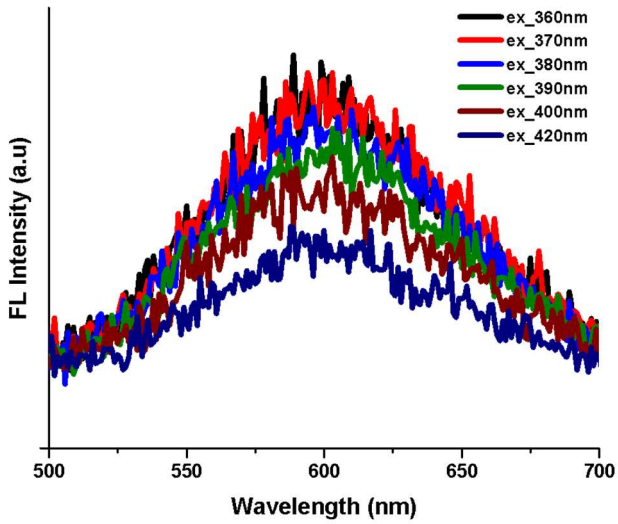

Figure 3.1.2.7: Emission spectra at different excitation wavelength 360 nm, 370 nm, 380 nm, 390 nm, 400 nm and 420 nm of QDs capped by MPA with x=0.6 composition ratio in mili-q water.

(b) Effect of adding base in the suspension of QDs capped by MPA:

In order to investigate the quenching effect of QDs after grafting them on amine modified silica helices, (high surface pH) two different types of bases (sodium hydroxide and ammonia) were used to adjust the pH of QDs suspension in water (figure 3.1.2.9). The excitation wavelength was 365nm for both sets of experiment.

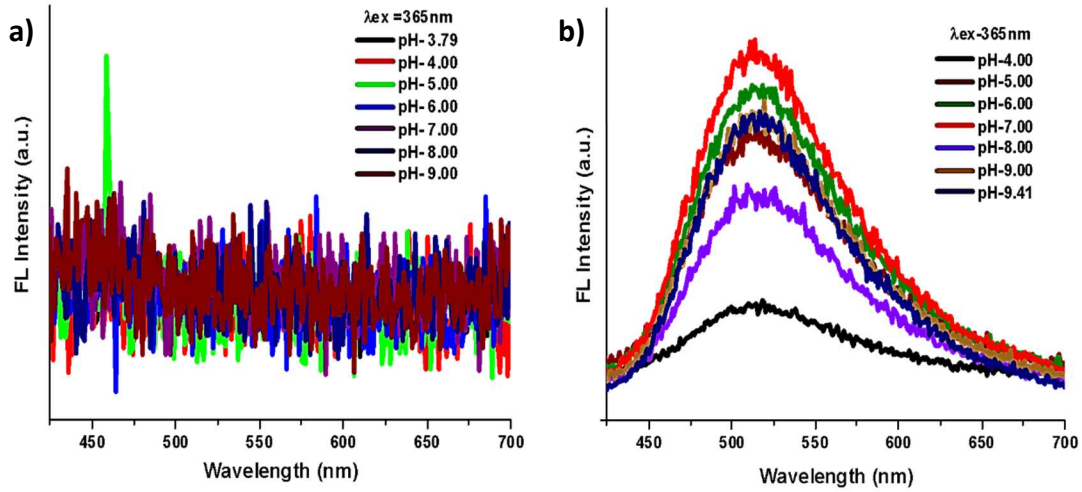

Figure 3.1.2.8: Effect of base on QDs (x=0.2) in water changing the pH (a) base NaOH, and (b) base NH_3.

It can be observed from figure 3.1.2.8a that the emission disappears upon addition of NaOH in the suspension of the QDs which does not recover upon decrease in pH. On the contrarily, the fluorescent property of QDs decreases by the addition of ammonia but is not totally lost upto pH 9.4 and is reversible back in acidic medium. This indicates that the quenching of these QDs occurs only in the presence strong base.

Finally, QDs capped by chiral ligand L- Cysteine, show different absorbance behaviour as compared to the QDs capped by achiral ligands. (Figure 3.1.2.9) L-cys@QDs shows induced circular dichroism signal in the range of wave length 250-300 nm which clearly comes from QDs and not from L-cys. [49]

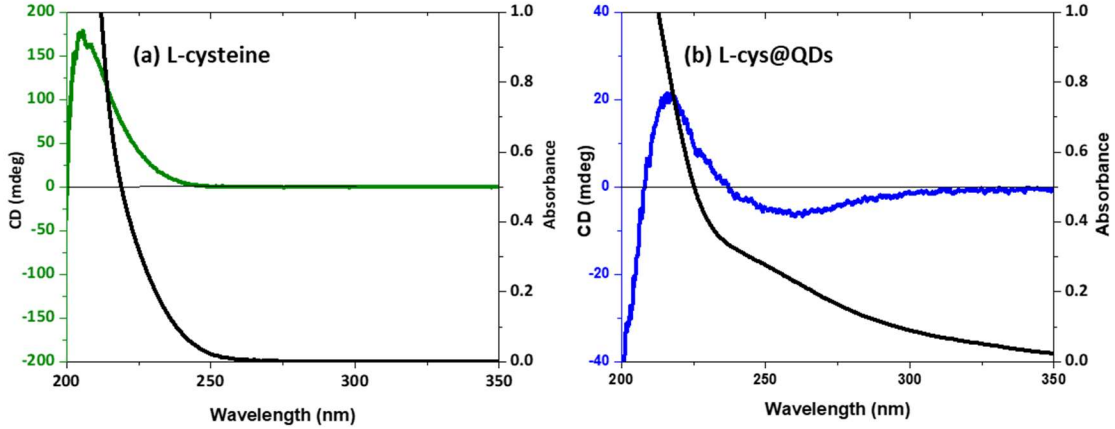

Figure 3.1.2.9: Absorbance and circular dichroism (CD) spectra (a) ligand L-cysteine, and (b) QDs capped by l-cysteine.

3.2 Grafting of Quantum dots $(ZnS)_{1-x}(AgInS_2)_x$ the surface of silica helix with different ligand:

In the previous section, we characterized quantum dots alone in suspension. In this section, we analyse the QDs grafted on silica helix with different ligand. The interaction between the QDs and helical silica is ionic bond. The fabrication is divided in 4 parts based on ligands: (a) Ammonium sulphide (AS), (b) 3 - mercaptopropionic acid (MPA), (c) l – cysteine, and (d) oleylamine (OLA). The procedure of the grafting of QDs is presented in figure 3.2.1.

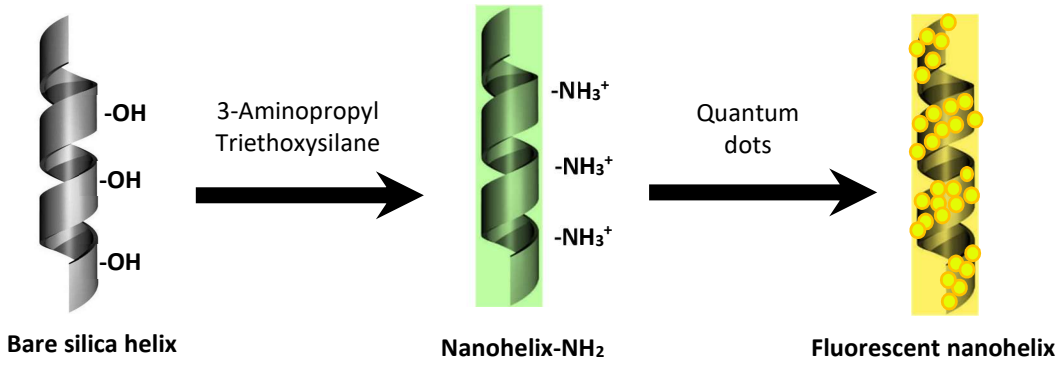

Figure 3.2.1: Schematic about grafting of QDs with different ligand capped by QDs.

3.2.1 Quantum dots capped by Ammonium sulphide (NH4)2S ligand:

The QDs are highly negatively charged as discussed in previous section and silica helix are positively charged after functionalisation of the silica surface by APTES. The concentration of silica helix is 0.5mg/ml fragmented by ultrasound before surface modification and weight concentration of QDs in milli-Q water is 1.0 mg/ml. After mixing the two, we waited for around 12-15h. Different conditions were applied to graft QDs: (a) pH of modified silica helix were adjusted in two cases: pH 5.0 and pH 7.0; (b) Changing the solvent. The results are as follows:

(a) pH 5.0 of APTES-silica:

When the pH of silica helices suspension in mill-Q water was adjusted to 5.0, the helix surface charge remains positive. As shown in figure 3.2.1.1 (A-a), upto 12 hours after mixing the $(NH_4)_2S$ QDs suspension and silica nanohelices, we could observe helical structure of silica with QD-like small particles grafted on their surface. However, the observation at 15 hours clearly shows that the silica helices are destroyed. At the same time silica helix were observed in same condition without QDs helix in water (figure 3.2.1.2). It is likely that the thiol S^{-2} ion acts as strong acid and react with Si-O bond. It clearly shows that the surface ligand is affecting the structural morphology of silica helix.

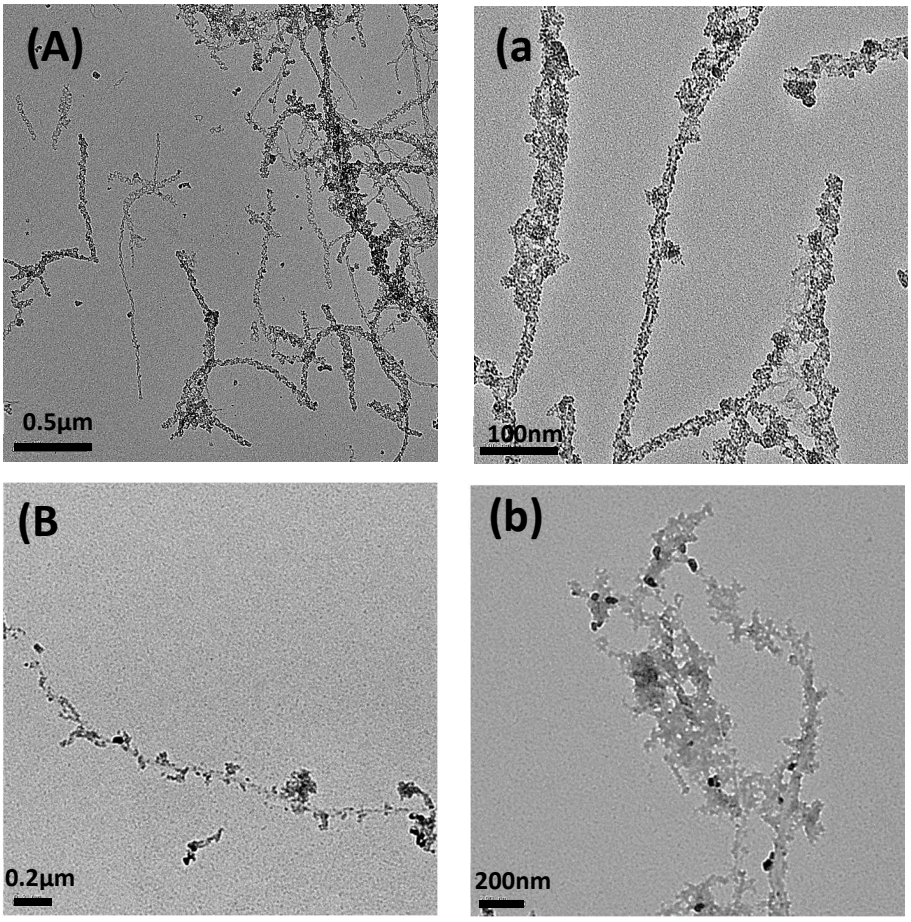

Figure 3.2.1.1: TEM image of (NH4)2S-QDs: (A-a) after 12h of grafting and (B-b) after 18h grafting.

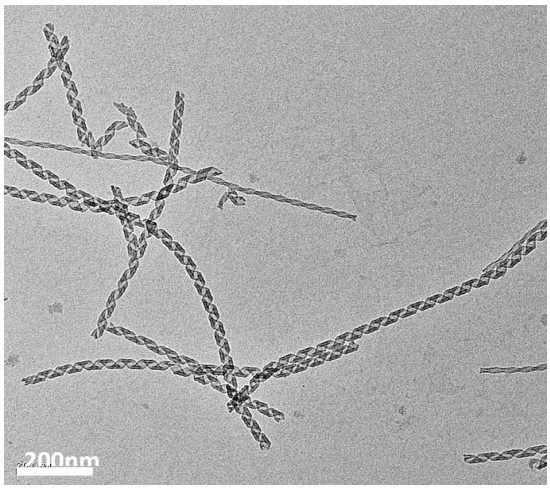

Figure 3.2.1.2: TEM image of amine modified silica in water after 48h.

(b) **pH 7.0 of APTES-silica:**

In this case, big aggregation of quantum dots were observed under TEM images (figure 3.2.1.3.). No grafting of QDs was observed on the surface of silica helices. It was observed by zeta potential measurements that the suspension of the APTES grafted helices are highly positive below pH 5.0, but decreases at pH around 7. The non-grafting of QDs on the surface of APTES grafted helices indicates that the surface charge of silica helices at pH7 is not sufficient for the electrostatic interaction between the QDs and the silica helices.

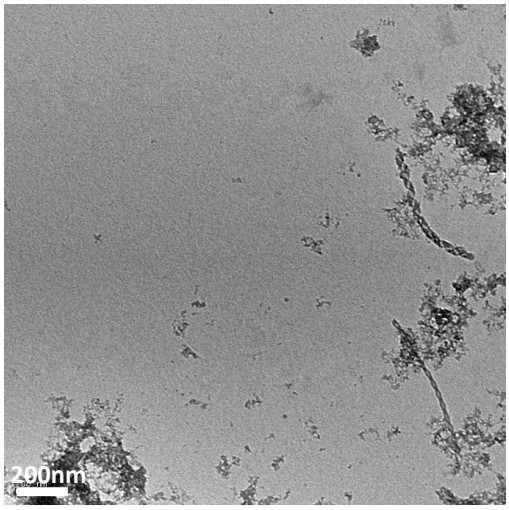

Figure 3.2.1.3: QDs aggregate and no grafting on silica helix.

Grafting of QDs in the mixture of ethanol and water: Silica helices and QDs are mixed in two water:ethanol ratios (1:2 and 2:3). The TEM images (figure 3.2.1.4.) show that there is no grafting of QDs on the surface of silica helices in both cases but only aggregates of QDs separated from bare silica helices were observed. The results above show that $(NH_4)_2S$ QDs cannot be grafted on silica nanohelices without destroying the helices regardless of pH or the presence ethanol.

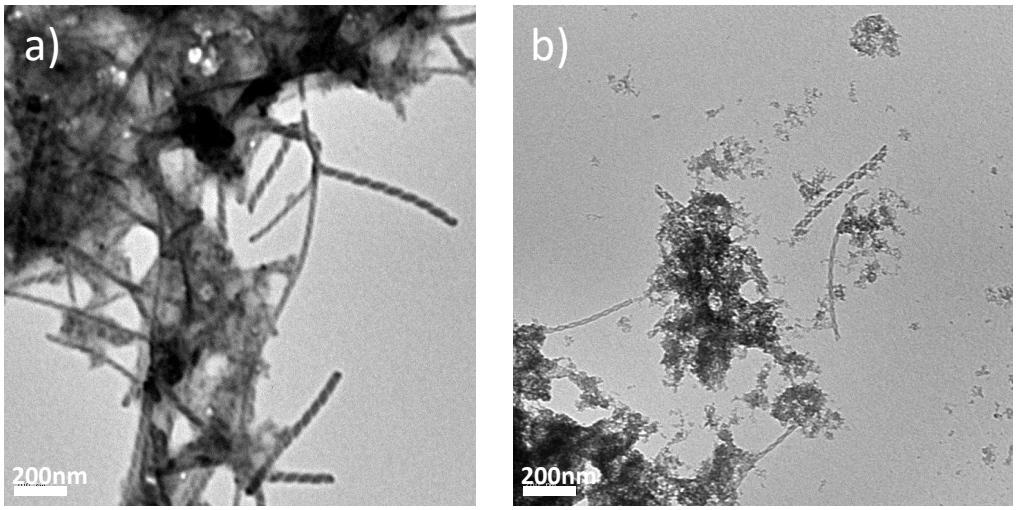

Figure 3.2.1.4: TEM images (a) 1:2 ratio of water and ethanol, and (b) 2:3 ratio of water and ethanol.

3.2.2 Quantum dots capped by 3-Mercaptopropionic acid ligand:

Instead of using $(NH_4)_2S$ ligands which destabilize silica helices, 3-mercaptopropionic acid was used as capping ligand for QDs. As we have shown in the previous section, the zeta potential measurement showed that QDs are highly negatively charged (figure 3.1.2.6). We used APTES modified silica helix in different pH.

(a) By adjusting the pH of APTES modified silica helix and QDs to 5:

To adjust the pH of the suspension, 10^{-3} M concentration acetic acid and sodium hydroxide were used. MPA-capped QDs aggregated in milli-Q water after 24h of dispersion in water due to the presence of carboxylic group which undergo formation of intermolecular hydrogen bond formation between the carboxylic groups of the ligand. [17] Therefore, to avoid aggregation of QDs pH was increased using sodium hydroxide. Before grafting the QDs, the pH of APTES modified silica helix and QDs was adjusted between pH 5.0. As shows in the

figure 3.2.2.1. The QDs were grafted homogenously on the surface of silica helix and morphology of helical silica remains protected unlike to previous case of grafting. Overall coverage of QDs was observed on the surface of silica helix. Here, the composition ratio of QDs was x = 1.0 (figure 3.2.2.1 (A, a)) and x = 0.6. It indicates that the capping ligand on the surface of QDs plays important role for the formation of ionic bond between the amine group on the surface of silica helix and carboxylic group on the surface of QDs. Lot of studies have been conducted on formation of ionic bond between amine and carboxylic group on different surfaces. [17, 18, 19] The stability of QDs grafted silica helix remains for 3 – 4 days (figure 3.2.2.1 (B, b)) However, the fluorescence decreased after 24h due to the quenching of QDs. (figure 3.2.2.2)

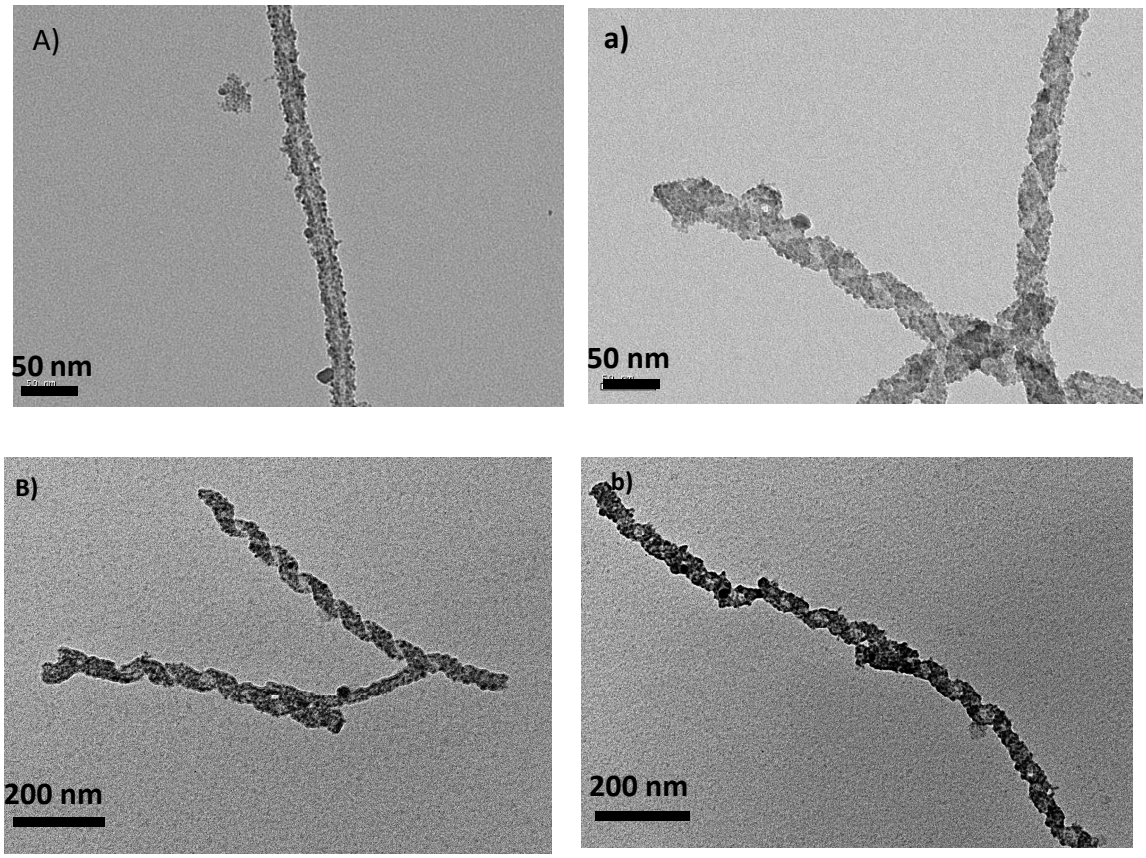

Figure 3.2.2.1: TEM images of QDs (x=1.0) grafted on the surface of silica helix at pH 5.0 of QDs and amine modified silica: (A, a) after 15 h of grafting fluorescent, and (B, b) after 3 days of grafting none fluorescent.

But in case of optical properties of QDs grafted silica helix. The absorbance did not vary strongly before or after grafting, but for the fluorescence, the emission from the QDs after grafting decreased a lot (figure 3.2.2.1(B, b)) after grafting.

(b) Without adding any acid or base in modified silica suspension or nanocrystals:

The absence of added acid or base, the pH is approximately 6.0 for the suspension of QDs (1.0 $mgml^{-1}$) which remain negatively charged for all the compositions of QDs as x=0.2, 0.4, 0.6, 0.8 and 1.0. For the suspension of amine modified helix, pH is around 7.0. When mixed, no aggregation was observed and homogenous grafting of QDs were observed as per the TEM images in figure 3.2.2.3. As previously indicated, some of these QDs have weak contrast, and along with their small sizes, it was difficult to do the statistics of the nanoparticles with respect to silica helices. The other alternative is to calculate through absorbance spectra. As we know no of particle in initial stage while mixing the silica helix with QDs.

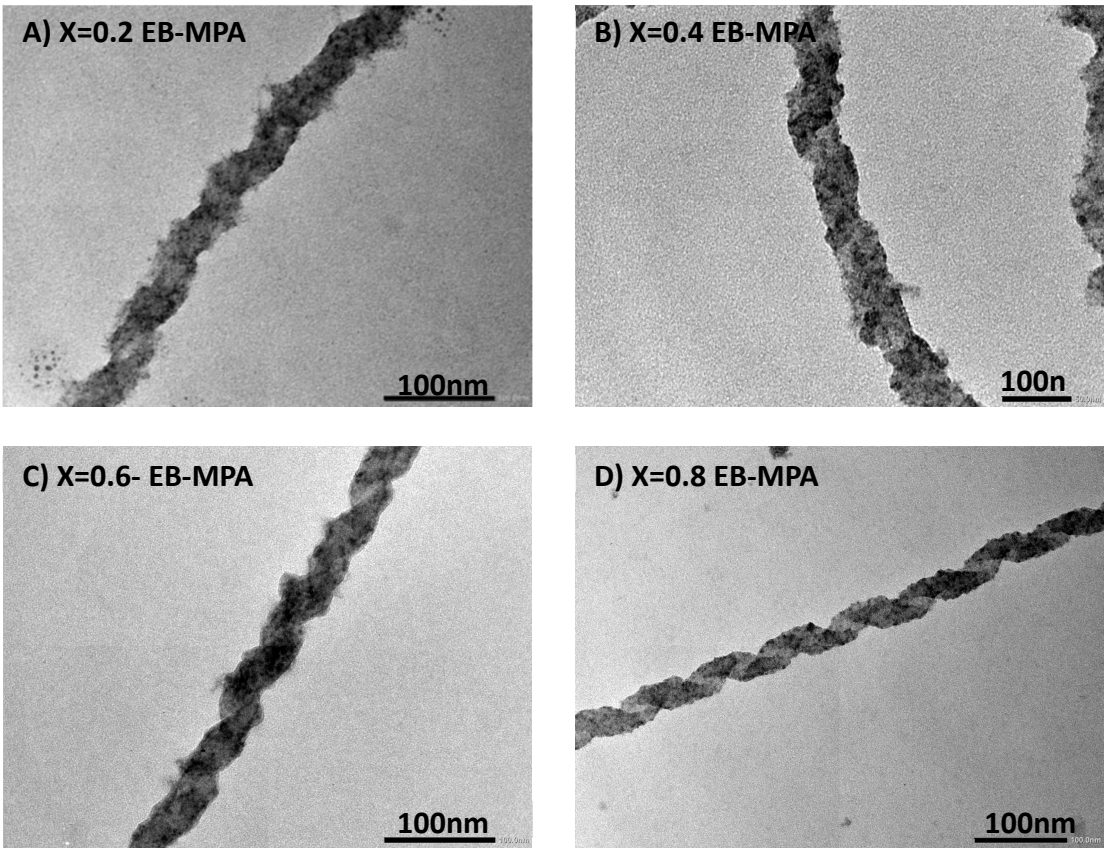

Figure 3.2.2.3: TEM images of QDs grafted on the surface on the surface of silica helix with different composition (A) x=0.2, (B) x=0.4, (C) x=0.6 and D) (x= 0.8) respectively at same conditions.

High resolution transmission electron microscopy (HRTEM), JEOL- 2200FS (UHR), was used in order to investigate the qualitative estimation of QDs(x=0.6) grafted on silica helix (figure 3.2.2.4). HRTEM confirms homogeneously covered silica helices by QDs. In addition,

Scanning Transmission Electron Microscopy (STEM) with Energy dispersive x-ray spectroscopy (EDX) were used to identify each element of QDs in x=0.6 composition ratio.

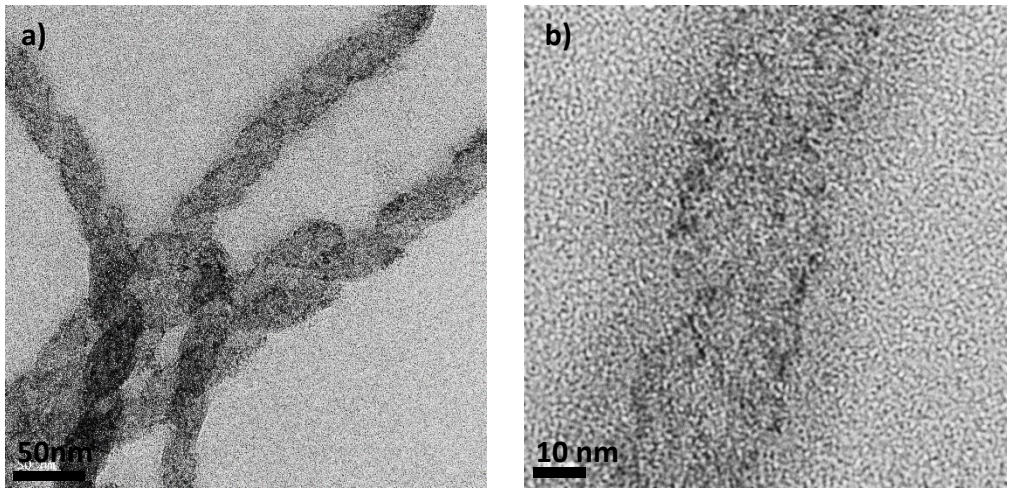

Figure 3.2.2.4: HRTEM images of QDs grafted on the surface on the surface of silica helix with different x=0.6 at different scale bar.

In figure 3.2.2.5 the mapping of the element is shown on STEM image while figure 3.2.2.6 shows the EDS spectrum, the peaks are X-rays given off as electrons return to the K- or the L-electron shell with respective elements. In STEM mode image of QDS@silicahelices (figure 3.2.2.5), each element of QDs was mapped using Si as a reference. Later, spectra (figure 3.2.2.6) were generated according to mapping done on the STEM. The quantitative estimation of each element is as shown in table 3.2. These images well demonstrate the deposition of QDs on silica helix.

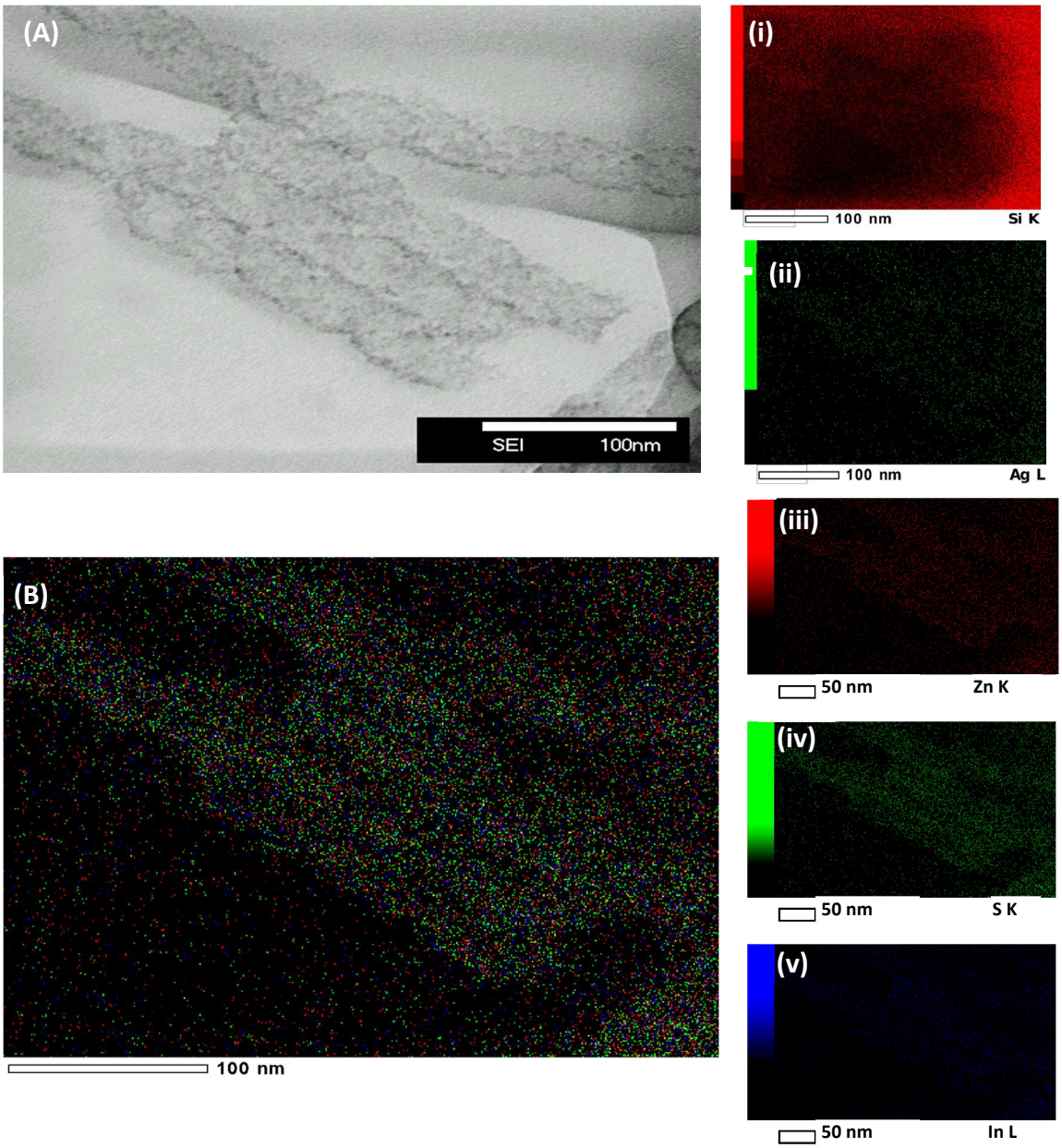

Figure 3.3.2.5: STEM image with mapping through EDS for each element present in the compositions of QDs grafted on the surface of silica helix. (A) STEM image of QDs0.6@silicahelices, (B) Mapping of all elements of QDs, and individual mapping of each element: (i) Si, (ii) Ag, (iii) Zn, (iV) S, and (v) In, respectively.

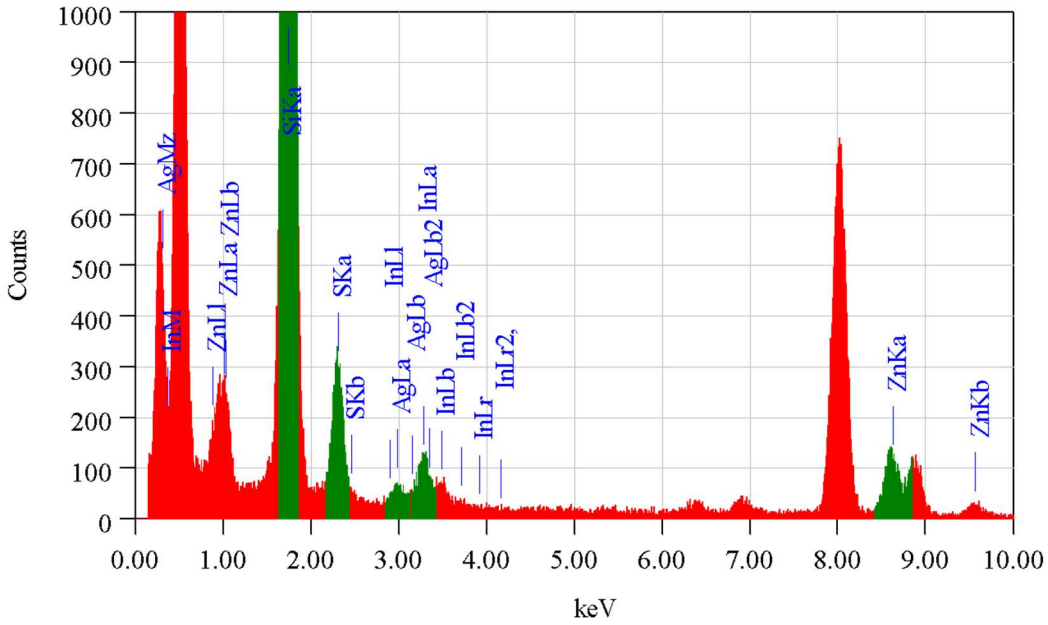

Figure 3.3.2.6: EDS spectrum of X-ray with respect to mapping done on TEM image.

Table 3.2: Thin Film Standless Quantitative Analysis (Fitting Coefficient: 0.6895)

Element	(keV)	Mass %	Counts	Sigma	Atom %	K
Si K (Ref.)	1.739	80.24	39055.27	0.54	89.39	1.0000
S K	2.307	5.69	2291.50	0.11	5.55	1.2090
Zn K	8.630	5.76	1617.72	0.14	2.76	1.7330
Ag L	2.984	2.21	289.49	0.23	0.64	3.7170
In L	3.286	6.09	800.72	0.25	1.66	3.7027
Total		100.00			100.00	

3.2.3 Quantum dots capped by Oleylamine:

We then tried to make distance shorter between QDs and amine modified silica helix. In this case we tried to replace oleylamine directly by amine (APTES) through amine modified helix to obtain chiroptical properties.

Oleylamine acts both as capping agent and as stabilizer during the synthesis of QDs. [1] Here the amine modified silica helix directly interact with OLA-QDs, the amine group of silica helix replaces the oleylamine molecule on the QDs, by strong electrostatic interaction between them due the function group.

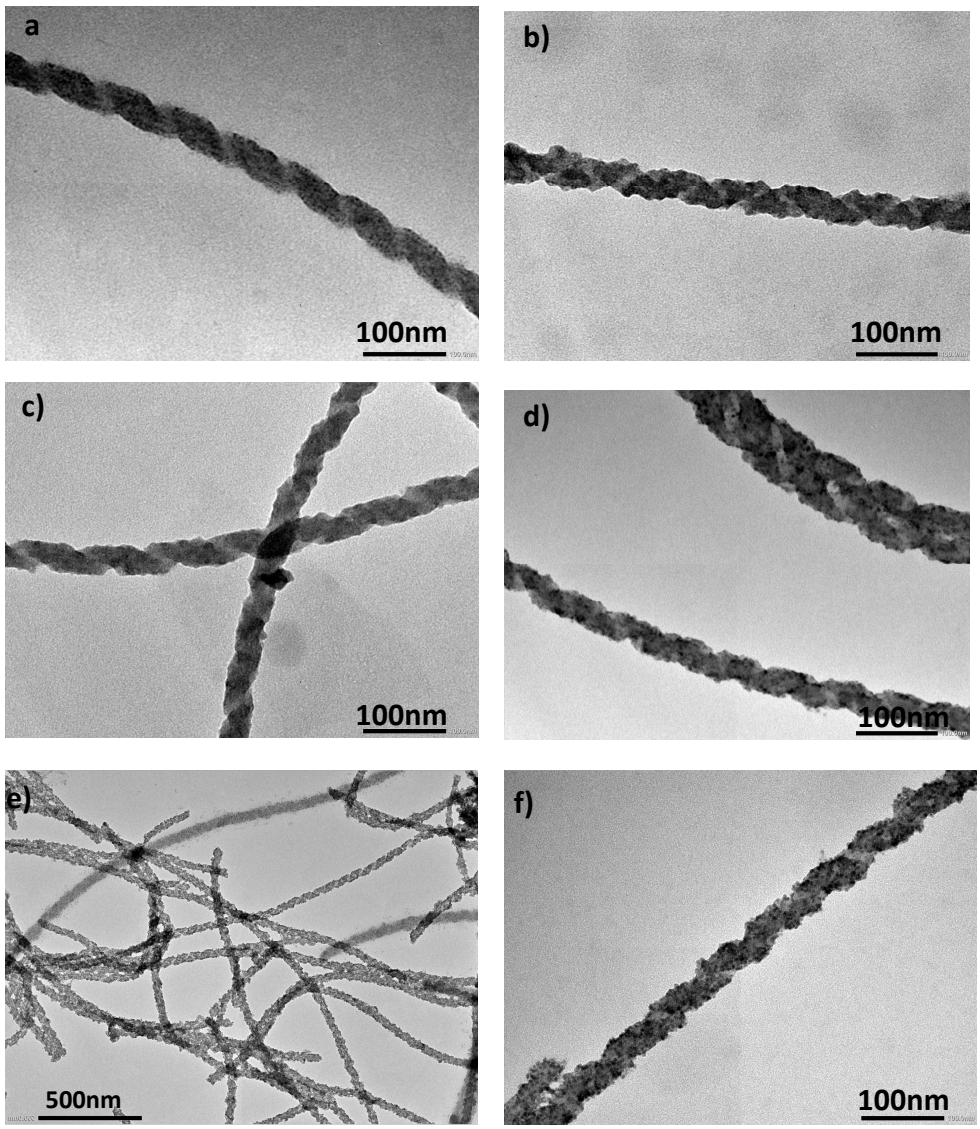

Figure: 3.2.3.1: TEM image of QDs grafted on the surface of silica helix in toluene with different composition ratio of QDs: (a) x=0.2, (b) x= 0.4, (c) x=0.6, (d) x=0.8 and (e, f) x= 1.0.

Because of the apolar character of the oleylamine, QDs grafted on the surface of the silica helix is dispersed in the nonpolar solvents like toluene. Figure 3.2.3.1 shows that the TEM image of oleylamine covered QDs grafted on the surface of silica helix. It also shows good homogeneous grafting of QDs on the surface of silica helix. Same phenomena was observed for each composition of QDs.

The images taken from confocal microscope (λex = 405nm) shows that the QD grafted silica helix are fluorescent in nature. The bright big spots in the image show the aggregation of the QD@helices. The enlarged image (right) clearly shows the long fluorescent fibre like structure of QD@helices. This was observed for all compositions of QDs grafted on silica helix. Samples are stable during more than 3 weeks in toluene.

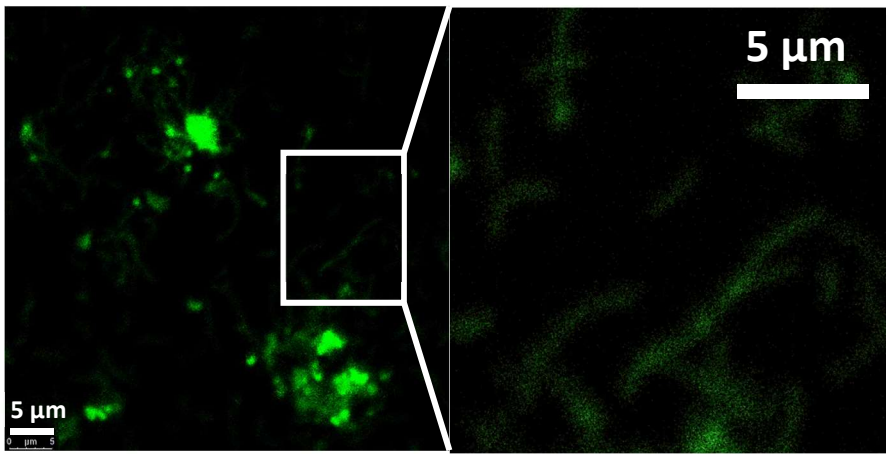

Figure: 3.2.3.2: Confocal microscopic image of QDs (x = 0.6) grafted on surface of silica helix, excitation wavelength 405 nm of laser in ethanol.

Globally, OLA-QDs grafted silica helices suspension are more turbid in water while in toluene, the suspension remains transparent.

3.2.4 Quantum dots capped by L- cysteine chiral ligand:

The results obtained by the chiral L-cysteine capped QDs are similar to those obtained by other ligands. The TEM image shows that QDs are grafted on silica helix uniformly, however, unlike MPA@helices or Oleylamine@helices, the helical structures are slightly destroyed (figure 3.2.4.1).

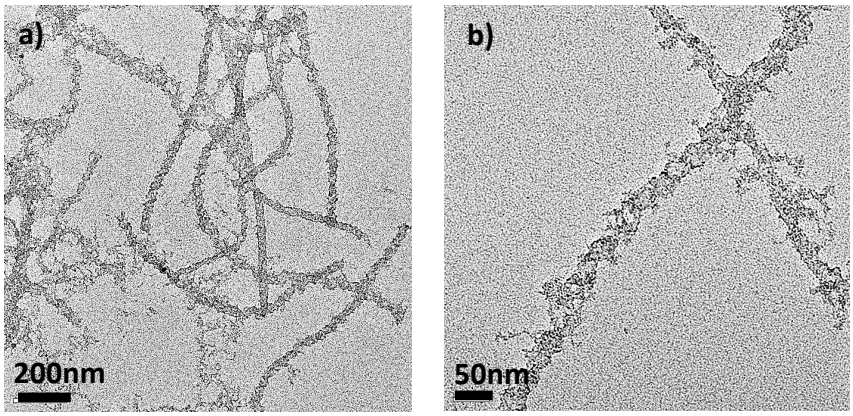

Figure: 3.2.4.1: TEM image of L-cys QDs (x=0.6) on the silica helix with different scale bare.

3.3 Optical and chiroptical properties of QDs grafted amine modified silica nano-helix: Capping ligand on QDs 3-mercaptopropionic acid, oleylamine and L-cysteine

In the previous section, we discussed about the microscopy and spectroscopy study QDs having different ligands as well as the TEM study on the QDs@silica nanohelices in different condition. Here, the major focus is on optical and chiroptical properties of QDs@silica nanohelices. The composite of QDs-Helices with ligands: 3-mercaptopropionic acid (MPA), Oleylamine (OLA) and L- cysteine (L-cys) are discussed while the ammonium sulphide@silica nanohelices was not studied due to the instability of helical structures as reported in previous sections.

In this section, we will discuss the impact of the organisation of these QDs on the surface of silica helices on their optical properties.

3- Mercaptopropionic acid QDs: MPA-capped QDs grafted on the surface of helical silica without addition of any acid or base (pH 5.5.0-6.2 of the mixture) (section 3.2.2(b)) are luminescent. Figure 3.4.1 absorbance of QDs individually dispersed in aqueous solution (supernatant after washing the QDs@Silica helices). The plot in the figure 3.4.1c represents the concentration of non-grafted QDs after each washing, estimated by using the Beer – Lambert law equations,

$$A = \varepsilon \, l \, C$$

Where, A represents measured absorbance at incident wavelength, l, the path length of the cell in centimetre, C, the concentration of given sample in molar and ε, the molar extinction coefficient.

For the QD nanoparticles, ε- molar extinction coefficient is unknown. Therefore in order to calculate the concentration of the non-grafted QDs, first, the ε- molar extinction coefficient needs to be calculated from a QDs suspension of a known concentration.

The quantity of the QDs with other compositions grafted on nanohelical silica was estimated using the same method.

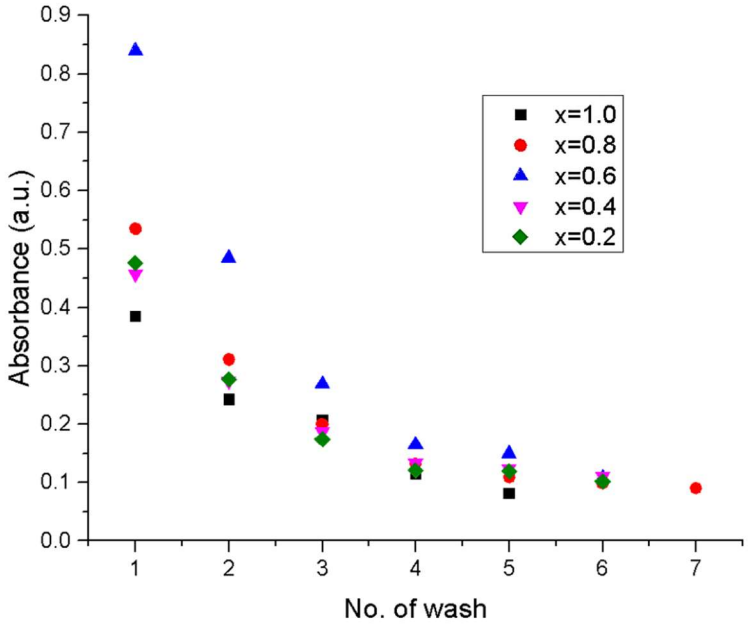

Figure 3.4.1: Plot of absorbance at 300nm vs no of wash: Supernatant collected after washing in each wash in each case of different compositions grafted on silica helix. (x= 0.2, 0.4, 0.6, 0.8 and 1.0).

As we have shown in the previous section, these QDs are homogenously grafted on the surface of silica helix. After the grafting in each case, a slight blue shift was observed from the emission spectra of QDs before grafting as shown in the figure 3.4.3. However, no chiral induction was observed in absorbance (CD) and emission state (CPL).

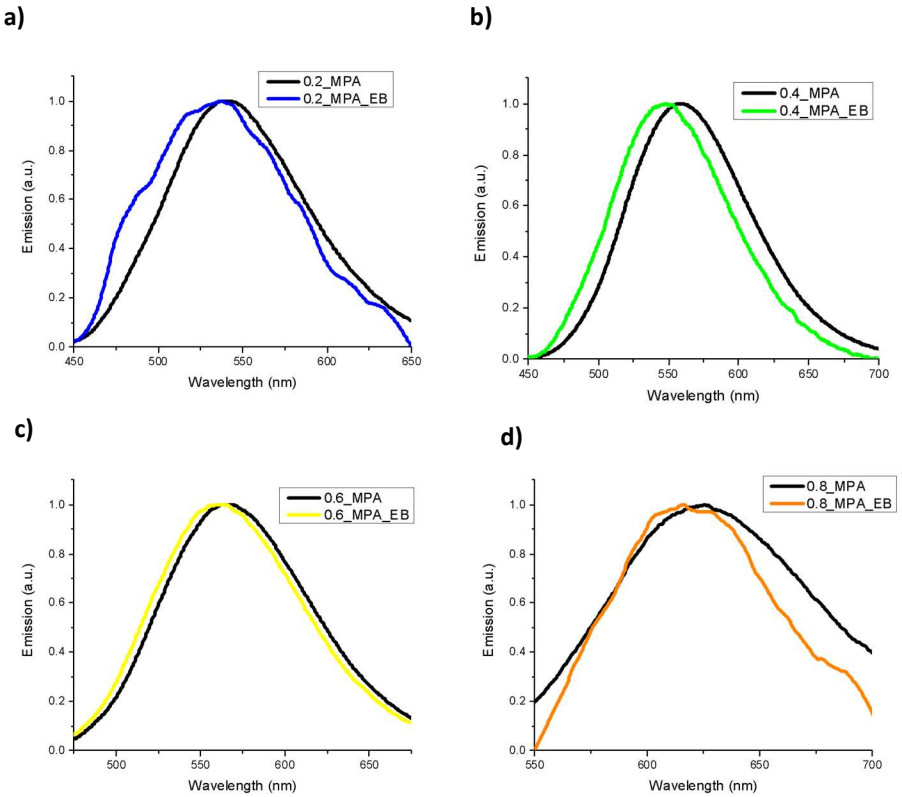

Figure 3.4.3: Emission spectra of QDs-MPA before (alone black line) and QDs-MPA after grafted on silica helix (color line) in each case of different compositions grafted on silica helix. (x= 0.2, 0.4, 0.6, and 0.8) excited at 365nm .

QDs capped oleylamine: As already shown in previous section with confocal images, OLA capped QDs @ silica helices are fluorescent. Here, QDs show blue shift after grafting in each case with different gaps depending on x values. For x=0.2, negligible blue shift was observed, for x = 0.4, 0.6 and 0.8, the blue shift was 12.0 nm, 22.0 nm and 52.0 nm respectively. As the ZnS component decreases QDs stronger blue shift was observed. There is no major change in observed before and after grafting.

Neither of the cases above, (QDs with 3-mercaptopropionic or oleylamine ligands) chiroptical properties were observed from the QDs grafted on the nanohelices in spite of the highly dense and homogeneous grafting of the QDs. Many literature including the ones from our group has reported the chiral induction on achiral gold or silver nanoparticles [3, 21] in interaction with chiral templates or chiral molecules. Also, core-shell type QDs such as (ZnSe)ZnS quantum dots as described by Huo and his co-workers demonstrated the induced

chirality when they were organized around the chiral glutamide molecules which self-assemble to form chiral nanofiber-like structure [22]

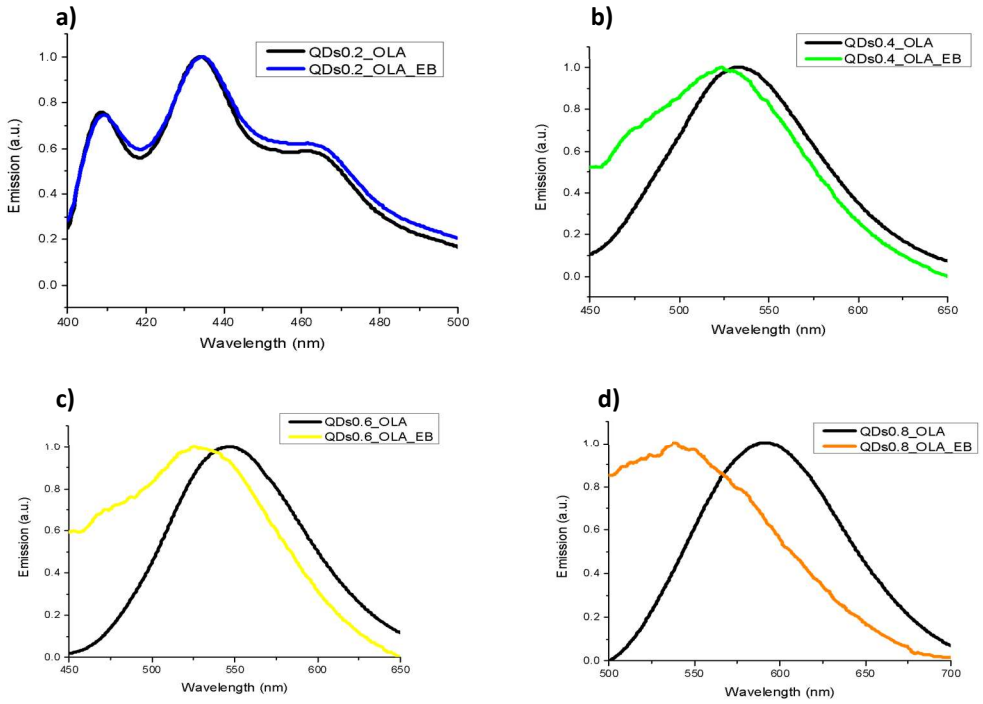

Figure 3.4.3: Emission spectra of QDs grafted on silica helix in each case of different compositions grafted on silica helix. (x= 0.2, 0.4, 0.6, and 0.8).

Such QDs show induced chirality at ground and excited states resulting in ICD and ICPL. The reason why in our case, the ZnS-$AgInS_2$ QDs do not show the chiral interaction with the chiral template is not clear but it might be that these QDs do not interact with each other as it is the case of the plasmonic particles or core-shell QDs. This can be because these multi-element (with high numbers of different atoms) form more non-organized composite structures (crystalline domains are randomly organized inside a QD), and that they have weak dipole moment, not allowing them to interact with each other. In order to observe the chiral organization-induced CD or CPL, It is likely that the achiral particles (metal nanoparticles or QDs) need to have strong inter-particle interaction such as high polarizability or strong dipole moment such as CdSe quantum dots. [23, 24]

Chiral ligand L-cysteine: Here, we investigated if the induction of chirality to the QDs from chiral molecules, L-cysteine, can be coupled with the mesoscopic nanohelical chirality. Indeed, the idea was to see if the handedness of the silica nanohelices would have any effect

on the ICD of the QDs from L-cysteine. The CD spectra (figure 3.4.4) of the L-cysteine capped QDs @ right handed vs left handed silica helices do not show differences, indicating that there is no impact due to the handedness of chiral helical silica. No impact of chirality from the ligand was observed on their CPL

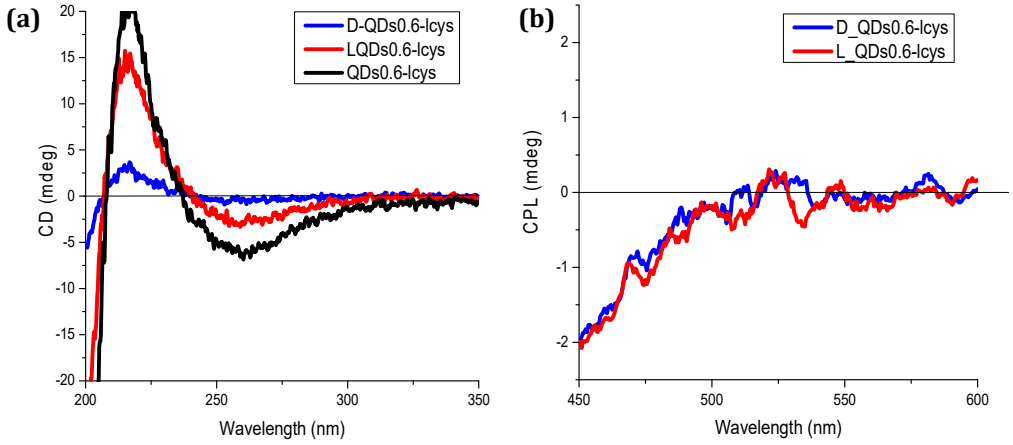

Figure3.4.4: (a) Circular dichroism (CD) of QDs-Lcys grafted on silica helices: L- helix-QDs, D-helix QDs, and QDs_l-cys alone and (b) circularly polarised luminescence (CPL) spectra for L- helix-QDs and D-helix-QDs excited at 365nm.

Conclusion:

We described the synthesis of $(ZnS)_{1-x}(AgInS_2)_x$ quantum dots with various ligands, its optical properties and various characterizations. These quantum dots were grafted on amine modified silica helix via electrostatic interaction in different environment and conditions. In the case of ammonium sulphide ligand, we observed that the helical structure of silica was destroyed due to the strong acidity of thiol S^{-2} ion which reacts with Si-O bond. In the case of ligands, 3-mercaptopropionic acid and oleylamine, homogeneous and dense grafting of the QDs were observed and nanohelices became fluorescent, and the nanohelical structure of silica was preserved after their grafting. These hybrid systems did not show induced CD (ICD) from the silica nanohelices to the achiral QDs. In the presence of chiral ligand L-cysteine, quantum dots were used to see chirality induction, however the effect of the mesoscopic chirality of the silica nanohelices on the ICD of L-cysteine to the QDs was not observed.

Experimental Section:

(a) Synthesis of Nanocrystal: Precursor prepared by using the 0.25M concentration of silver nitrate, Indium hydroxide, the mole ratio is as mentioned in the table. Once the precursor is prepared by thermal decomposition reaction carried out with 3.0 cm^3 oleylamine at 180°C for 15 minutes under nitrogen. Once reaction is completed, product centrifuged and collected washed by methanol and re-dispersed in non-polar solvent such as toluene.

(b) Ligand exchange: Ammonium sulphide by phase transfer method the ligand mixed 0.33 ml ligand used for 1 mg of QDs was taken. At room temperature with constant stirring in solvent formamide and nonpolar solvent such as toluene or hexane. Reaction was carried out once the reaction is finished it will be indicate by colour change of polar solvent with respect to colour of QDs. Product in formamide collected and precipitated and washed out by acetonitrile. Re-dispersed in water. Similar strategy was applied on for ligand 3-mercaptopropionic acid and l-cysteine.

(c) QDs grafted silica helix after ligand exchange in Ammonium sulphide (AS)/ 3-Mercaptopropionic acid (MPA)/ L--cysteine: The concentration of amine modified silica 0.5 mg/ml and 10 mg in case of composition. 30 µl of silica (0.0 15mg) mixed with 1 mg /ml of QDs and 8 similar batches were prepared. After mixing the tubes were sonicated for 10 min in water bath and left on bio-shaker overnight for grafting at room temperature. Next day QDs grafted silica washed out several times by water until the supernatant becomes colourless. Here, the mili-q water is used as a solvent for silica helix and QDs.

To adjust pH: 10^{-2} - 10^{-4} M solution of sodium hydroxide, hydrochloric acid and acetic acid were used, respectively.

(d) QDs capped by oleylamine grafted silica helix: Amine modified helices were redispersed in toluene with QDs in order to do direct ligand exchange. The ligand OLA get replaces by the APTES ligand which is there on the surface of silica helices. The QDs replace grafting of QDs was carried in toluene here the concentration of silica is 0.5 mg/ml and 6.0 mg/ml of QDs. The QDs of mixed by 1.0 mg step by step until the suspension becomes saturated with coloured supernatant in each step 6 h gap was maintained and overall reaction

of grafting QDs was carried out 48h. The product was collected by centrifuge and redispersed in toluene.

Reference:

1. Torimoto, T.; Adachi, T.; Okazaki, K.; Sakuraoka, M.; Shibayama, T.; Ohtani, B.; Kudo, A.; Kuwabata, S. Facile Synthesis of ZnS−AgInS 2 Solid Solution Nanoparticles for a Color-Adjustable Luminophore. Journal of the American Chemical Society 2007, 129 (41), 12388–12389. https://doi.org/10.1021/ja0750470.
2. Attoui, M.; Pouget, E.; Oda, R.; Talaga, D.; Le Bourdon, G.; Buffeteau, T.; Nlate, S. Optically Active Polyoxometalate-Based Silica Nanohelices: Induced Chirality from Inorganic Nanohelices to Achiral POM Clusters. Chemistry - A European Journal 2018, 24 (44), 11344–11353. https://doi.org/10.1002/chem.201801905.
3. Cheng, J.; Le Saux, G.; Gao, J.; Buffeteau, T.; Battie, Y.; Barois, P.; Ponsinet, V.; Delville, M.-H.; Ersen, O.; Pouget, E.; et al. GoldHelix: Gold Nanoparticles Forming 3D Helical Superstructures with Controlled Morphology and Strong Chiroptical Property. ACS Nano 2017, 11 (4), 3806–3818. https://doi.org/10.1021/acsnano.6b08723.
4. Jagadeeswararao, M.; Dey, S.; Nag, A.; Rao, C. N. R. Visible Light-Induced Hydrogen Generation Using Colloidal (ZnS) 0.4 (AgInS 2) 0.6 Nanocrystals Capped by S 2− Ions. Journal of Materials Chemistry A 2015, 3 (16), 8276–8279. https://doi.org/10.1039/C5TA01240F.
5. Anderson, N. C.; Hendricks, M. P.; Choi, J. J.; Owen, J. S. Ligand Exchange and the Stoichiometry of Metal Chalcogenide Nanocrystals: Spectroscopic Observation of Facile Metal-Carboxylate Displacement and Binding. Journal of the American Chemical Society 2013, 135 (49), 18536–18548. https://doi.org/10.1021/ja4086758.
6. Knauf, R. R.; Lennox, J. C.; Dempsey, J. L. Quantifying Ligand Exchange Reactions at CdSe Nanocrystal Surfaces. Chemistry of Materials 2016, 28 (13), 4762–4770.
7. Nishida, N.; Yao, H.; Kimura, K. Chiral Functionalization of Optically Inactive Monolayer-Protected Silver Nanoclusters by Chiral Ligand-Exchange Reactions. Langmuir 2008, 24 (6), 2759–2766. https://doi.org/10.1021/la703351p.
8. Tamang, S.; Beaune, G.; Texier, I.; Reiss, P. Aqueous Phase Transfer of InP/ZnS Nanocrystals Conserving Fluorescence and High Colloidal Stability. ACS Nano 2011, 5 (12), 9392–9402. https://doi.org/10.1021/nn203598c.
9. Tamang, S.; Beaune, G.; Texier, I.; Reiss, P. Aqueous Phase Transfer of InP/ZnS Nanocrystals Conserving Fluorescence and High Colloidal Stability. ACS Nano 2011, 5 (12), 9392–9402. https://doi.org/10.1021/nn203598c.
10. Nag, A.; Kovalenko, M. V.; Lee, J.-S.; Liu, W.; Spokoyny, B.; Talapin, D. V. Metal-Free Inorganic Ligands for Colloidal Nanocrystals: S 2– , HS – , Se 2– , HSe – , Te 2– , HTe – ,TeS 3 2– , OH – , and NH_2 – as Surface Ligands. Journal of the American Chemical Society 2011, 133 (27), 10612–10620. https://doi.org/10.1021/ja2029415.
11. Kim, E.; Ruankham, P.; Lee, J.; Hachiya, K.; Sagawa, T. Ag–In–Zn–S Quantum Dots for Hybrid Organic–Inorganic Solar Cells. Japanese Journal of Applied Physics 2016, 55 (2S), 02BF06. https://doi.org/10.7567/JJAP.55.02BF06.
12. Powder Diffraction File; The JCPDS International Centre for Diffraction Data: Swarthmore, PA, 1990; No. 251330.
13. Powder Diffr. file; the JCPDS International Centre for Diffraction Data: Swarthmore 1990, No.50566.
14. Shukla, N.; Liu, C.; Jones, P. M.; Weller, D. FTIR Study of Surfactant Bonding to FePt Nanoparticles. Journal of Magnetism and Magnetic Materials 2003, 266 (1–2), 178–184.

https://doi.org/10.1016/S 0304-8853(03)00469-4.
15. Théo Chevallier. Photoluminescence et couplage plasmonique des nanocristaux d'AgInS2-ZnS. Science des matériaux [cond-mat.mtrl-sci]. Université Grenoble Alpes, 2015. Français. ⟨NNT : 2015GREAY092⟩.
16. Lifson, S.; Hagler, A. T.; Dauber, P. Consistent Force Field Studies of Intermolecular Forces in Hydrogen-Bonded Crystals. 1. Carboxylic Acids, Amides, and the C:O.Cntdot..Cntdot..Cntdot.H- Hydrogen Bonds. *Journal of the American Chemical Society* **1979**, *101* (18), 5111–5121. https://doi.org/10.1021/ja00512a001
17. Pengo, P.; Polizzi, S.; Pasquato, L.; Scrimin, P. Carboxylate−Imidazole Cooperativity in Dipeptide-Functionalized Gold Nanoparticles with Esterase-like Activity. *Journal of the American Chemical Society* **2005**, *127* (6), 1616–1617. https://doi.org/10.1021/ja043547c.
18. Chandra, S.; Das, P.; Bag, S.; Laha, D.; Pramanik, P. Synthesis, Functionalization and Bioimaging Applications of Highly Fluorescent Carbon Nanoparticles. *Nanoscale* **2011**, *3* (4), 1533. https://doi.org/10.1039/c0nr00735h.
19. Zheng, Y.; Duanmu, C.; Gao, Y. A Magnetic Biomimetic Nanocatalyst for Cleaving Phosphoester and Carboxylic Ester Bonds under Mild Conditions. *Organic Letters* **2006**, *8* (15), 3215–3217. https://doi.org/10.1021/ol061098a.
20. Reiss, P.; Protière, M.; Li, L. Core/Shell Semiconductor Nanocrystals. *Small* **2009**, *5* (2), 154–168. https://doi.org/10.1002/smll.200800841.
21. Kumar, J.; Kawai, T.; Nakashima, T. Circularly Polarized Luminescence in Chiral Silver Nanoclusters. Chemical Communications 2017, 53 (7), 1269–1272. https://doi.org/10.1039/C6CC09476G.
22. Huo, S.; Duan, P.; Jiao, T.; Peng, Q.; Liu, M. Self-Assembled Luminescent Quantum Dots To Generate Full-Color and White Circularly Polarized Light. *Angewandte Chemie* **2017**, *129* (40), 12342–12346. https://doi.org/10.1002/ange.201706308.
23. Purcell, A. R. T.; T Seideman, T.; Modeling the Chiral Imprinting Response of Oriented Dipole Moments on Metal Nanostructures ACS Photonics 2018, 5, 4801-4809. DOI: 10.1021/acsphotonics.8b00911.
24. Gao, X.; Zhang, X.; Zhao, L.; Huang, P.; Lv, J.; Qiu, X.; Wei, H.-S.; Tang, Z.; Distinct Excitonic Circular Dichroism between Wurtzite and Zincblende CdSe Nanoplatelets. Nano Lett. 2018, 18, 6665-667. DOI: 10.1021/acs.nanolett.8b01001

Chapter 4: Synthesis and characterization of fluorescent polymer particles, and polymer coated chiral silica template

Chapter 4: Synthesis and characterization of fluorescent polymer particles, and polymer coated chiral silica template

Table of contents

4. Introduction

The brief description about the roles of polymers in chiral supramolecular structures was given in chapter 1. The application of optically active polymers became a hot topic in recent years. Some popular applications of chiral polymers include their use in molecular recognition, molecular scaffold approach with controlled alignment of functional group such as chromophores locally, or in the solid state which can lead to liquid crystal materials.

In this chapter, we will demonstrate the synthesis of polymer particles by one step polymerization and their coating on the surface of silica nanohelices. The polymer particles were synthesized from various monomers such as 2,6 dihydroxynaphthalene (DHN), 2,6-dihydroxy anthracene (DHA) and 9,9-bis(4-hydroxyphenyl)fluorene (BHF) by one step polymerization using microwave reactor with different size range between 30 -300nm. These polymer particles are fluorescent similar to inorganic quantum dots unbounded to size. The size of these organic polymer particles can be controlled by playing with parameters. More in detail, 2,6-dihydroxy anthracene (DHA) polymer nanoparticle were studied. These particles have high quantum yield, and their optical properties were studies in a different environment. **The work presented here was performed by Hiroki Noguchi, Nobuo Yamada, and myself and led to a publication as it is described later. My contribution in this part of the chapter is mainly on the synthesis of DHA nanoparticles**

In the second part, by using the same technique of one-step polymerization the polymer coated on the surface of chiral nano-helical silica. The monomer 2,6-dihydroxy anthracene (DHA) was used for polymerization. These polymerized particles were used for their coating on the surface of silica nanohelices. **For this part of the chapter, all the work presented here was done by me and a publication is submitted as described later.**

4.1 Synthesis and characterization of polymer nanoparticles with different monomer.

The fluorescent nanoparticles have attracted attention in the last two decades. [1-4] Their application has a wide range in the photonics, biosensors, cell labelling, optical signals, etc. In the previous chapters we have discussed the fluorescent quantum dots which are very well known for their unique features and used in many applications such as solar cell, displays, optical devices, and many more. [5-8] However, they have limitations in terms of stability and quenching. Also their dispersion in various solvents can lead to the modification of the particle parameters. Therefore, to overcome these barriers, the other alternative is to make organic fluorescent particles free from heavy metals, halogens, toxic elements.

Fluorescent quantum dots from organic molecules are fabricated in two ways: Doping of dyes in nano-size carriers as colloidal silica, magnetic nanoparticles, and graphene. [9-12] The other way is to introducing luminophore at the side chain of monomer, which can be polymerized. [13] However, in the case of doping of dyes there are unavoidable barriers to overcome such as quantification of dyes in the carriers to be introduced, prevention elution of the dyes, complex structures and low stability of dyes in the systems.

Here, we introduced an innovative way to solve such problems. Original organic nanoparticles composed of monomers such as naphthalene, anthracene, fluorine, etc., are produced as the main chain skeleton without a heterocyclic structure. Therefore, they are not prepared from doping of dyes or by branching them synthetically to a polymer side chain as compared available luminescent particles. [14, 15, 16] In short, this unique method involves a polymerization reaction by a one-pot, one-step process that produces spherical particles with sizes from the nanoscale to microscale. The final product was collected and purified by using centrifuge in respective solvents, without any surfactant. The emergence of fluorescence occurs from the polymer main chain, no carrier is present, or elution phenomena occurred. The monomer are 2,6 -dihydroxynapthalene (DHN), 2,6-dihydroxy anthracene (DHA) and 9,9-bis(4-hydroxyphenyl)fluorene (BHF) with cross-linkers 1,3,5-trimethyl-1,3,5-triazinane (TMTA), hexamethylenetetramine (HMT), respectively by one-pot synthesis. The

scheme for one-pot synthesis is as shown in figure 4.1.1. (**In the context of my thesis, I performed the synthesis of DHA nanoparticles**)

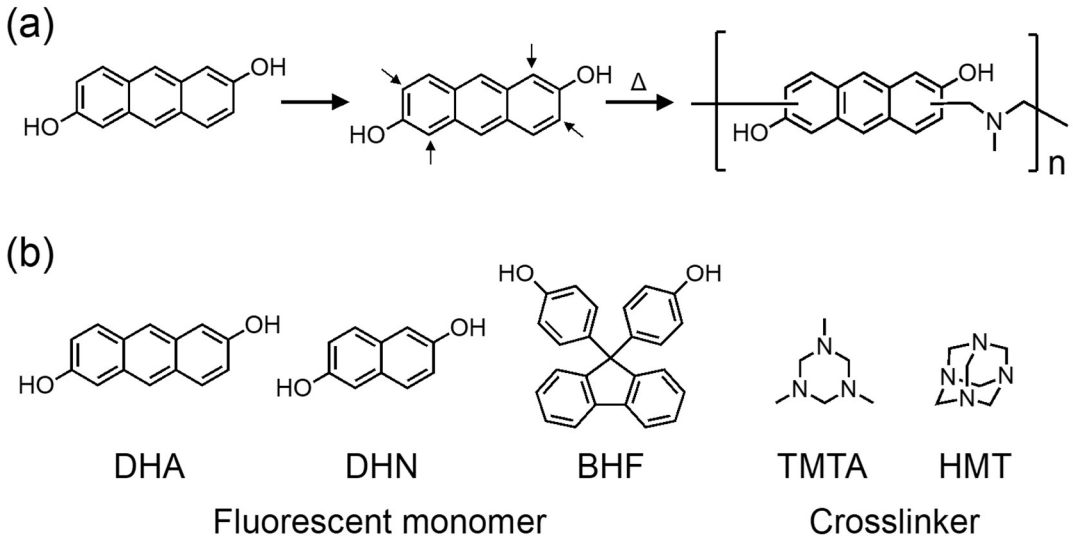

Figure 4.1.1: One-post synthesis of formation of polymer particle: (a) Estimated reaction mechanism between the monomer and the cross-linker, and (b) Chemical structure of monomers and cross-linkers.

The particle size was measured by TEM images (figure 4.1.2). The size of the particle depends on various factors such as the monomer concentration, type of monomer and solvent used to synthesize the polymer particles. Table 4.1 represents the reaction parameters concerning particle size. The reaction was carried out in the microwave reactor with a constant time for three minutes, and by varying the temperature. (**For the rest of the characterizations of polymer nanoparticles were performed by M. Yamada and Dr. Noguchi**)

Table 4.1: Reaction parameters and the average size of the polymer particle.

Abbreviation	Monomer		Crosslinker		Solvent Mixture	Solvent ratio [a]	Temperature (°C) [b]	Diameter (nm) [c]
	Type	mM	Type	mM				
Ant10-T_8W_2	DHA	10	TMTA	10	T: W	8:2	150	30
Ant20-T_8W_2	DHA	20	TMTA	20	T: W	8:2	150	86
Ant30-T_8W_2	DHA	30	TMTA	30	T: W	8:2	150	103
Ant10-D_8W_2	DHA	10	TMTA	10	D: W	8:2	150	39
Ant20-D_8W_2	DHA	20	TMTA	20	D: W	8:2	150	123
Ant10-E_8W_2	DHA	10	TMTA	10	E: W	8:2	150	167
Naph30-E_5W_5	DHN	30	TMTA	30	E: W	5:5	150	434
Flu30-E_8W_2	BHF	30	HMT	30	E: W	5:5	200	315

[a] Solvent ratio, [b] the temperature was maintained for 3 min in a microwave reactor. [c] Particle diameters were determined from TEM images using image analysis software.
Solvent: T- THF, D-DMF, E-Ethanol, W-water.

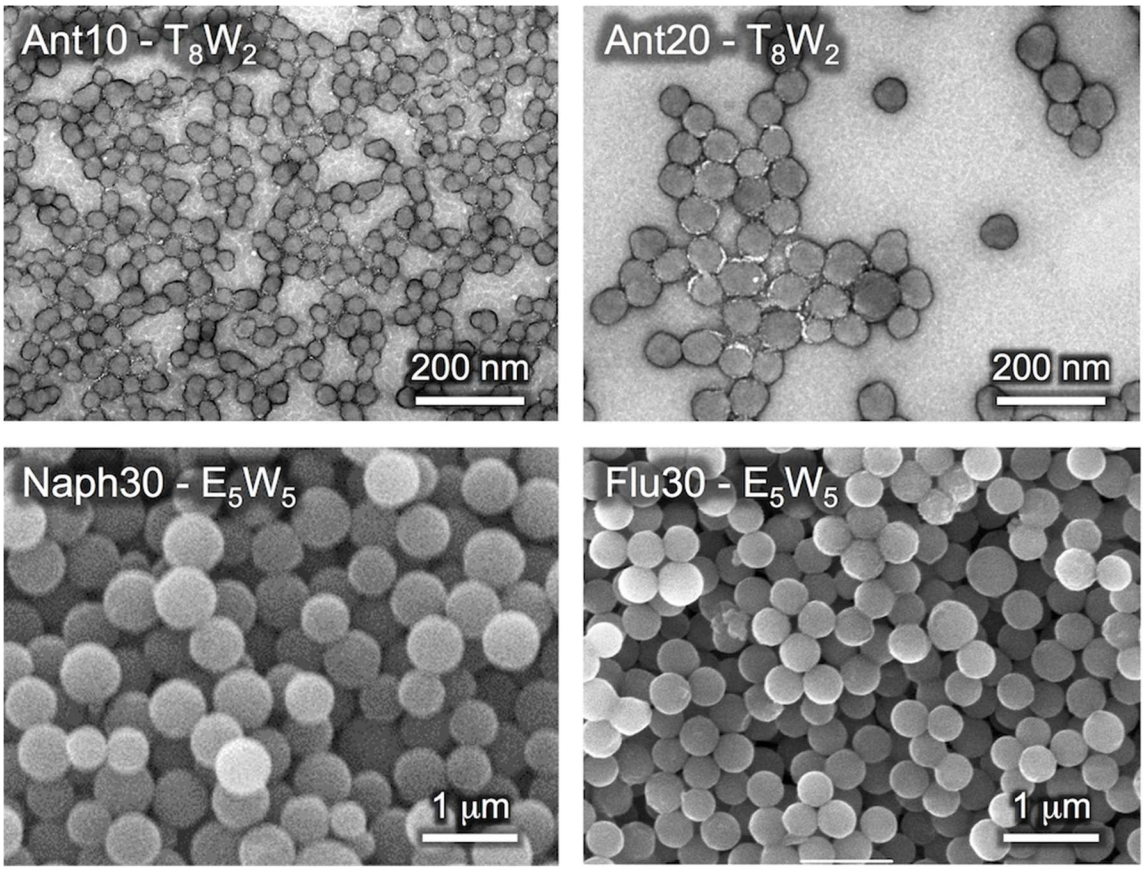

Figure 4.1.2: TEM images: (A) Ant10-T_8W_2 nanoparticles and (B) Ant20-T_8W_2 nanoparticles stained with 1.0 wt% uranyl acetate for TEM, SEM images : (C) Naph30-E_5W_5 nanoparticles and Flu30-E_5W_5 nanoparticles were coated by osmium oxide with the thickness of 5nm.

We found that the monomers DHN and BHF with respective cross-linkers TMTA and HMT, the particle size was found to be larger than the monomer 2,6-DHA. Therefore, our primary focus was on the properties of 2,6-DHA particles due to size variations.

(C)

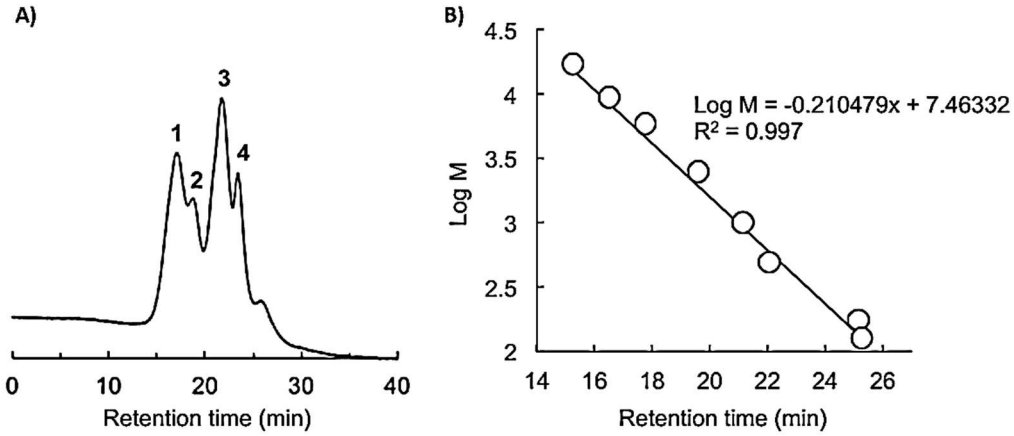

Table 4.2: Data from size exclusion chromatography

No.	tR (min)	Mn	Mw	Mw/Mn	Polymerization degree
1	17.1	8128	9919	1.22	37
2	18.8	2890	3047	1.05	11
3	21.7	805	922	1.14	3
4	23.4	286	307	1.07	1.1

Figure 4.1.3: (A) Size exclusion chromatography of washed out supernatant of Ant10-T_8W_2 nanoparticles, (B) plot for retention time vs Log M, and (C) Table 4.2: Data from size exclusion chromatography.

Size exclusion chromatography was performed on the unreacted molecules after the polymerization reaction to create nanoparticles. The degree of polymerization was calculated from molecular weight M_w of polymer $C_{17}N_1H_{15}O_2$. In the case of Ant10-T_8W_2, the oligomers with molecular weight < 9900 were found (figure 4.1.3), higher molecular weight oligomers or polymer were not found.

The scheme 1a of the expected reaction mechanism indicates that there are multiple reaction sites in the monomer. For 2,6-DHA monomer, since there are four active sites at the 1st, 3rd, 5th and the 7th carbons directly located next to the phenoxy group, the cross-linker, $-CH_2N(CH_3)CH_2-$ as an active species, can react with an anthracene ring at multiple positions. [17, 18, 19] On the other hand, the elementary analysis of 2,6-DHA nanoparticles shows that

the measured value of C/N ratio are found to be similar to the theoretically calculated values as the composition ratio of the anthracene component and $-CH_2N(CH_3)CH_2-$ to be 1:1.

Table 4.3: The elementary analysis of DHA-based nanoparticles in different solvents.

Abbreviation	C %	N %	H %	C/N	DHA content %
Ant10-T_8W_2	76.54	5.93	4.70	12.91	75.4
Ant10-D_8W_2	78.02	5.59	3.89	13.96	77.5
Ant10-E_8W_2	77.89	6.02	4.03	12.94	75.5
Calculated	76.96	5.28	5.70	14.58	79.2

It is reasonable to estimate that anthracene and $-CH_2N(CH_3)CH_2-$ are alternately polymerized at 1:1, but since DHA contains four active sites, it seems that multi-crosslinking partially progresses. This presumed structure corresponds well with the fact that the produced nanoparticles are insoluble and swell in various solvents. Therefore, the particles produced should be classified as "gel" type one. Due to the complicated crosslinking structure, the exact chemical structure has not yet been identified. The elementary analysis results indicate that the fluorescent component concentration remains high in the particle. For example, it was estimated that the anthracene contents were 75.4 wt% in the Ant10-T_8W_2 nanoparticles, 77.5 wt% in the Ant10-D_8W_2 nanoparticles and 75.5 wt% in the Ant10-E_8W_2 nanoparticles whereas the theoretical estimated value in the 1-1 polymer was 79.2 wt %. This is the first example of nanoparticles in which the fluorescent component can be immobilized at such high values. As described above, this cannot be realized in the conventional organic particles prepared by doping or side chain branching methods. These nanoparticles were found to be insoluble but well dispersible in various solvents such as water, methanol, ethanol, DMF, DMSO, ethyl acetate, THF, toluene, and chloroform.

4.1.1 Polymer-nanoparticle dispersity in an aqueous media:

Since all of the produced nanoparticles also exhibited good dispersibility in (good compatibility with) an aqueous system, it could be inferred that polar groups exist on the particle surface. By analysing the reaction route shown in Scheme 1, it is considered that tertiary amine due to $-CH_2N(CH_3)CH_2-$as well as phenolic OH groups remained on the particle surface. To support these estimations, Figure 4.1.1.1 shows that Ant_{10}-T_8W_2 particles disperse in an aqueous solution with a wide range of pH. The solutions exhibited an orange color in an acidic aqueous solution and a red-purple color in an alkaline aqueous solution.

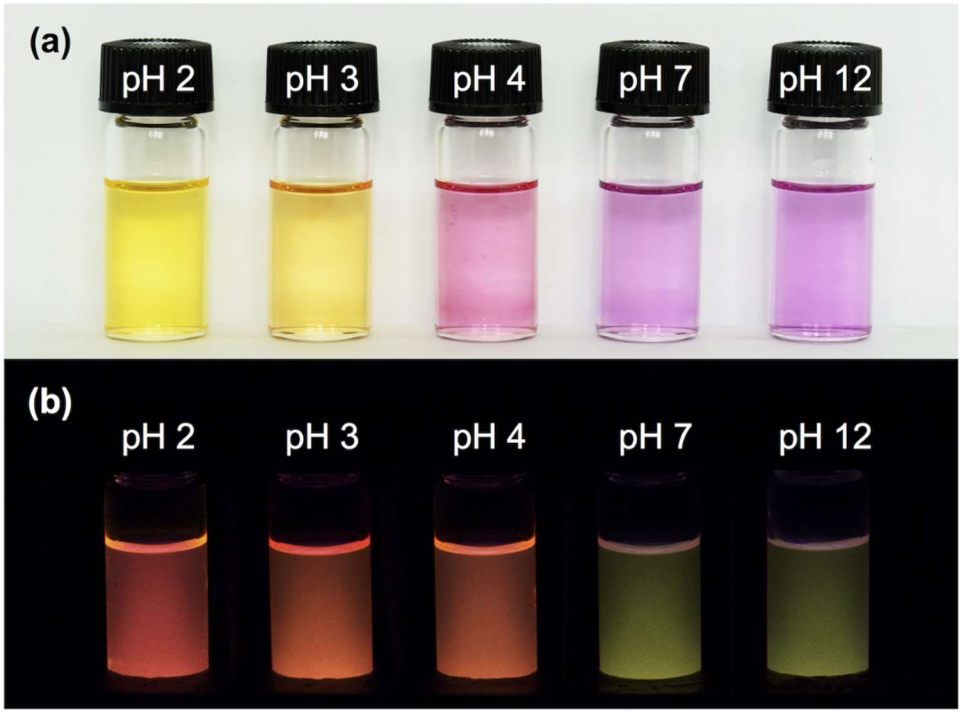

Figure 4.1.1.1: Ant10-T_8W_2 nanoparticles pH dependency in an aqueous media, (a) under normal light (b) excitation at 365nm.

The ξ – potential measurement result shows that it can be seen that the Ant10-T_8W_2 particles are positively charged under acidic conditions and negatively charged under alkaline conditions. That is, Ant10-T_8W_2 are ampholytic. Accordingly, the fluorescence color also varied with the pH. As shown in 4.1.1.1, a yellow-green color (λem = 546 nm) under alkaline conditions and a red-orange color (λem = 620 nm) under acidic conditions were observed

when the solutions were excited at 365 nm. This color change can be attributed to the structural change (pI = 5.5) between the states I and II indicated in Figure 4.1.1.2

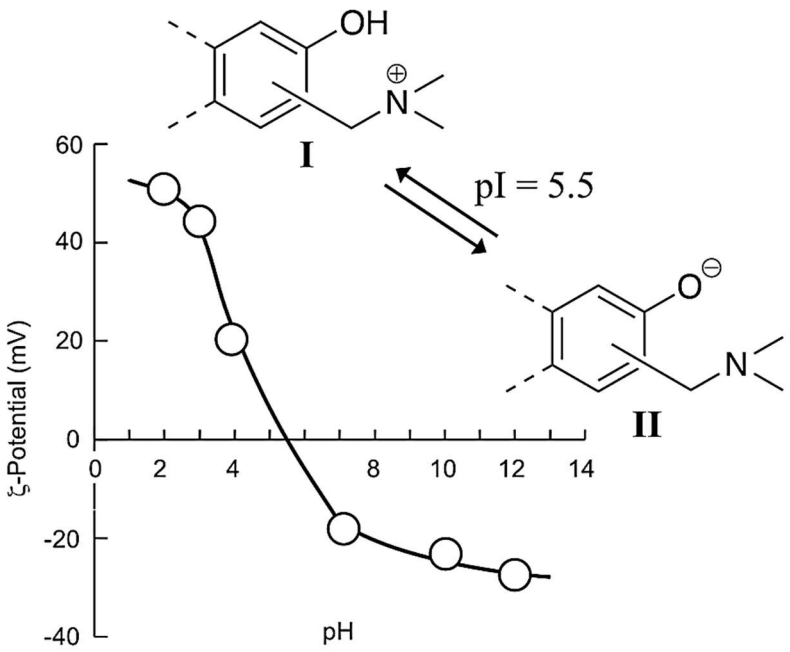

Figure 4.1.1.2: ξ - potential plot of Ant10-T_8W_2 nanoparticles in different pH in an aqueous media.

4.1.2 Optical properties of polymer nanoparticles:

The nanoparticles prepared from different monomers exhibit fluorescent properties. Here, we will discuss more in details about 2,6-DHA nanoparticles. In the case of 2,6-DHA nanoparticles, the monomer itself is fluorescent. Figure 4.1.2.1 represents the UV-visible absorbance and emission spectra of monomer and nanoparticle, respectively. The absorbance peak in case of the nanoparticle is different from the absorbance of monomer with the emergence of the new peaks between 475 nm – 700nm (figure 4.1.2.1a).

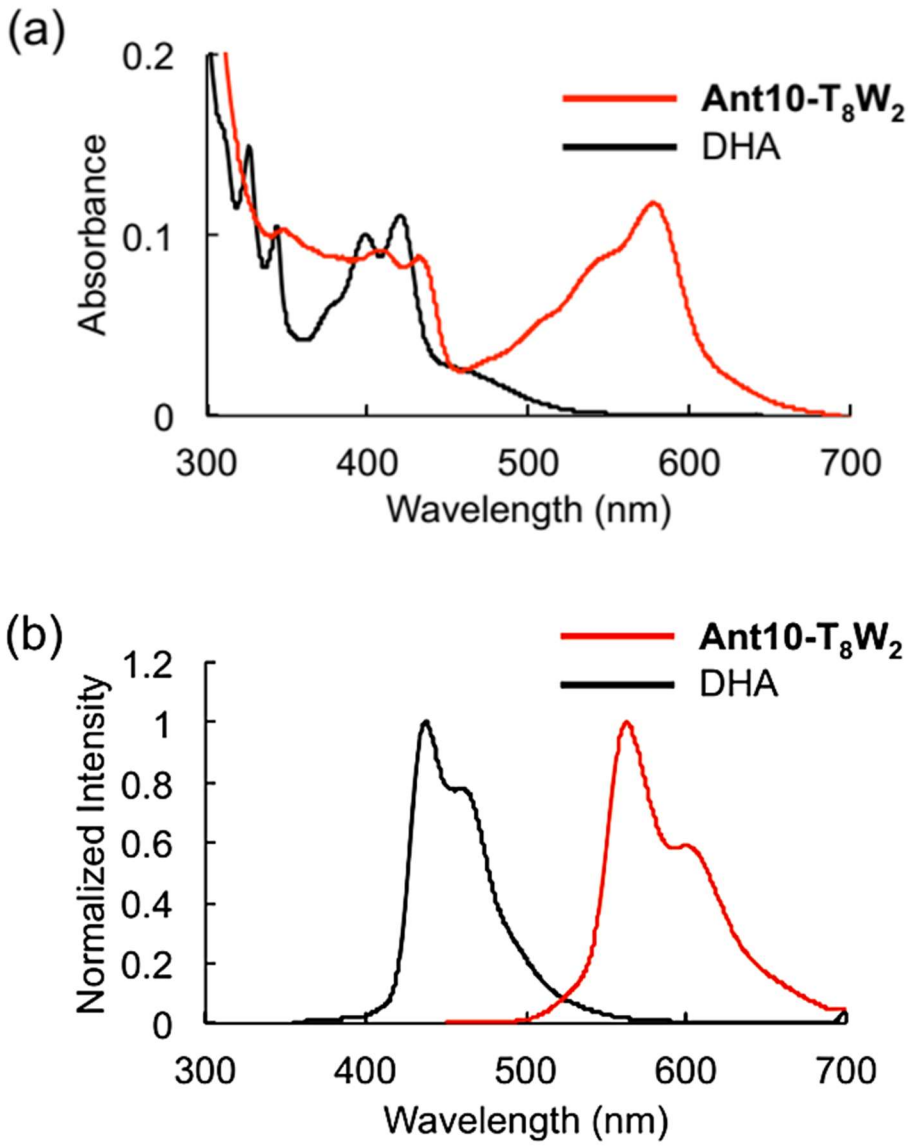

Figure 4.1.2.1: Optical properties: (a) UV-visible absorbance spectra, (b) Emission spectra excited at 350nm in particular cases of monomer 2,6-dihydroanthracene and Ant10-T_8W_2 nanoparticles in DMF.

The DHA-based nanoparticles have sufficient hydrophobicity to be dispersed in an organic solvent, and thus, they exhibit an amphiphilic nature: they can be dispersed in both water and organic solvents. Figure 4.1.2.1a shows that Ant10-T_8W_2 is dispersed in various organic solvents to produce a clear solution. The high transparency can be about a result of not only reduced agglomeration but also the fact that the refractive index of the organic nanoparticles is close to that of the solvent although strong light scattering is often observed in inorganic nanoparticles with a high refractive index.

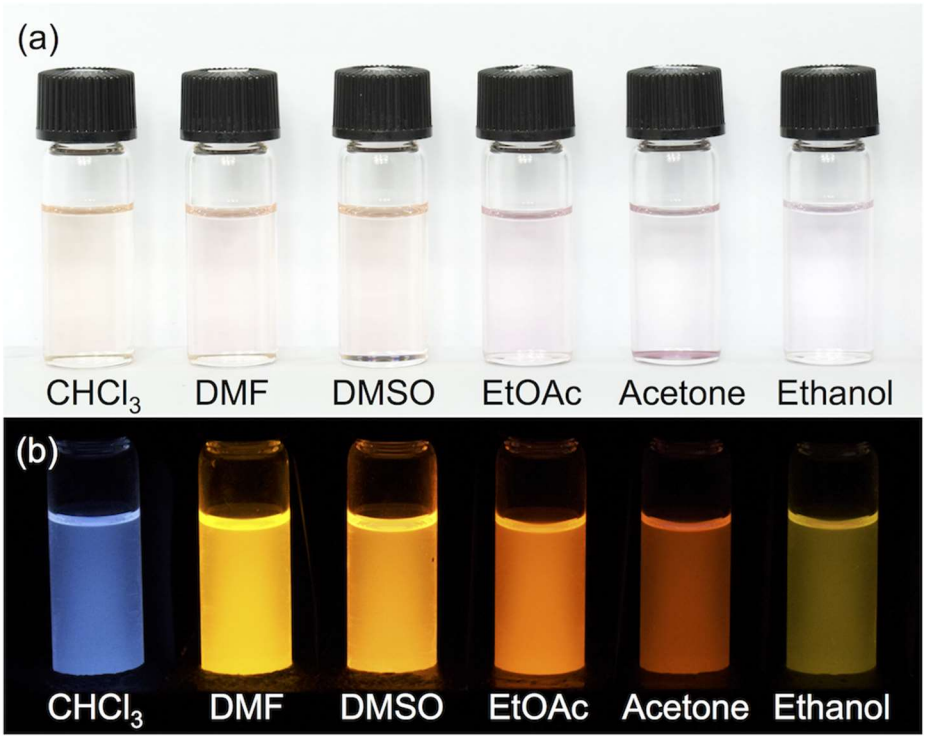

Figure 4.1.2.2: Ant10-T_8W_2 nanoparticles dispersed in different organic solvents (5.0 $mgml^{-1}$): (a) Under normal light, (b) excited at 365 nm. EtOAc: ethyl acetate.

Figure 4.1.2.2 shows the luminescence color of **Ant10-T_8W_2** dispersion in organic solvents upon irradiation with UV light of 365 nm. Interestingly, the luminescence color depended remarkably on the type of solvent. Therefore, we focused on the mixed solvent systems, i.e., DMF-chloroform or ethyl acetate-chloroform systems, which had the most different luminescence colors, and the relationship between the composition ratio and luminescence color was investigated. As evident from Figure 4.1.2.3, the solvent change induced remarkable difference of the emission bands when the dispersions were excited at 350 nm: λ_{em} appeared at 437 nm in chloroform, but they were observed at 116 - 127 nm longer wavelengths such as 564 nm and 553 nm in DMF and ethyl acetate, respectively. Such a fluorescence solvatochromism [20] is a typical phenomenon in which a Stokes shift appears

due to the influence of the polarity, viscosity, etc., of the solvent in contact with the fluorescent unit.

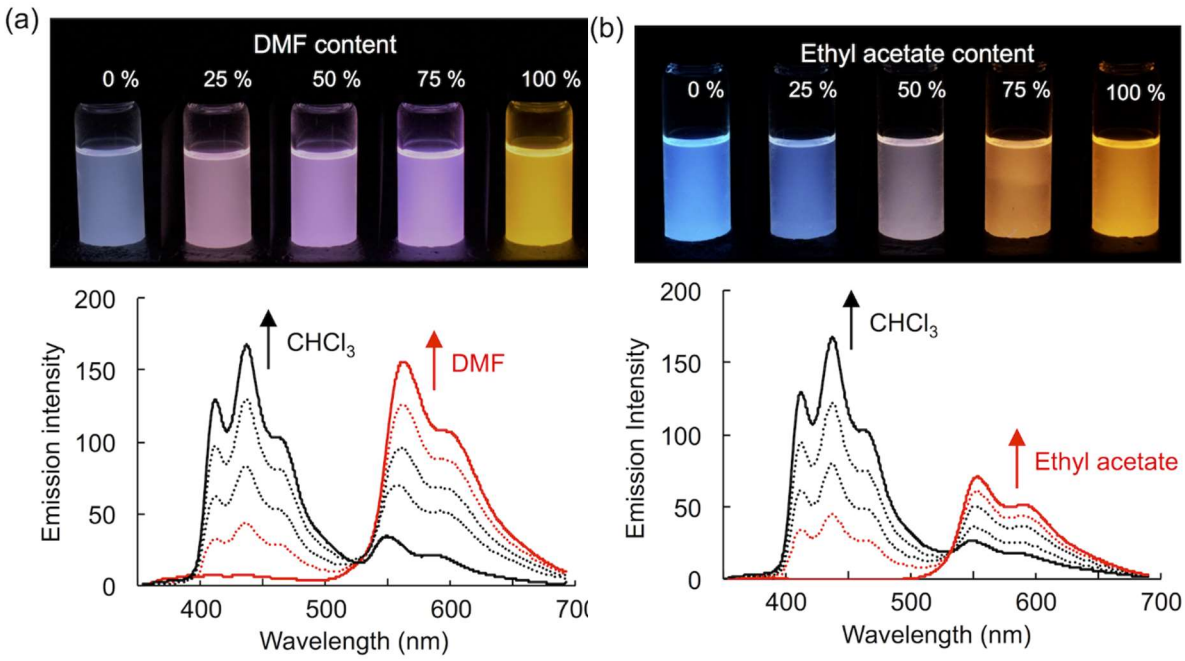

Figure 4.1.2.3: Ant_{10}-T_8W_2 nanoparticles dispersed in (a) chloroform and DMF mixtures and (b) chloroform and ethyl acetate mixtures with emission spectra, respectively.

As it was clear from figure 4.1.2.2, the fluorescent intensity was dependent on the solvent. Also, this can be explained to be a result of the difference in the swelling degree. When plotting the swelling degree and the relative quantum yield (QY) to the monomer (Figure 4.1.2.4), it was revealed that a high QY was observed under a high swelling degree. For example, the highest QY (108 %) was observed for the highest swelling degree (8.0) in DMF, and the lowest QY (0.4 – 12) was observed in water, in which the swelling degree was in 2.2 – 2.5. This suggests that the swelling property of the nanoparticles promotes the isolation of the polymer main chain, which is a luminescent component, and the luminescence efficiency becomes closer to that of the monomer as the isolation progresses. However, the relative QY of Ant10-T_8W_2 in DMF reached 108 %, which was a little higher than that in monomeric DHA. This is estimated to be because the fluorescent component is completely isolated in DMF and also because the $-CH_2N(CH_3)CH_2-$ moiety can act as an auxochrome group for the anthracene moiety.

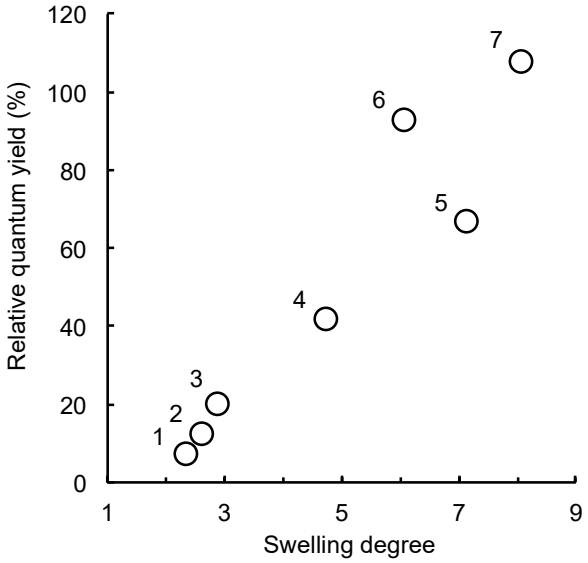

Figure 4.1.2.4: Correlation plots between swelling degree of polymer particle and relative quantum yield of Ant10-T_8W_2 to DHA in various solvents. 1: Water (pH 12), 2: water (pH 2), 3: ethanol, 4: ethyl acetate, 5: DMSO, 6: chloroform, 7: DMF.

Table 4.4: Fluorescent properties of polymer particle with size variation and monomer in various solvents.

Solvent	Diameter nm	Swelling degree	Quantum yield (λ_{em})	
			Monomer	Particle
None	30	1.0	-	-
Water (pH 2.0)	75	2.5	21 (434)	12 (620)
Water (pH 12.0)	67	2.2	5 (513)	0.4 (546)
Ethanol	83	2.8	17 (433)	20 (549)
DMF	241	8.0	22 (436)	108 (564)
DMSO	212	7.1	22 (440)	67 (563)
Ethyl acetate	140	4.7	18 (434)	42 (553)
Chloroform	180	6.0	20 (531)	92 (437)

The calculation of quantum yield (QY) was determined from uv-absorbance and emission spectra area calculated by integration,

$$QY = QY_{st} \frac{I_x A_{st}}{I_{st} A_x} \frac{n_x^2}{n_{st}^2}$$

Where, abbreviation A - absorbance, I - integrated emission spectra, n - refractive index, and subscript 'st'- quinine sulphate, subscript 'x'- samples. The QY of quinine sulphate was 54% as a measurement standard was dissolved in 0.1M H_2SO_4 aqueous solution (λ_{ex} -350 nm).

On the other hand, it is not easy to explain the complicated red shift in the DHA particles comparing with the monomer. One of the possible explanation is considered by an aggregation effect among the anthracene moieties. However, dilution with good solvents such as DMF promoted the solvation of an anthracene moiety to increase the fluorescent intensity as shown in Table 4.4 and figure 4.2.1.4, therefore an aggregation-induced red shift is not suitable for our results. The other possible mechanism for the red shift can be induced by an electron-donating, auxochromic effect due to the substitution of $–CH_2N(CH_3)CH_2–$ moiety onto the anthracene ring. However, the substitution positions as well as the number of the substituents per an anthracene ring could not be identified while they were determined to occur at 2 - 4 positions according to the elemental analysis (Table 4.3). In addition, the $–CH_2N(CH_3)CH_2–$ moiety can be a cause of ring expansion to expand π-conjugated structures.[18, 21] Therefore, it is reasonable why the DHA particles exhibit complicated absorption bands in the wide range up to 450 nm as well as the specific absorption around 575 nm.

Due to the swelling property of nanoparticles and high dispersity, these particles can be utilized to create thin films. By using poly(methyl methacrylate) (PMMA) incorporating emissive nanoparticles in the form of thin films are created (figure 4.1.2.5).

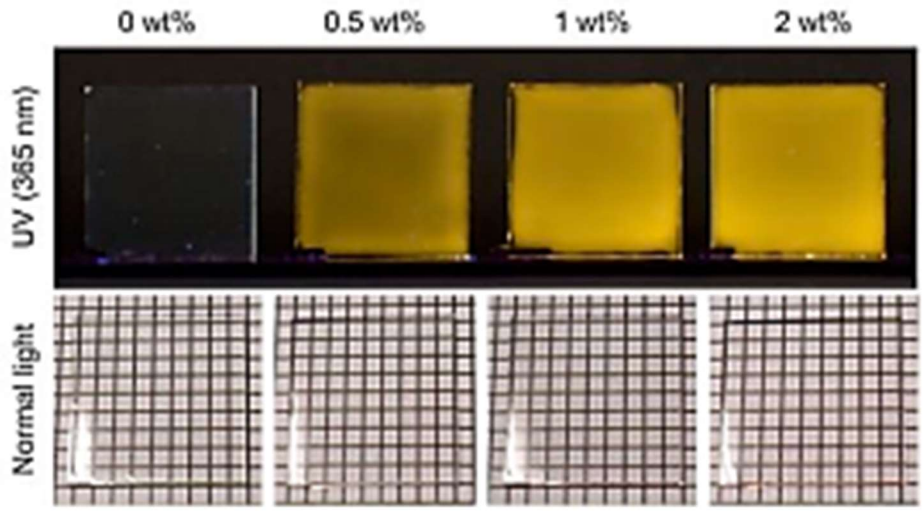

Figure 4.1.2.5: Normal and emitted photo images of Ant10-T_8W_2 (0 ~ 2 wt%) containing PMMA films. Composite films were prepared by casting on a glass plate from Ant10-T_8W_2 and PMMA dispersed in ethyl acetate excited at 365 nm.

An article was published based on the results of polymer particles entitled as:

Emission color control in polymer film by memorized fluorescence solvatochromism due to a new class of totallyorganic fluorescent nanogel particles.' Chemistry- A European Journal, 2019. https://doi.org/10.1002/chem.201901239.
Nobuo Yamada, Hiroki Noguchi, Yoshifumi Orimoto, Yutaka Kuwahara, Makoto Takafuji, Shaheen Pathan, Reiko Oda, Almara Mahammadali Rahimli, Mahammadali Ramazanov, and Hirotaka Ihara.

4.2 Fabrication of polymer coated nanohelical silica.

In the previous section, we studied in detail the polymer particles synthesized from different monomers. In this section, our focus is on the fabrication of emissive polymer coated silica nanohelices to induce chirality on their optical properties. This approach was inspired based on the fact that the polymerization of 1,5-dihydroxynaphthalene through crosslinking with 1,3,5-trimethyl-1,3,5-triazinane (TMTA) produces black polymers from a ring extension reaction leading to carbon-like structures. [18] The monomer 2,6- Dihydroxyanthracene(DHA) with the cross-linker 1,3,5-trimethyl-1,3,5-triazinane (TMTA), were used. The polymerization occurs on the surface of bare silica helix. The scheme for the polymer coating is represented in figure 4.2.1**. All the work presented here was performed by myself.**

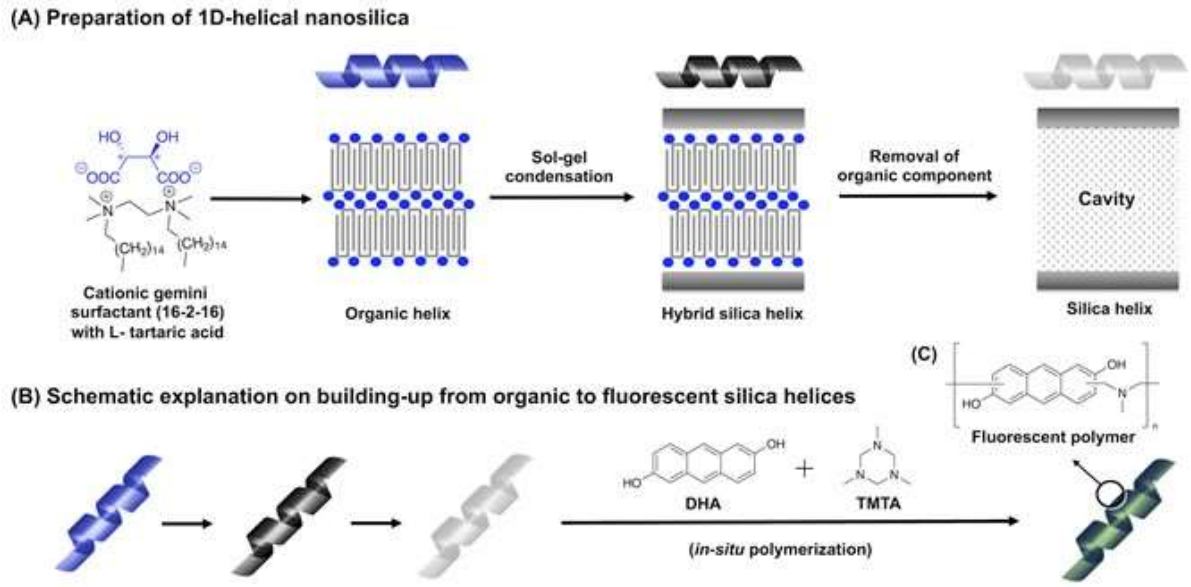

Figure 4.2.1: Schematics of polymer coated silica helix.

4.2.1. 2,6- Dihydroxyanthracene polymer coated nano-helical silica:

In the section 4.1, we discussed about the 2,6- DHA polymer nanoparticles which are highly fluorescent with good quantum yield. Therefore, it can be a good candidate to induce chirality on their optical properties using silica nano helices as templates. The fluorescent polymer-coating on the nanosilica helices was carried out as follows: 2,6-dihydroxyanthracene (2,6-DHA) was used as the main monomer for fluorescent functionalization (Figure 4.2.1B). This approach was inspired based on the fact that the polymerization of 1,5-dihydroxynaphthalene through crosslinking with 1,3,5-trimethyl-1,3,5-triazinane (TMTA) produces black polymers from a ring extension reaction leading to carbon-like structures,[18] whereas the corresponding 2,6-isomer provides colored and fluorescent polymers. [22] Based on these findings, the hybridization of 1D helical nanosilica with a fluorescent polymer was achieved. The nanosilica and 2,6-DHA (1 mM) were mixed at a 1 : 1 weight ratio in ethanol. TMTA was added to the mixture, and polymerization was then conducted at 150 ˚C for 5 min using a microwave reactor. The product was collected through centrifugation, purified with ethanol, and washed several times until the supernatant became colorless despite the initial reddish color of the supernatant.

It was confirmed that the 1D morphology with a helical form was maintained after the polymerization process. Similar procedures were performed using water or a mixture of water and THF, although the helical structures collapsed in these solvent systems. This is probably caused by the alkaline behavior of the TMTA, where the pH of the solvent system was between 8.5 and 9.0, thereby leading to a hydrolysis of the Si-O bonds. Based on these fundamental results, we used ethanol without water as a solvent to perform polymerization. Ethanol was considered as the best solvent for the stability of helical nanosilica.

The color of the product obtained was brownish green (Figure 4.2.2a) after drying, and the TEM images show only a helical morphology (Figure 4.2.2c) similar to the original nanosilica helices. Therefore, the change in color from white to brownish green can be explained by the coloration of the nanosilica. By comparing their detailed morphologies before and after polymerization, the diameter, width, and thickness of the product slightly increased in the original silica, whereas there was no significant change in the helical pitch, as shown in Table 1. Figures 4.2.2B and 4.2.2C show transmission electron microscopy (TEM) images of the nanosilica obtained, of which the diameter and helical pitch were determined

to be 30 and 69 nm (Table 4.2.1), respectively. The other parameters (Table 4.2.1) include a width and thickness of 29 and 15 nm, respectively, which were measured based on the scheme shown in the TEM image of Table 4.2.1.

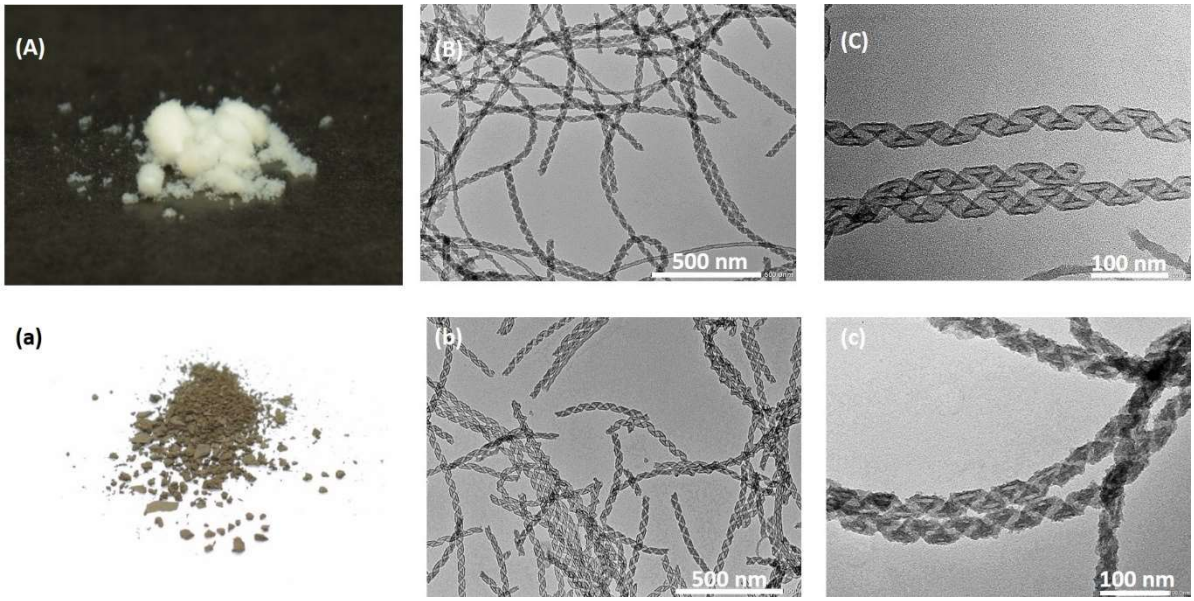

Figure 4.2.2: (A) White powders from bare silica helices and (B-C) their TEM images. (a) Brownish green powders from the polymer-coated silica helices and (b-c) their TEM images.

Table 4.2.1 Comparison of the measured parameters on silica helices before and after polymerization.

Parameters	Bare silica nanohelices (nm)	Polymer coated nanohelices (nm)	Change nm
Diameter	30	34	4
Pitch	69	68	1
width	29	33	4
thickness	15	17	2

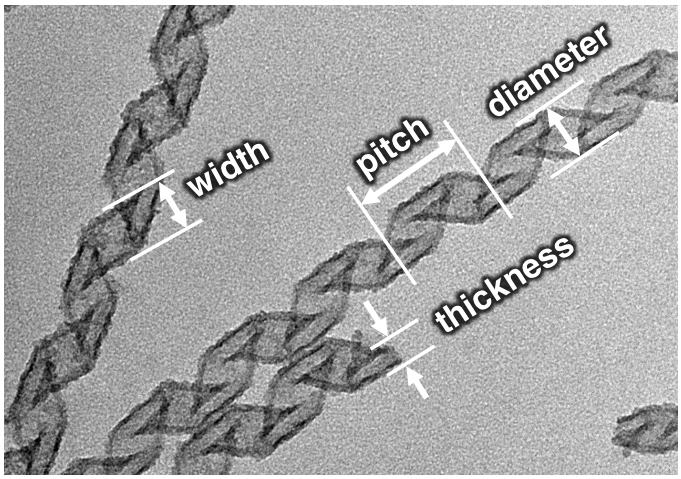

Figure 4.2.3: Schematics of measurement of parameters in TEM images.

The mechanism of polymer deposition on the silica is yet to be determined because 2,6-DHA has four reactive sites at the next positions (1-, 3-, 5- and 7-positions) of the phenolic carbon, although it is estimated that two distinct mechanisms may be possible: first, through direct polymerization on the silica surface, and second, through a deposition of the produced oligomers onto a silica surface. Both processes likely occur competitively through a weak interaction between the Si-OH and nitrogen atoms of a cross-linker. The estimated reaction between the monomer DHA and cross-linker is as shown in the figure 4.2.4.

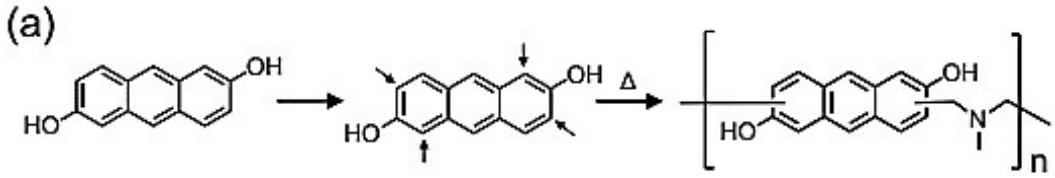

Figure 4.2.4: Estimated reaction scheme of polymer.

An elemental analysis promotes further discussion regarding this problem. The estimated chemical structure of the polymer is shown in Figure 4.2.4. If the polymerization involves a one-to-one addition reaction based on the estimated structure (Figure 4.3.2), the C/N value should be 14.58 based on $C_{14}H_{10}O_2$ and $CH_2N(CH_3)CH_2$ from 2,6-DHA and TMTA; however, the observed C/N value was 10.15 in the polymer@silica helices, where the C and N contents were 14.42% and 1.42%, respectively. This increase in the N content suggests multiple introductions of $CH_2N(CH_3)CH_2$ on the anthracene moiety leading to the promotion

of crosslinking structures. These results indicates the presence of polymer on the surface of silica helices.

ξ-potential analysis:

A ξ-potential analysis provides additional information on the surface structure. Therefore, the ξ-potential analysis was performed on bare silica and polymer coated silica nanohelices. The bare silica helices exhibited +14 ± 1.5 and -25 ± 2.5 mV at pH 4 and 8.5, respectively, which could be explained by the presence of $Si^{+}OH$ and SiO^{-}. In contrast, the distinct increases in these values were observed to be +21.4 ± 1.9 and -48.0 ± 2.0 mV at pH 4.0 and 8.5 through the introduction of the anthracene-derived polymer. These results strongly suggest the co-existence of additional basic and acidic sources from $CH_2N(CH_3)CH_2$ and the phenolic OH groups of the surface polymer.

4.3 Optical properties of 2,6- Dihydroxyanthracene polymer coated silica nano helices:

In this section we will describe the optical properties of polymer@silica nanohelices the synthesis of which has been described in the section 4.2.

After the polymerization and the purification, the polymer@silicahelices were dispersed in ethanol and their optical properties were studied and compared with the monomers co-suspended with bare silica helices in ethanol. The figure 4.3.1a and b represent the monomer absorbance and emission spectra respectively, while the figure 4.3.1c and 4.3.1d, represents DHA polymer coated silica helices absorbance and emission after the polymerization reaction. We observe that with the polymerization, the peaks observed with monomers disappear leading to a gradually decreasing curve as a function of the increasing wavelength. (Figure 4.3.1a).

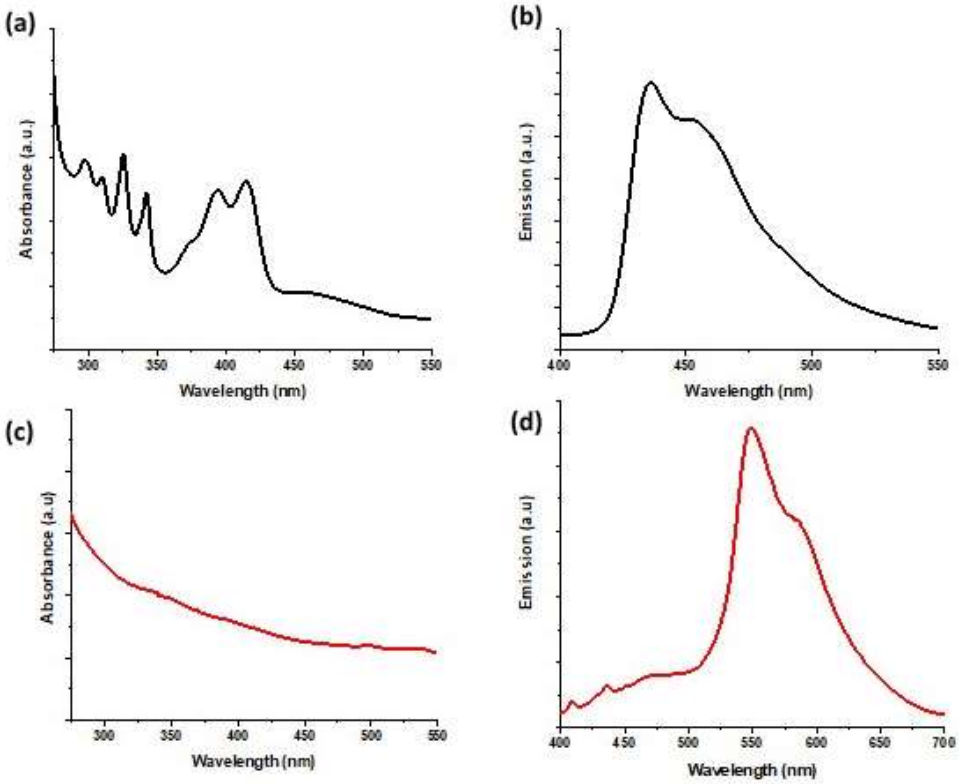

Figure 4.3.1: (a) Absorbance spectra of monomer with silica before polymerization, (b) absorbance spectra of polymer coated helical silica, and (c) Emission spectra of polymer, excited at 365 nm.

The versatility of the polymer-silica hybrids can be emphasized by their unique fluorescent (FL) property. Figures 4.3.2a and 4.3.2b show a comparison of the fluorescent colors in aqueous dispersion states excited at 365 nm between the polymer-silica hybrids and bare silica. The distinct difference demonstrates that the coated-organic component on the silica is not due to the monomer adsorption; however, the pH-dependent Stokes shift in the polymer-silica hybrid agrees with the pH-dependent change of the dissociation states between phenolic OH and O^- on the anthracene moiety in the polymer layer.

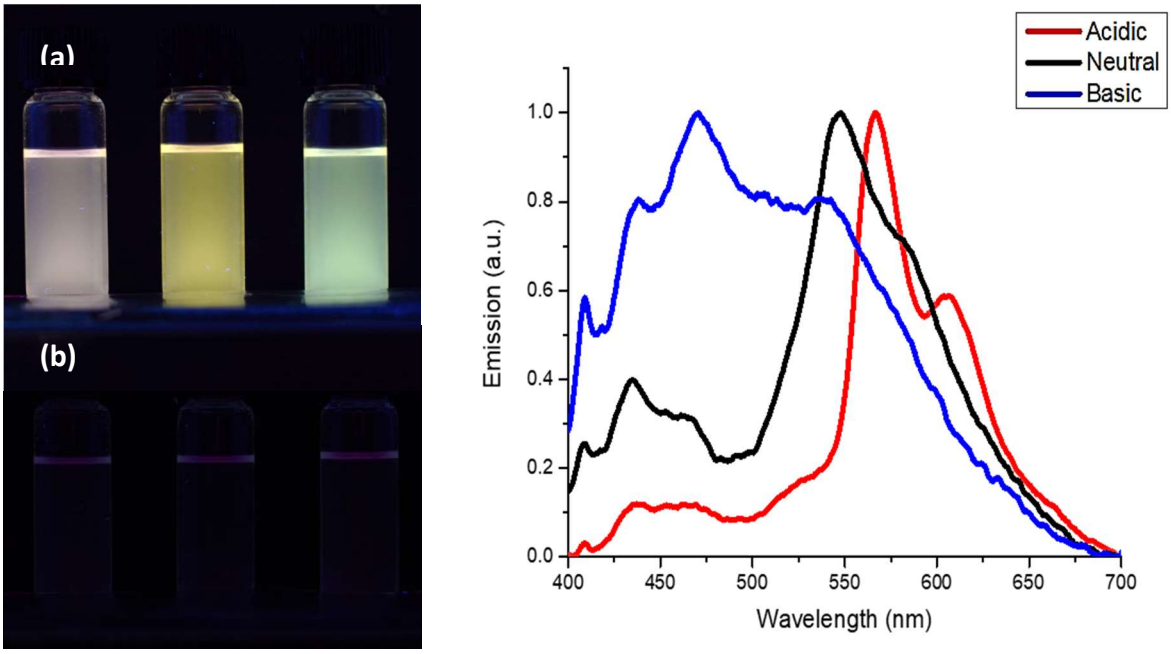

Figure 4.3.2: (a) Emission colors of the polymer-silica hybrids and (b) the bare silica helices in aqueous media with different pH under UV-lamp excited at 365 nm. (c) Normalized emission spectra of the polymer-silica hybrid with different pH levels excited at 365 nm. Concentration of silica: 0.25 mg ml^{-1}. The sample pH was adjusted to be pH 2, pH 7 and pH 11 using 0.1 M HCl and 0.1 M NaOH.

The uniqueness of the FL property can also be emphasized based on the solvent dependency. As shown in Figure 4.3.3, good dispersity in various organic solvents was observed, indicating an effective hydrophobicity from the coated polymer, and a distinct fluorescent solvatochromism was observed. [20] This is one of the characteristic phenomena of a 2,6-DHA-derived polymer, and it was estimated that the fluorescent solvatochromism is induced through the “on-off” switch in the intramolecular hydrogen bonding interaction between $CH_2N(CH_3)CH_2$ from the cross-linker and phenolic OH groups from the anthracene moiety: the estimated interaction mechanism is proposed in figure 4.3.3c where the st can be formed in acidic or polar solvents such as DMSO, but the state II based on intramolecular hydrogen bonding interaction is formed in a non-polar solvent such as toluene. In a basic condition, the phenolic anion state generated is probably similar to that in the state II. The detailed discussion will be done in a future report with further investigation.

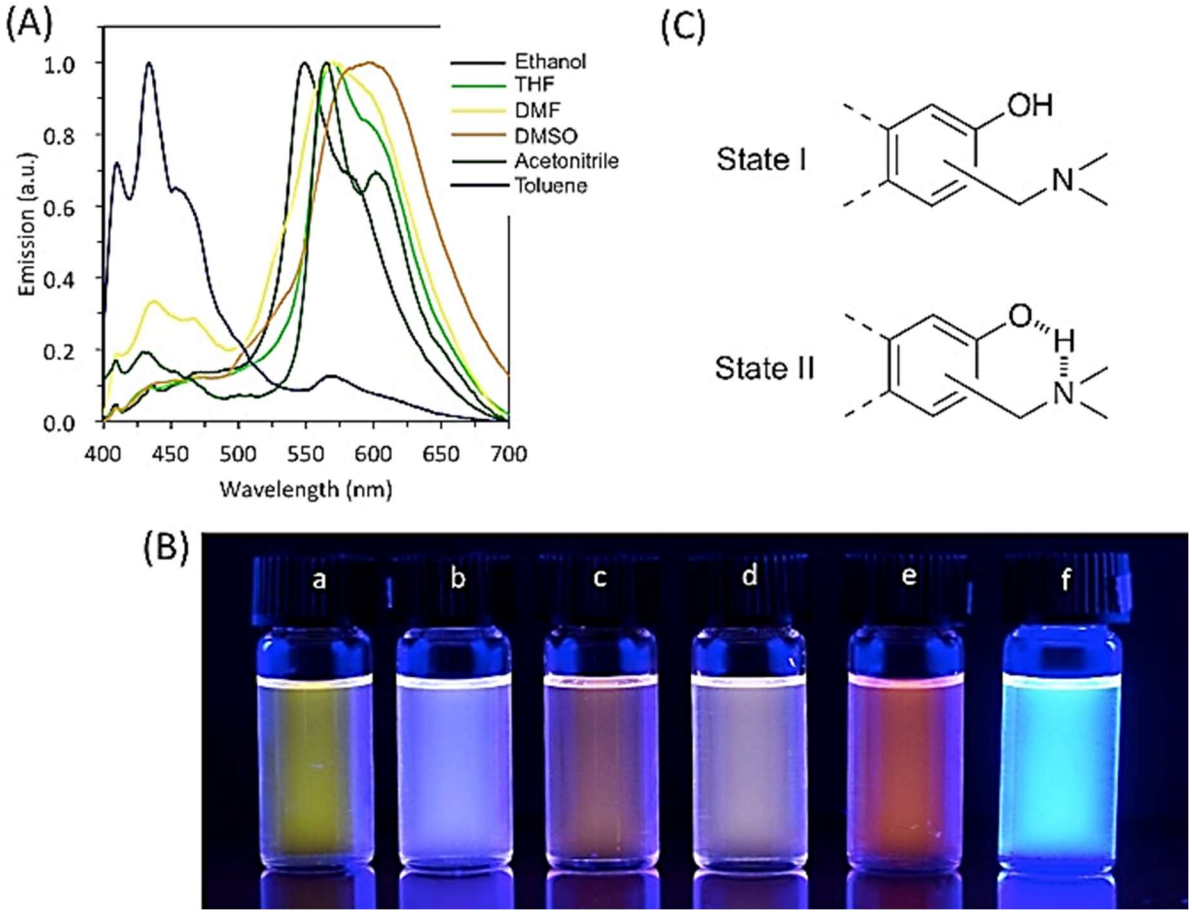

Figure 4.3.3: Solvent-dependent changes in (A) the fluorescent spectra and (B) the luminescent color in the polymer-silica hybrid dispersed in various organic media:(a) ethanol, (b) tetrahydrofuran, (c) dimethyl-formamide, (d) dimethylsulfoxide, (e) acetonitrile, and (f) toluene, under a UV-lamp excited at 365 nm. (C) Estimated mechanism on the fluorescent solvatochromism in the polymer component.

The chiroptical properties (both absorbance and emission) of these on polymer coated silica nanohelices (L-& D-type) were investigated. No chiral induction was observed in terms of circular dichroism (CD) and circularly polarised luminescence (CPL) for the optical properties of the polymers adsorbed on the silica nanohelices.

Based on the results of polymer coated silica nanohelices an article was submitted and accepted as:

'Fabrication of fluorescent one dimensional nanocomposite through one-pot self-assembling polymerization' in Chemistry letter.

Shaheen Pathan, Hiroki Noguchi, Nobuo Yamada, Yutaka Kuwahara, Makoto Takafuji, Reiko Oda, and Hirotaka Ihara·.

Conclusion

In this chapter, we first presented the synthesis of fluorescent nanoparticles from different monomers such as DHN, DHA and BHM via one-step polymerization. And, detailed study about DHA nanoparticles with various characterizations were performed. It was shown that these polymer particles are fluorescent with good quantum yield and show strong solvochromism.

The DHA polymer was also deposited on the surface of chiral silica nano twisted ribbons and nano helices via one-step polymerization. The polymer@nanohelices exhibit fluorescence properties similar to the polymer particles. The fluorescent silica is optically inactive, they are not able to show chiroptical properties. In brief, we were able create fluorescent one dimensional nanostructure using chiral silica nanostructure.

Experimental Section

The other types of anthracene-based nanoparticles were prepared according to the similar procedure to **Ant10-T_8W_2** by changing the initial concentration and solvent system.

Preparation of Naph30-E_5W_5. 2,6-Dihydroxynaphthalen (96.9 mg, 0.60 mmol) and 1,3,5-trimethyl-1,3,5-triazinane (77.5 mg, 0.60 mmol) were dissolved in 20 mL of an ethanol-water mixed solvent (5 : 5). The mixture was placed into a 30 mL glass vessel, and then heated at 150 ˚C for 3 min with stirring (300 rpm) in the microwave reactor. The resultant solution was filtered with cellulose acetate membrane filter (pore diameter = 0.2 μm) and the residual product, **Naph30-E_5W_5** was collected. The product was washed with ethanol and dried in vacuum. **Naph30-E_5W_5** was obtained as brown powders.

Preparation of Flu-E_5W_5. 9,9’-Bis(4-hydroxyphenyl)fluorene (210.25 mg, 0.60 mmol) and Hexamethylenetetramine (84.11 mg, 0.60 mmol) were dissolved in 20 mL of ethanol-water mixed solvent (5 : 5). The mixture was placed into a 30 mL glass vessel, and then heated at 200 ˚C for 30 min with stirring (300 rpm) in the microwave reactor. The resultant solution was filtered with cellulose acetate membrane filter (pore diameter = 0.2 μm) and the residual product, **Flu-E_5W_5** was collected. The product was washed with ethanol and dried in vacuum. **Flu-E_5W_5** was obtained as yellow powder.

Reference:

1. Shen, S.; Wang, Q. Rational Tuning the Optical Properties of Metal Sulfide Nanocrystals and Their Applications. *Chemistry of Materials* **2013**, *25* (8), 1166–1178. https://doi.org/10.1021/cm302482d
2. Hua, F.; Swihart, M. T.; Ruckenstein, E. Efficient Surface Grafting of Luminescent Silicon Quantum Dots by Photoinitiated Hydrosilylation. *Langmuir* **2005**, *21* (13), 6054–6062. https://doi.org/10.1021/la0509394.
3. Oosterkamp, T. H.; Fujisawa, T.; van der Wiel, W. G.; Ishibashi, K.; Hijman, R. V.; Tarucha, S.; Kouwenhoven, L. P. Microwave Spectroscopy of a Quantum-Dot Molecule. *Nature* **1998**, *395* (6705), 873–876. https://doi.org/10.1038/27617.
4. Zhang, Y.; Clapp, A. Overview of Stabilizing Ligands for Biocompatible Quantum Dot Nanocrystals. *Sensors* **2011**, *11* (12), 11036–11055. https://doi.org/10.3390/s111211036.
5. Giri, S.; Sykes, E. A.; Jennings, T. L.; Chan, W. C. W. Rapid Screening of Genetic Biomarkers of Infectious Agents Using Quantum Dot Barcodes. *ACS Nano* **2011**, *5* (3), 1580–1587. https://doi.org/10.1021/nn102873w.
6. Giansante, C.; Raffy, G.; Schäfer, C.; Rahma, H.; Kao, M.-T.; Olive, A. G. L.; Del Guerzo, A. White-Light-Emitting Self-Assembled NanoFibers and Their Evidence by Microspectroscopy of Individual Objects. *Journal of the American Chemical Society* **2011**, *133* (2), 316–325. https://doi.org/10.1021/ja106807u.
7. Mitchell, P. Turning the Spotlight on Cellular Imaging. *Nature Biotechnology* **2001**, *19* (11), 1013–1017. https://doi.org/10.1038/nbt1101-1013.
8. Chan, W. C. Quantum Dot Bioconjugates for Ultrasensitive Nonisotopic Detection. *Science* **1998**, *281* (5385), 2016–2018. https://doi.org/10.1126/science.281.5385.2016.
9. Hsieh, C.-J.; Chen, Y.-C.; Hsieh, P.-Y.; Liu, S.-R.; Wu, S.-P.; Hsieh, Y.-Z.; Hsu, H.-Y. Graphene Oxide Based Nanocarrier Combined with a PH-Sensitive Tracer: A Vehicle for Concurrent PH Sensing and PH-Responsive Oligonucleotide Delivery. *ACS Applied Materials & Interfaces* **2015**, *7* (21), 11467–11475. https://doi.org/10.1021/acsami.5b02397.
10. Kaewsaneha, C.; Tangboriboonrat, P.; Polpanich, D.; Elaissari, A. Multifunctional Fluorescent-Magnetic Polymeric Colloidal Particles: Preparations and Bioanalytical Applications. *ACS Applied Materials & Interfaces* **2015**, *7* (42), 23373–23386. https://doi.org/10.1021/acsami.5b07515.
11. Lee, J. E.; Lee, N.; Kim, H.; Kim, J.; Choi, S. H.; Kim, J. H.; Kim, T.; Song, I. C.; Park, S. P.; Moon, W. K.; et al. Uniform Mesoporous Dye-Doped Silica Nanoparticles Decorated with Multiple Magnetite Nanocrystals for Simultaneous Enhanced Magnetic Resonance Imaging, Fluorescence Imaging, and Drug Delivery. *Journal of the American Chemical Society* **2010**, *132* (2), 552–557. https://doi.org/10.1021/ja905793q.
12. Stoica, G.; Castelló Serrano, I.; Figuerola, A.; Ugarte, I.; Pacios, R.; Palomares, E. Layered Double Hydroxides as Carriers for Quantum Dots@silica Nanospheres. *Nanoscale* **2012**, *4* (17), 5409. https://doi.org/10.1039/c2nr31550e.
13. Breul, A. M.; Hager, M. D.; Schubert, U. S. Fluorescent Monomers as Building Blocks for Dye Labeled Polymers: Synthesis and Application in Energy Conversion, Biolabeling and Sensors. *Chemical Society Reviews* **2013**, *42* (12), 5366.

https://doi.org/10.1039/c3cs35478d.
14. Li, Z.; Lu, J.; Li, S.; Qin, S.; Qin, Y. Orderly Ultrathin Films Based on Perylene/Poly(*N* -Vinyl Carbazole) Assembled with Layered Double Hydroxide Nanosheets: 2D Fluorescence Resonance Energy Transfer and Reversible Fluorescence Response for Volatile Organic Compounds. *Advanced Materials* **2012**, *24* (45), 6053–6057. https://doi.org/10.1002/adma.201203040.
15. Kasuya, M.; Taniguchi, T.; Kohri, M.; Kishikawa, K.; Nakahira, T. Preparation of Polymer Latex Particles Carrying Salt-Responsive Fluorescent Graft Chains.
16. Liu, T.; Meng, Y.; Wang, X.; Wang, H.; Li, X. Unusual Strong Fluorescence of a Hyperbranched Phosphate: Discovery and Explanations. *RSC Advances* **2013**, *3* (22), 8269. https://doi.org/10.1039/c3ra22680h.
17. Uyar, T.; Hacaloglu, J.; Ishida, H. Synthesis, Characterization, and Thermal Properties of Alkyl-Functional Naphthoxazines. *Journal of Applied Polymer Science* **2013**, *127* (4), 3114–3123. https://doi.org/10.1002/app.37692.
18. Murakami, A.; Noguchi, H.; Kuwahara, Y.; Takafuji, M.; Nozato, S.; Sun, R.; Nakasuga, A.; Ihara, H. Non-Conductive, Size-Controlled Monodisperse Black Particles Prepared by a One-Pot Polymerization and Low-Temperature Calcination. *Chemistry Letters* **2017**, *46* (5), 680–682. https://doi.org/10.1246/cl.170084.
19. Khan, M. N.; Orimoto, Y.; Ihara, H. Amphiphilic Spherical Nanoparticles with a Nitrogen-Enriched Carbon-like Surface by Using β-Lactoglobulin as a Template. *Chemical Communications* **2018**, *54* (94), 13204–13207. https://doi.org/10.1039/C8CC07532H.
20. a) C. Reichardt, *Chem. Rev.* **1994**, *94*, 2319-2358; b) E. Yamaguchi, C. Wang, A. Fukazawa, M. Taki, Y. Sato, T. Sasaki, M. Ueda, N. Sasaki, T. Higashiyama, S. Yamaguchi, *Angew. Chem. Int. Ed.* **2015** *54*, 4539-4543; *Angew. Chem.* **2015,** 127, 4622-4626 c) A. S. Klymchenko, Acc. Chem. Res. **2017**, *50*, 366-375.
21. Hano, N.; Takafuji, M.; Noguchi, H.; Ihara, H. Monodisperse Surface-Charge-Controlled Black Nanoparticles for Near-Infrared Shielding. *ACS Applied Nano Materials* **2019**. https://doi.org/10.1021/acsanm.9b00555.
22. a) Ihara, H.; Takafuji, M.; Kuwahara, Y.; Noguchi, H.; Yamada, N.; JP Pat. Appl. JP 2018 189735, **2018**.

General conclusion and perspectives

In this work, we focused on the fabrications of optically active chiral nanostructures. To achieve this goal, the inorganic helices were formed via sol-gel method using organic helical self–assemblies of achiral Gemini surfactant molecules with chiral tartrate counterion, together called as Gemini tartrate used as templates. These inorganic silica helices were used as template to 1) graft inorganic quantum dots ZnS-$AgInS_2$ with different capping ligands, or to 2) deposit the fluorescent anthracene derivative polymer on their surface. To investigate the chiroptical properties, circular dichroism and circularly polarised luminescence characterization were performed.

As it was shown in Chapter 3, we synthesized inorganic $(ZnS)_{x-1}(AgInS2)_x$ QDs with different compositions ratio (x=0.2, 0.4, 0.6, 0.8, and 1.0) and their characterization was performed by TEM, Fourier-transform infrared spectroscopy (FTIR) and zeta potential measurements. Four different types of ligands were used to cap the quantum dots via phase ligand exchange as follows: ammonium sulphide (AS), 3-mercaptopropionic acid (MPA), l-cysteine (L-Cys) and the fourth one is oleylamine (OLA). These QDs are grafted on the surface of amine-modified silica helices through ionic interaction. Different conditions were used to graft these QDs on the surface of silica helices, and their optical properties were studied using absorption and emission spectroscopy. It was clearly observed that the properties of these QD@silica nanohelices depend strongly on the ligands. For all the cases, the TEM characterization shows that QDs are grafted on the surface of silica helices. However, in the case of AS-capped QDs, the helical morphology of silica helices after grafting is rapidly destroyed probably due to S^{2-} ions of the ligand which act as strong acids and break Si-O bond. While, in the cases of QDs with other three ligands MPA, OLA and L-cys, dense and homogeneous grafting of the QDs on the nanohelices were observed and the morphologies of these helices preserved after the grafting as observed by HRTEM images, energy-dispersive x-ray (EDX) analysis performed in STEM mode, For the OLA-QDs@silica helices, along with the TEM images, confocal microscopy was also used to observe fluorescent long fiber-like structures. The spectroscopic studies on these QDs@silica helices were performed. The UV-Vis absorbance of MPA- and OLA capped QDs upon grafting no major changes were observed,

it may be due to their broad absorbance with no particular peaks and no ICD was observed. On the other hand, in the case of L-cysteine ligand which is chiral, QDs alone show induced circular dichroism (CD) between the wavelength 250 nm - 290 nm. However, their grafting on the silica nanohelices does not show any influence on the ICD. For the fluorescence spectroscopy, the blue shift was observed in the both cases of MPA and OLA after grafting in comparison to bare QDs. In sum, in spite of the homogeneous and dense grafting of the QDs and well preserved nanohelices (MPA, OLA, L-Cys), we could not observe induced CD or CPL. However, we are able to prepare fluorescent silica nanohelices by grafting QDs which are stable in polar and non-polar solvents.

The ZnS-$AgInS_2$ QDs do not show the chiral interaction with the chiral template might be that these QDs do not interact with each other as it is the case of the plasmonic particles or core-shell QDs, due to their non-organized composite structures (crystalline domains are randomly organized inside a QD), and that they have weak dipole moment, not allowing them to interact with each other. In order to observe the chiral organization-induced CD or CPL, It is likely that either the achiral particles (metal nanoparticles or QDs) have strong inter-particle interaction such as high polarizability or strong dipole moment unlike CdSe nanocrystals.

In the last chapter 4, we introduced the syntheses and the characterisation of organic fluorescent polymer particles with size ranging from nm - µm from different monomer such as 2,6 -dihydroxynapthalene (DHN), 2,6-dihydroxy anthracene (DHA) and 9,9-bis(4-hydroxyphenyl)fluorene (BHF) with two different cross-linkers 1,3,5-trimethyl-1,3,5-triazinane (TMTA) and hexamethylenetetramine (HMT). The reaction is a one-step polymerization. The size of the particles was investigated by TEM and SEM. For the synthesis of polymer particles the parameters such as concentration, solvent, time and temperature played important role. Furthermore, solvatochromism was observed due to variation of different solvents with swelling effect. The swelling effect on particle in wet and dry conditions were observed. The relative quantum yield of DHA polymer particles in different solvents were calculated. The highest quantum yield was observed in DMF by 108 %. The other characterization such as, EA, zeta potential were performed to investigate their physiochemical properties.

In the second part of the chapter 4, the DHA polymer was adsorbed or deposited on the surface of silica twisted ribbons and nanohelices. The deposition of different types of polymers on the silica helix was investigated by TEM, confocal microscopy, EA, absorption, and emission spectroscopy. The fluorescence properties at different pH in aqueous media and in different solvent were studied. The ensemble of these results showed that we are able to create the hybrid fluorescent one dimensional helical structure by organic polymer coating on silica nanohelices.

These polymers @silica nanohelices also did not show ICD or ICPL. This may be because the deposited polymer is not thick enough (~2nm), the intermolecular (between anthracene) interaction within the deposited polymer is not strong enough. Indeed we have shown that when the molecules grafted on the surface of the silica nanohelices do not interact with each other, but separately grafted, they did not show ICD or ICPL. In our case, probably homogeneous multi-layer of aromatic polymer films may lead to the ICD or ICPL.

The present study was focused on the creation of optically active chiral nanostructures using chiral templates. Our results confirm that we created fluorescent one dimensional silica nanohelices by grafting inorganic quantum dots or by coating with organic polymer with different techniques of fabrication while protecting helical structural morphology of chiral silica template and also preserving the photochemical properties of fluorophore. These fluorescent one dimensional nanostructure can be utilized for the nano-photonic applications or creating composite material. We also created fluorescent and solvochromic polymer particles which can also be used to create thin films. In the context of the study, we could not observe the chiroptical properties of these fluorescent chiral fibers, which may be due to the choice of the QDs and the types of the polymers used for the study. Indeed, for the future work it may be interesting to choose di-component QDs such as CdSe which are known to show organization induced CD or CPL. For the Fluorescent polymer coating of the silica helice, we may investigate the effect of the thickness of the polymers (higher number of multi-layer) on the ICD or ICPL.